(3)

AD-A192 881

HDL-CR-88-052-1

March 1988

Research in Electromagnetic Shielding Theory: Part 1. Shielding by Rectangular Enclosures

by Richard L. Monroe

Prepared by

Sol Telecommunications Services, Inc.
2000 Corporate Ridge, Suite 810
McLean, VA 22102

Under contract

DAAL02-86-C-0052

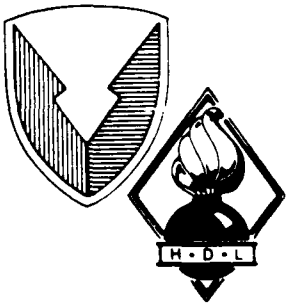

U.S. Army Laboratory Command
Harry Diamond Laboratories
Adelphi, MD 20783-1197

SECURITY CLASSIFICATION OF THIS PAGE

REPORT DOCUMENTATION PAGE

Form Approved
OMB No 0704-0188
Exp. Date Jun 30, 1986

1a. REPORT SECURITY CLASSIFICATION UNCLASSIFIED	1b. RESTRICTIVE MARKINGS None
2a. SECURITY CLASSIFICATION AUTHORITY	3. DISTRIBUTION/AVAILABILITY OF REPORT Unlimited
2b. DECLASSIFICATION/DOWNGRADING SCHEDULE	
4. PERFORMING ORGANIZATION REPORT NUMBER(S)	5. MONITORING ORGANIZATION REPORT NUMBER(S) HDL-CR-88-052-1
6a. NAME OF PERFORMING ORGANIZATION Sol Telecommunications Services 6b. OFFICE SYMBOL (If applicable)	7a. NAME OF MONITORING ORGANIZATION USALABCOM
6c. ADDRESS (City, State, and ZIP Code) 2000 Corporated Ridge, Suite 810 McLean, VA 22102-7805	7b. ADDRESS (City, State, and ZIP Code) 2800 Powder Mill Road Adelphi, MD 20783-1197
8a. NAME OF FUNDING/SPONSORING ORGANIZATION USALABCOM 8b. OFFICE SYMBOL (If applicable) AMSLC	9. PROCUREMENT INSTRUMENT IDENTIFICATION NUMBER DAAL02-86-C-0052
8c. ADDRESS (City, State, and ZIP Code) 2800 Powder Mill Road Adelphi, MD 20783-1197	10. SOURCE OF FUNDING NUMBERS PROGRAM ELEMENT NO: 6.2120 PROJECT NO: IL162 120-AH25 TASK NO: WORK UNIT ACCESSION NO:
11. TITLE (Include Security Classification) Research in Electromagnetic Shielding Theory: Part 1. Shielding by Rectangular Enclosures	
12. PERSONAL AUTHOR(S) Richard L. Monroe	
13a. TYPE OF REPORT final 13b. TIME COVERED FROM May'86 TO Mar'88 14. DATE OF REPORT (Year, Month, Day) 1988 March 31 15. PAGE COUNT 162	
16. SUPPLEMENTARY NOTATION HD XE76E3; AMSCODE: 612120.H25	
17. COSATI CODES FIELD / GROUP / SUB-GROUP	18. SUBJECT TERMS (Continue on reverse if necessary and identify by block number) Electromagnetic shielding, shielded enclosures, Maxwell's equations, shielding effectiveness, transient analysis, MIL-STD-285, IEEE-299, impedance boundary conditions.

19. ABSTRACT (Continue on reverse if necessary and identify by block number)

General expressions for the electric and magnetic fields at any point inside slotted and continuous, rectangular enclosures exposed to arbitrary external, time harmonic source fields are obtained under the assumption that the enclosures are constructed from good conductors and the slot is small compared to the wavelength of the source field. These expressions consist of infinite series summed over the TE waveguide modes where each term is the product of one or more mode functions and a Fourier coefficient that depends on the spatial variation of the source magnetic field. The Fourier coefficients were evaluated in closed form for two cases: the outside surface of the slot exposed to a spatially uniform magnetic field and the outside surface of one wall of the continuous enclosure exposed to a spatially uniform magnetic field.

Frequency domain calculations based on these expressions showed that for frequencies below the enclosure cutoff frequency, the magnetic field at all locations inside a typical slotted enclosure is independent of frequency. For the same range of frequencies

20. DISTRIBUTION/AVAILABILITY OF ABSTRACT ☒ UNCLASSIFIED/UNLIMITED ☐ SAME AS RPT. ☐ DTIC USERS	21. ABSTRACT SECURITY CLASSIFICATION same as
22a. NAME OF RESPONSIBLE INDIVIDUAL W. Coburn	22b. TELEPHONE (Include Area Code) (703) 490-2320 22c. OFFICE SYMBOL SLCHD-NW-EC

DD FORM 1473, 84 MAR

83 APR edition may be used until exhausted.
All other editions are obsolete.

SECURITY CLASSIFICATION OF THIS PAGE

the field inside a continuous enclosure is a monotonically decreasing function of frequency. At frequencies above cutoff, the fields in both slotted and continuous enclosures show very complex behavior associated with cavity resonances.

The frequency domain series for the internal magnetic fields were transformed into time domain expressions which were used to plot the transient response of the internal magnetic fields at various locations when one wall or one slot is exposed to time-varying external fields. It was found that the properties of the field inside a continuous enclosure are determined to a great extent by the characteristic diffusion time of the enclosure wall and the duration of the incident field. The former determines the fastest rise time of the internal field and the latter determines its largest value. The transient field inside an enclosure with an air-filled slot consists of the sum of two parts: the stationary field and the propagating field. The stationary field dominates close to the slot where it forms a reduced replica of the external field. Its peak field decreases rapidly with distance from the slot so that at most locations it is negligible compared to the propagating field. The latter travels at approximately the speed of light and undergoes repeated reflections from the walls of the enclosure. The peak value of the stationary field depends principally on the length of the slot, while the peak of the propagating field depends on the rise time of the external field. That is, longer slots produce larger stationary fields and faster rise times produce larger propagating fields.

Calculations based on the frequency domain expressions were used to compare the theoretical results with two sets of experimental data, and satisfactory agreement was found.

Accession For	
NTIS GRA&I	☑
DTIC TAB	☐
Unannounced	☐
Justification	
By	
Distribution/	
Availability Codes	
Dist	Avail and/or Special
A-1	

CONTENTS

APPENDIX

FIGURES

1. INTRODUCTION

An electromagnetic shield is a structure fabricated from one or more sheets of electrically conducting material, usually copper, steel, or aluminum, that is used to reduce the intensity of electric and magnetic fields entering a designated region (the shielded volume) from external sources such as antennas, transmission lines, lightning, and electromagnetic pulse (EMP). It does this by forming a barrier between the shielded volume and the source that reflects and absorbs most of the electromagnetic field before it can enter. Shields can be simple open structures such as a single flat sheet of steel placed between a source and the shielded volume. Or, they can be much more complicated closed form structures that approximate continuous metallic shells. The latter are usually circular cylinders or rectangular parallelepipeds (boxes). The volume enclosed by such a shield may, or may not, coincide with the shielded volume. It does if the source of interest is located outside of the enclosure. However, if the source is inside, then the shielded volume is the (unlimited) region outside the enclosure. On the other hand, if there are sources of interest both inside and outside, then both regions are shielded volumes with respect to one source or the other. That is, a closed shield may be used to exclude designated fields from a limited region, it may confine fields to a limited region, or it may separate the effects of two sources by excluding the

fields of one source from the region while confining the fields of the other source.

Closed-form shields are prefered to open shields for most applications because of their generally greater efficiency as measured by the reduction in field intensity at a given location when that location is included in a shielded volume. The reason for this is simply that they usually have smaller open (non-metallic) areas through which fields can reach the shielded volume without incurring the large reflection and absorption losses associated with direct penetration of the metal barrier. Open shields, by their very openness, usually provide relatively large areas where incoming fields can bypass the metal barrier. For example, a shield consisting of a flat, rectangular, steel sheet of modest thickness exacts huge losses on the part of the incoming field that takes a straight line all-metal path to the shielded volume. If this were the only path to the shielded volume, its efficiency would be very high. However, this structure also provides longer but less lossy paths through the (infinite) area at and beyond the perimeter of the sheet by which part of the field can reach the shielded volume through the process of diffraction. This diffracted field usually dominates the directly transmitted field and, thus, severely limits the efficiency of the shield. Without changing the frequency of the source field, the only way the efficiency can be improved is by increasing the size (area) of the sheet- an approach that is often impractical.

A simple closed-form shield can be constructed from the rectangular steel sheet by bending it into a circular cylinder and joining the adjacent edges with a continuous weld. Since the diffraction field can now avoid all-metal paths only by entering or leaving the enclosed volume through the finite (circular) areas at the ends of the cylinder, we can expect the efficiency of this shield to be significantly greater than that of a flat sheet with the same composition, thickness, and surface area. Much greater efficiency can be achieved by welding steel sheets to both ends. These minimize diffraction effects and insure that fields enter or leave the enclosure by all-metal paths. In this way, a closed-form shield can be transformed into a continuous metal shell.

By a similar process in which six rectangular steel sheets are welded along their edges, a continuous metal shell can be constructed in the form of a rectangular parallelepiped. This enclosure, like the cylindrical enclosure, constitutes an ideal electromagnetic shield in the sense that its efficiency cannot be significantly improved without increasing the thickness of the shell or changing its composition. It does, in fact, realize the full shielding potential of a given thickness of steel in this form. This structure is also ideal in the sense that it represents a limit that can only be approached by practical shields.

In practice, perfect metallic continuity must always be sacrificed for access areas in the form of doorways, hatches, and other entry points for people, equipment, or supplies. These openings or discontinuities inevitably reduce the efficiency of a practical shield below that of the ideal by allowing fields to reach the interior by nonmetallic paths just as in the case of an open shield. Thus, practical closed-form shields must be open to some extent. To minimize their effect, large openings are usually provided with metal closures (doors or panels) that are intended (when in place) to establish continuity by maintaining metal to metal contact at their boundaries with the rest of the shield. Unfortunately, perfect contact between two pieces of metal cannot usually be maintained except by welding or some other type of permanent connection that would defeat the purpose of the opening. Consequently, closures are almost never completely successful in achieving continuity, although some may approach it. In general, the effect of the closure is to replace an original large opening by one or more smaller ones in the form of gaps arranged along the seams where it meets the body of the shield. These openings are frequently sufficient to reduce the efficiency of the structure well below that of a comparable ideal shield, and, if numerous enough and large enough, are capable of compromising its performance. Consequently, the treatment of seam discontinuities is crucial to both the theory and practice of electromagnetic shielding

This report presents a theoretical investigation of the rectangular enclosure as an ideal shield and as a shield with one or more seam discontinuities in the form of narrow rectangular slots. The investigation uses a recently developed shielding theory for generalized structures composed of flat metal sheets to obtain general expressions for the electric and magnetic fields at points inside continuous and discontinuous rectangular enclosures when an external surface is exposed to fields from an arbitrary, time harmonic, electromagnetic source. These general expressions are reduced to explicit expressions when the source field is spatially uniform over the outside surface of the enclosure and for the less restrictive case where the field is uniform over the discontinuity. The latter are used to calculate and plot frequency domain fields at selected points inside both continuous and discontinuous enclosures. Comparison of the calculations shows the large effect of even small discontinuities on the shielding effectiveness (efficiency) of the enclosure. Analogous results are obtained in the time domain by computing and plotting inverse LaPlace transforms of the frequency domain expressions for several types of transient source fields. In the case of the discontinuous enclosure these calculations reveal a very complicated time history for the internal fields due to multiple internal reflections.

The following section reviews the general shielding theory based on impedance boundary conditions and summarizes its principal results. Section 3 uses these results to construct the gen-

eral expressions for internal electric and magnetic fields as doubly infinite series summed over the TE_{nm} modes for a rectangular waveguide. Fourier coefficients appearing in the series are evaluated in section 4 for the cases of interest, and, in section 5, the frequency domain series are transformed to the time domain using term-by-term inversion . In section 6, calculations are carried out using some of the expressions obtained in the preceding sections, and these are compared to measurements performed by two groups of experimental investigators.

2. A SHIELDING THEORY BASED ON IMPEDANCE BOUNDARY CONDITIONS

In 1985, Monroe[1] described a general theory of electromagnetic shielding that improved on and extended the classic transmission theory of Schelkunoff.[2] The new theory improved on the old one by replacing its transmission line model and eliminating certain unnecessary assumptions. The transmission line model was replaced by an Impedance Boundary Condition (IBC)[3,4] which had not previously been used explicitly to solve shielding problems. This approximate boundary condition performs the same function as the transmission line model in that it allows one to represent the field passing through a wall of the shield as a plane wave traveling perpendicular to that wall. It also provides a way to calculate this field in terms of the source field incident on the outside of the shield. Its advantage over the transmission line model is that it can be applied to a very much larger class of

---

[1] R. L. Monroe, A Theory of Electromagnetic Shielding with Applications to MIL-STD 285, IEEE-299, and EMP Simulation, Harry Diamond Laboratories, HDL-CR-85-052-1, Adelphi, MD (February 1985).

[2] S. A. Schelkunoff, Electromagnetic Waves, Van Nostrand, Princeton, NJ (1943).

[3] T. B. A. Senior, Appl. Sci. Res., 8 (B) (1960), 418.

[4] T. B. A. Senior, IEEE Trans. on Antennas Propagt., AP-29, No. 2 (1981), 826.

sources and shields, including shields that have been rendered discontinuous by one or more slot-like apertures. In fact, the restrictions on applying IBC's are so weak that there is virtually no electromagnetic shield to which an IBC could not be applied. Thus, with the aid of IBC's, one can develop a theory of shielding for a wide range of sources and shields that fall outside the scope of Schelkunoff's theory.

2.1 Impedance Boundary Conditions

An IBC is a relationship between an impedance function and an electromagnetic field at the interface between two electrically distinct media where the impedance function characterizes one medium and the electromagnetic field is defined in the other medium. In its most frequently applied form, the IBC relates tangential field components at the interface to the impedance looking into one of the media. With the two media labeled M1 and M2 as shown in figure 1, this condition can be written in vector form as follows:

$$\bar{n} \times (\bar{n} \times \overline{E1}) = - \eta 2 \ (\bar{n} \times \overline{H1}) \qquad (2.1)$$

where $\overline{E1}$ and $\overline{H1}$ are the electric and magnetic fields in M1, $\bar{n}$ is the unit vector normal to the interface pointing outward from M2, $\eta 2$ is the impedance looking into M2, and it is understood that (2.1) applies only at the interface. Equation (2.1) is an approximation that cannot be used to replace standard boundary conditions in the general case. However, in many cases of interest, it

IMPEDANCE BOUNDARY CONDITION
$\bar{n} \times (\bar{n} \times \overline{E1}) = -\eta 2\ (\bar{n} \times \overline{H1})$

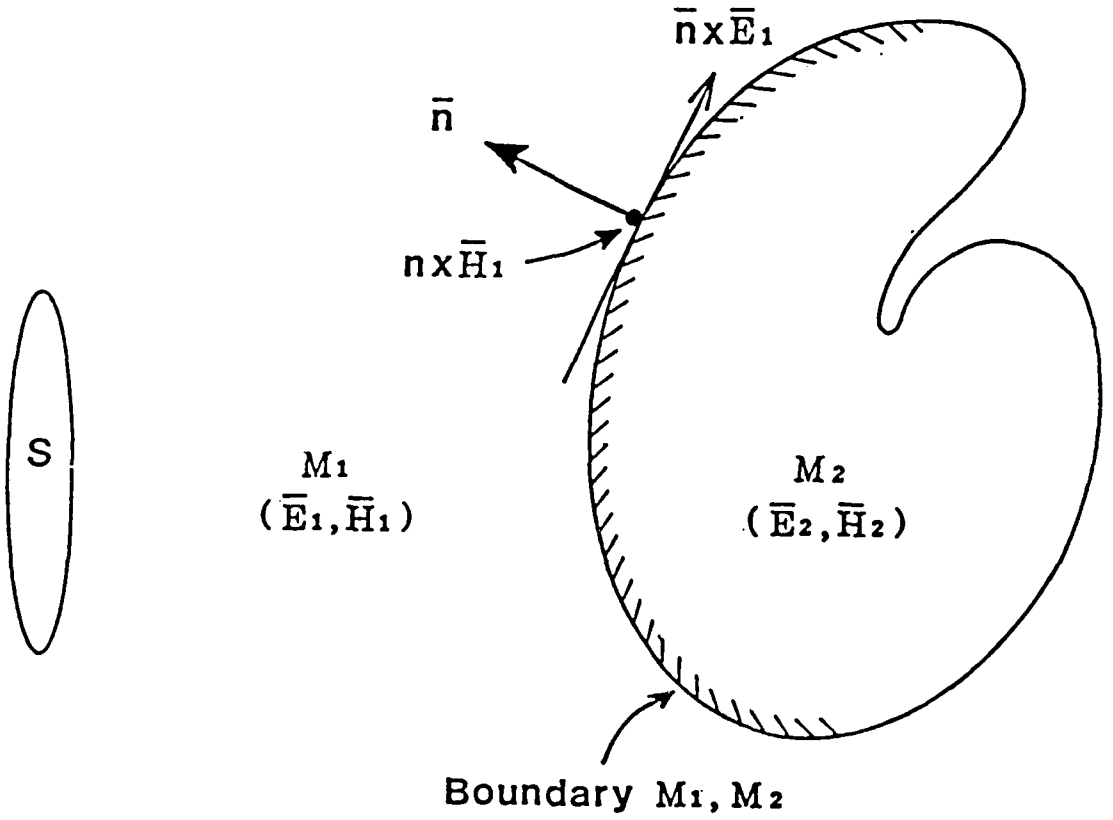

Figure 1. A medium M1 containing a source S and an electromagnetic field $\overline{E1}$, $\overline{H1}$ whose tangential components $\bar{n} \times \overline{E1}$ and $\bar{n} \times \overline{H1}$ at the boundary between M1 and a second medium M2 act as a primary source for the field $\overline{E2}$, $\overline{H2}$ in M2. (Reproduced from ref 1.)

has been shown that (2.1) is a valid approximation, and, in these cases, the IBC can be used to simplify the problem of determining the fields in M1 and M2.

This simplification derives from the fact that (2.1) decouples the fields in M1 from those in M2 in a way that does not introduce spatial derivatives of the fields at the interface. This means that $\overline{E1}$ and $\overline{H1}$ can be computed independently of the fields ($\overline{E2}$,$\overline{H2}$) in M2 and that both sets of fields can be obtained by applying standard techniques to Maxwell's equations. One first solves Maxwell's Equations for $\overline{E1}$ and $\overline{H1}$ using (2.1) to replace M2 and then solves for $\overline{E2}$ and $\overline{H2}$ in M2 using $\overline{E1}$ and $\overline{H1}$ at the interface to replace M1. Since this two-step process will usually be much easier than solving Maxwell's equations directly for $\overline{E1}$, $\overline{H1}$, $\overline{E2}$, and $\overline{H2}$, the utility of (2.1) is obvious. Moreover, if one is interested only in the fields in M1, then $\overline{E2}$ and $\overline{H2}$ need not be computed at all. Conversely, if one is primarily interested in $\overline{E2}$ and $\overline{H2}$, then it is only necessary to solve for $\overline{E1}$ and $\overline{H1}$ at the interface in order to determine the fields throughout M2. The latter describes the usual situation in shielding problems where the interior of M2 can be identified with the shield, M1 is the region containing one, or more, electromagnetic sources, and only the fields transmitted into the shielded volume are of interest.

To take advantage of the IBC, it is necessary to establish the validity of (2.1) at the interface that defines the problem of interest. In general, this requires one to show that $\overline{E2}$ and $\overline{H2}$ propagate into M2 along $\bar{n}$ as approximate plane waves. One way to do this is to show that the variation of $\overline{E2}$ and $\overline{H2}$ along $\bar{n}$ is much larger than the variation of $\overline{E1}$ and $\overline{H1}$ at the interface in directions transverse to $\bar{n}$. Specifically, one can show that the normal derivatives of $\overline{E2}$ anf $\overline{H2}$ are much larger in magnitude than the transverse derivatives of $\overline{E1}$ and $\overline{H1}$ at the interface. Since electromagnetic shields are intended to produce just such variations, it is not suprising that most of these structures will be found to satisfy IBC's. Indeed, it can be argued that no structure can be an effective shield unless it does satify an IBC at all points on its surface.

The validity of (2.1) has been demonstrated under relatively weak restrictions in the case of a planar interface separating two homogeneous half-spaces as shown in figure 2, where M1 is free space and M2 consists of a material with complex permittiviy $\epsilon 2$ and permeability $\mu 2$. With this arrangement, equation (2.1) can be written in scalar form as follows:

$$E1_x = -\eta 2\, H1_y \quad , \quad E1_y = \eta 2\, H1_x \qquad \text{at } z = 0, \qquad (2.2)$$

where

$$\eta 2 = (\mu 2/\epsilon 2)^{1/2} \qquad (2.3)$$

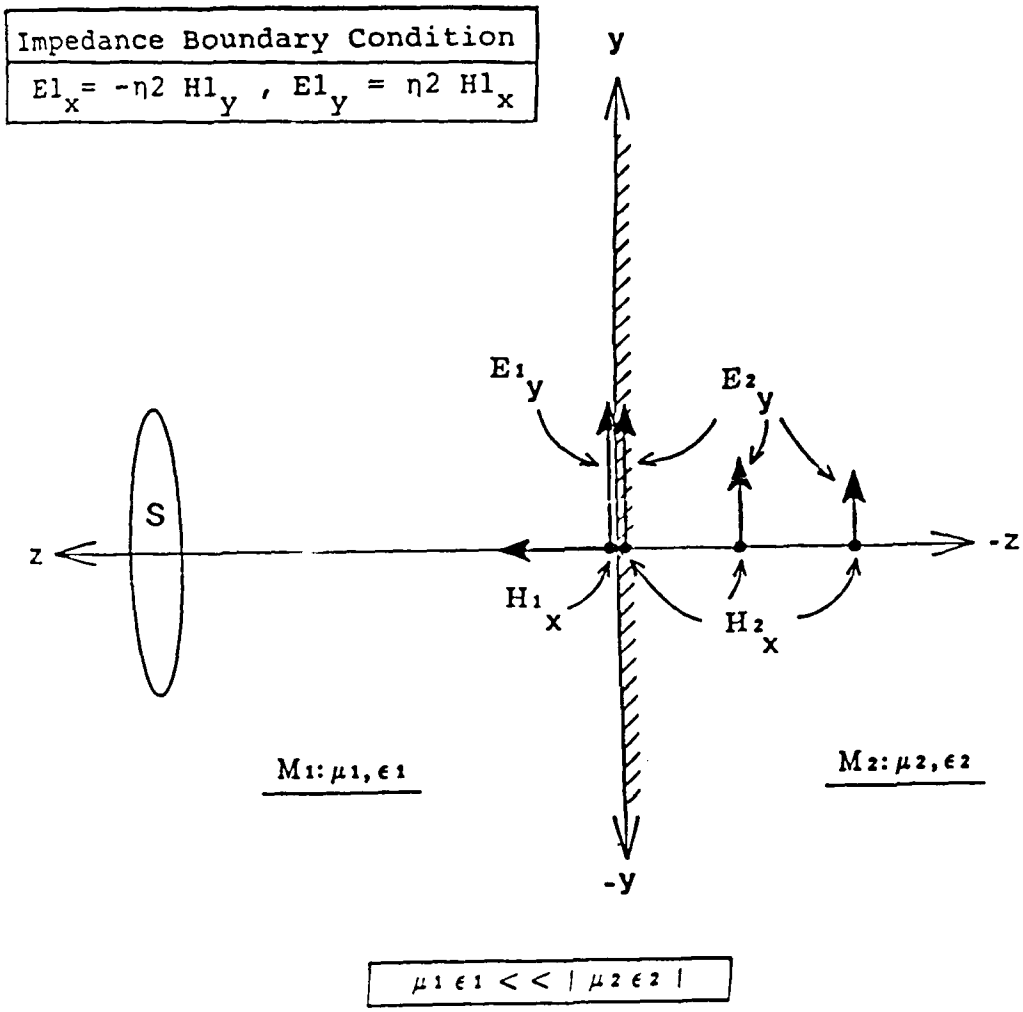

Figure 2. Two half-spaces M1 and M2 with a planar interface where an impedance boundary condition is satisfied by virtue of the relation $\mu 1\ \epsilon 1 << |\mu 2\ \epsilon 2|$. (Reproduced from ref 1.)

and the fields are referred to a rectangular coordinate system with its origin at the interface and its z axis directed out of M2 ($\bar{n} = \hat{i}_z$). A condition sufficient to insure the accuracy of (2.2) is

$$| \mu 2 \, \epsilon 2 | >> \mu 1 \, \epsilon 1 = \mu_o \, \epsilon_o \tag{2.4}$$

where $\epsilon 2$ is given by

$$\epsilon 2 = \epsilon^* - j \, \sigma 2/\omega \quad , \quad \epsilon^* > 0 \tag{2.5}$$

and ϵ_o and μ_o are the permittivity and permeability of free space. In (2.5), $\sigma 2$ is the conductivity ofthe half-space M2 and a harmonic time variation of the form $\exp(j\omega t)$ has been assumed.

When (2.4) is satisfied, the fields in M2 are constrained to propagate along the z axis (in the -z direction) like plane waves, and the validity of (2.2) is assured. The components $E2_x$, $H2_y$, $E2_y$, and $H2_x$ satisfy the one-dimensional, homogeneous wave equation with solutions of the form

$$\begin{aligned} E2_x(x,y,z) &= E2_x(x,y,0) \exp(\gamma 2 \, z) \\ H2_y(x,y,z) &= H2_y(x,y,0) \exp(\gamma 2 \, z) \\ E2_y(x,y,z) &= E2_y(x,y,0) \exp(\gamma 2 \, z) \\ H2_x(x,y,z) &= H2_x(x,y,0) \exp(\gamma 2 \, z) \end{aligned} \tag{2.6}$$

where $E2_x(x,y,0)$, $H2_y(x,y,0)$, $E2_y(x,y,0)$, and $H2_x(x,y,0)$ are the the tangential components of the field transmitted into M2 at the interface z = 0 due to the fields in M1 and the propagation constant $\gamma 2$ is given by

$$\gamma 2 = j\omega(\mu 2 \, \epsilon 2)^{1/2} \, . \tag{2,7}$$

When $E2_x(x,y,0)$, $H2_y(x,y,0)$, $E2_y(x,y,0)$, and $H2_x(x,y,0)$ are

known, equation (2.6) can be used to compute the fields at any point in M2.

Equation (2.2) is frequently referred to as the Leontovich Boundary Condition[5] although it was apparently used before Leontovich by Rytov,[6] Alpert,[7] and Feinberg[8] during World War II in their work on ground wave propagation. Since then, these and other investigators have shown that (2.2) is not limited in application to half-spaces but can be applied directly to more complicated structures. For example, if the half-space M2 is replaced by a sheet of the same material with a uniform thickness d as shown in figure 3, then the fields inside the sheet still satisfy the one-dimensional wave equation and propagate like plane waves parallel to the z axis provided (2.4) remains valid. The IBC is again applicable at z = 0 in the form given by (2.2) if an additional condition is satisfied:

$$\delta_s < d \tag{2.8}$$

where

$$\delta_s = 1/\omega \mid \mathrm{Im}((\mu 2 e 2)^{1/2}) \mid \tag{2.9}$$

is the skin depth of the sheet (M2.) The skin depth is a measure

---

[5] M. A. Leontovich, Investigation of Radiowave Propagation, Part II, Moscow: Academy of Sciences (1948).

[6] S. M. Rytov, J. Exp. Theor. Phys. USSR, 10 (1940),180.

[7] I. L. Alpert, J. Tech. Phys. USSR, 10 (1940), 1358.

[8] E. L. Feinberg, J. Phys. USSR, 8 (1944), 317.

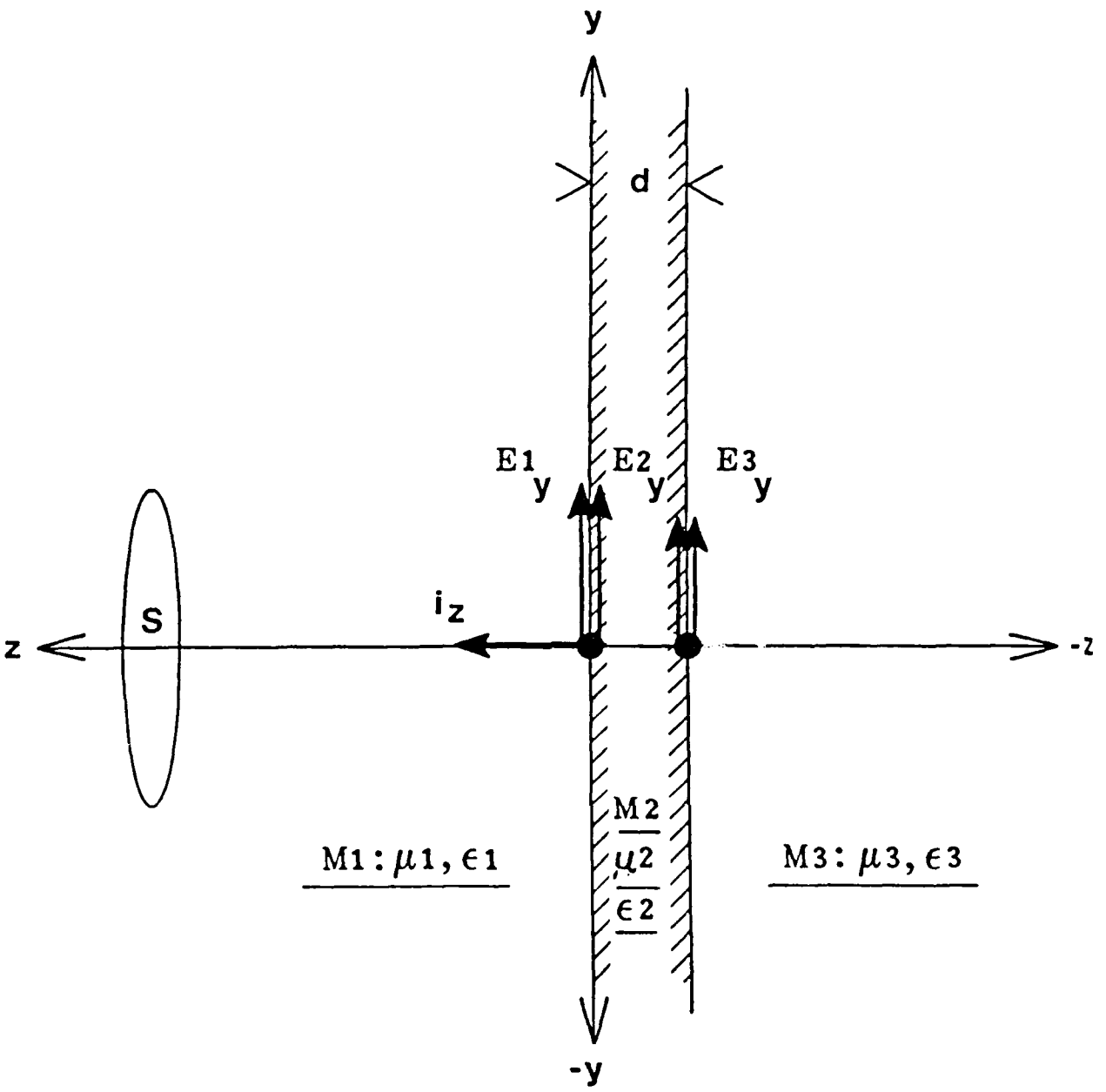

$$\mu_1 \epsilon_1 << |\mu_2 \epsilon_2|$$

$$\delta_s = 1/\omega \, \mathrm{Im}(\sqrt{\mu_2 \epsilon_2}) < d$$

Figure 3. A planar sheet of uniform thickness d separating media where an impedance boundary condition is satisfied at z = 0 by virtue of the relations $\mu_1 \epsilon_1 << |\mu_2 \epsilon_2|$ and $\delta_s < d$. (Reproduced from ref 1.)

of the rate at which the magnitude of the field decreases as it propagates in M2. Since fields decrease in amplitude by a factor of $e^{-1} = 0.37 = 8.5$ dB while traveling a distance equal to one skin depth, condition (2.8) means that fields making a round trip from z = 0 to z = - d and back to z = 0 will be reduced by at least a factor of $e^{-2} = 0.14 = 17$ dB. This condition is necessary to prevent fields reflected at z = -d from reaching z = 0 in sufficient strength to interfere with $\bar{E}\bar{1}$ and $\bar{H}\bar{1}$ at the interface and render (2.2) inaccurate. This also means that internally reflected fields at z = 0 can be neglected and that the fields at z = 0 traveling into M2 are again given by (2.6). In other words, (2.8) eliminates standing waves in the sheet, and allows one to represent the fields propagating into the sheet at z = 0 as simple traveling waves just as in the case of the infinite half-space. Condition (2.8) is easily satisfied by most electromagnetic shields composed of flat sheets since these structures are designed to reduce the fields reaching z = -d by far more than 8.5 dB. In fact, it will usually be found that quality shields satisfy the much more stringent condition $\delta_s << d$ at most frequencies of interest.

If a rectangular slot is cut through the uniform, homogeneous sheet in figure 3 and the rectangular volume of the slot is filled by a material with permeability $\mu 2'$ and permittivity $\epsilon 2'$, then the sheet is rendered locally inhomogeneous and anisotropic - inhomogeneous because the effective permeability, permittivity,

and impedance of the slot differ from those of the solid sheet and anisotropic because these quantities depend on the orientation of the slot. If the slot is oriented as shown in figure (a), then $E1_x$ and $H1_y$ will see a different impedance looking into the slot than will $E1_y$ and $H1_x$. With these two impedances denoted η_x^2 and η_y^2, a generalized IBC can be written

$$E1_x = -\eta_x^2 H1_y \ , \quad E1_y = \eta_y^2 H1_x \ , \quad \text{at } z = 0 \tag{2.10}$$

where η_x^2 and η_y^2 are functions of x and y, $\mu 2'$ and $\epsilon 2'$, and the dimensions of the slot are α and β. A similar IBC can be written for the vertical slot shown in figure 4.

A condition sufficient to insure that the fields in the slot $E2'_x$, $H2'_y$, $E2'_y$, and $H2'_x$ propagate parallel to the z axis in the manner of plane waves is

$$\begin{vmatrix} \eta_x^2 \\ \\ \eta_y^2 \end{vmatrix} << Z_o = (\mu_o/\epsilon_o)^{1/2} . \tag{2.11}$$

Since η_x^2 and η_y^2 can be defined in terms of effective slot permeabilities and permittivities,

$$\eta_x^2 = (\mu_x^2/\epsilon_x^2)^{1/2}$$
$$\eta_y^2 = (\mu_y^2/\epsilon_y^2)^{1/2} \tag{2.12}$$

where μ_x^2 , $\mu_y^2 \geq \mu_o$. Condition (2.10) then implies

$$\begin{vmatrix} \mu_x^2 \epsilon_x^2 \\ \\ \mu_y^2 \epsilon_y^2 \end{vmatrix} >> \mu_o \epsilon_o \tag{2.13}$$

which is completely analogous to (2.4). The fields in the slots

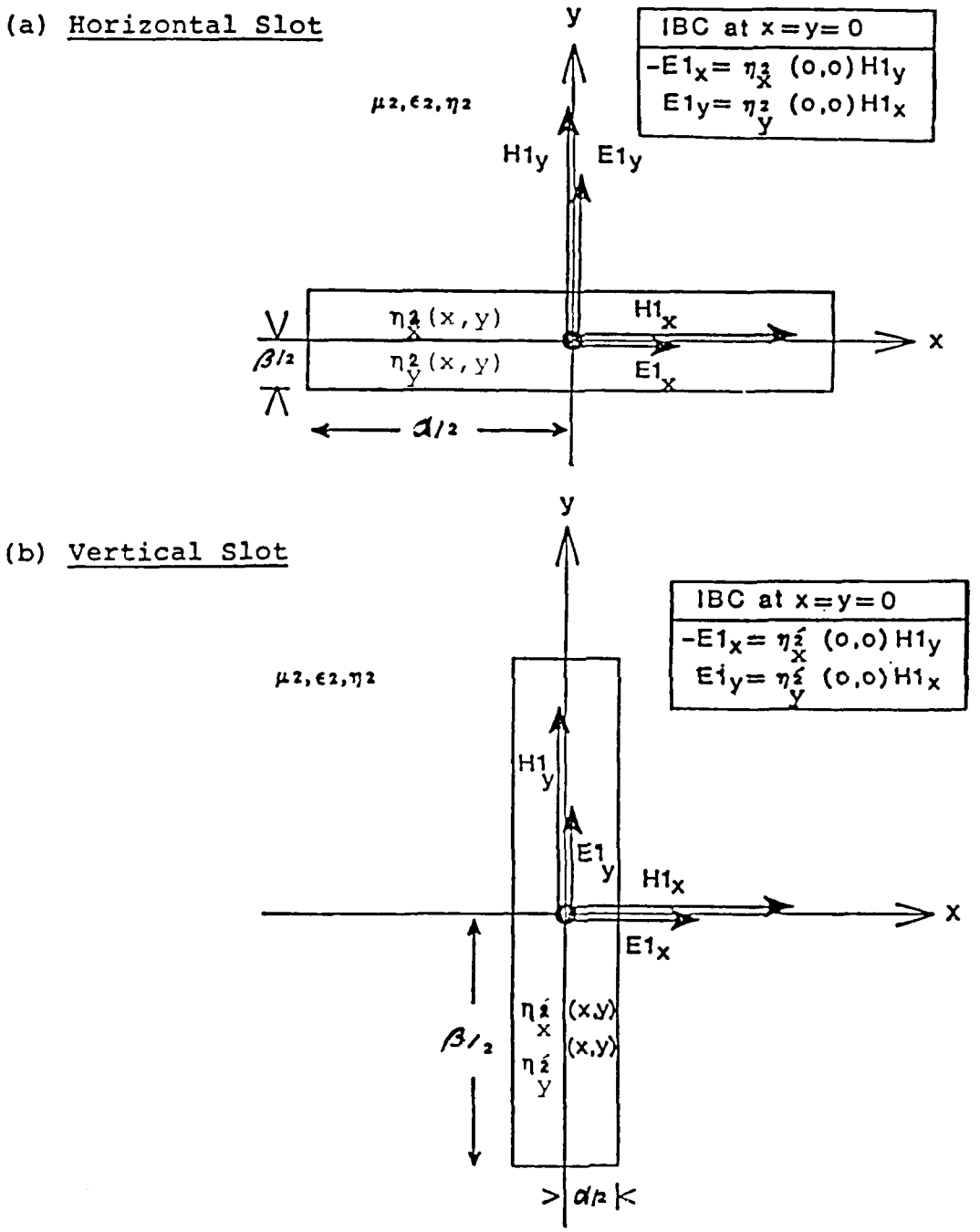

Figure 4. Impedance boundary conditions at the center of horizontal (a) and vertical (b) slots. (Reproduced from ref 1.)

satisfy separate homogeneous wave equations corresponding to η_x^2 and η_y^2. The solutions to these equations give the following expressions for the slot fields at z = 0 propagating in the -z direction:

$$\begin{aligned} E2'_x(x,y,z) &= E2'_x(x,y,0)\ \exp(\gamma 2_x\ z) \\ H2'_y(x,y,z) &= H2'_y(x,y,0)\ \exp(\gamma 2_x\ z) \\ E2'_y(x,y,z) &= E2'_y(x,y,0)\ \exp(\gamma 2_y\ z) \\ H2'_x(x,y,z) &= H2'_x(x,y,0)\ \exp(\gamma 2_y\ z) \end{aligned} \qquad (2.14)$$

where the propagation constants are given by

$$\begin{aligned} \gamma 2_x &= j\omega\ \mu_x^2\ /\ \eta_x^2 \\ \gamma 2_y &= j\omega\ \mu_y^2\ /\ \eta_y^2\ . \end{aligned} \qquad (2.15)$$

For air-filled slots with dimensions that are small compared to the wavelength of $\overline{E1},\overline{H1}$, the slot permeabilities μ_x^2 and μ_y^2 are real and equal to the permeability of free space μ_o and the slot impedances are

$$\begin{aligned} \eta_x^2 &\cong j\omega\ L_x \\ \eta_y^2 &\cong j\omega\ L_y \end{aligned} \qquad (2.16)$$

where L_x , L_y > 0 are inductances. In this case, (2.15) reduces to $\gamma_x^2 = \mu_o\ /L_x$ and $\gamma_y^2 = \mu_o\ /L_y$. Equation (2.14) becomes

$$\begin{aligned} E2'_x(x,y,z) &= E2'_x(x,y,0)\ \exp(z\ \mu_o/L_x) \\ H2'_y(x,y,z) &= H2'_y(x,y,0)\ \exp(z\ \mu_o/L_x) \\ E2'_y(x,y,z) &= E2'_y(x,y,0)\ \exp(z\ \mu_o/L_y) \\ H2'_x(x,y,z) &= H2'_x(x,y,0)\ \exp(z\ \mu_o/L_y)\ . \end{aligned} \qquad (2.17)$$

The latter show that the slot acts like a waveguide below cutoff resulting in an exponential decay of the slot fields for $z < 0$. The rates of decay depend primarily on the dimensions of the slot α and β. As α and β decrease, L_x and L_y also decrease, and the rate of decay increases. The air-filled slot is a structure of considerable importance in shielding theory since Jarva [9] has shown that it can be used as a working model for the most common types of defects (discontinuities) that occur in practical shields

The slotted sheet like the homogeneous sheet must satisfy an additional condition involving skin depth and sheet thickness in order to insure that (2.10) is valid at the interface between M1 and the slot. Here there are two skin depths, δ_x and δ_y, which in the case of the air-filled slot can be written as follows:

$$\delta_x = L_x/\mu_o$$
$$\delta_y = L_y/\mu_o \qquad (2.19)$$

and the condition (analogous to (2.8) is

$$\frac{\delta_x}{\delta y} < d \; . \qquad (2.20)$$

This condition insures that the impedance at $z = 0$ is unaffected by reflections at $z = -d$. When (2.13) and (2.20) are satisfied, the IBC (2.10) is a valid local boundary condition at the interface between M1 and the slot, and the fields in the slot

---

[9] W. Jarva, IEEE Trans. EMC, EMC-12 (1970), 12.

traveling away from the interface are plane waves given by (2.14). If a sheet has more than one slot, then (2.10) can be applied at each slot provided the appropriate conditions are satisfied and the impedances of the slots can be determined.

2.2 Shielding by Continuous Structures Composed of Good Conductors

IBC's were developed originally to simplify external scattering and propagation problems in which the sole objective is to compute the fields in M1:

$$\overline{E1} = \overline{E1}^s + \overline{E1}^r$$
$$\overline{H1} = \overline{H1}^s + \overline{H1}^r \qquad (2.21)$$

where $\overline{E1}^s$ and $\overline{H1}^s$ are the fields generated by the source and $\overline{E1}^r$ and $\overline{H1}^r$ are the reflected and diffracted fields in M1 due to M2. In most cases, the source fields are known functions of position in M1 and the external problem reduces to that of determining the reflected and diffracted fields. An IBC applied at the interface between M1 and M2 simplifies such a problem by decoupling the fields in M1 from those in M2. This allows one to solve the external problem without the necessity of solving the internal problem for $\overline{E2}$ and $\overline{H2}$. However, in many applications, such as underground communication and electromagnetic shielding, the internal problem is of equal or greater importance than the external problem, and it is natural to ask if an IBC can be used

to simplify the problem of computing $\overline{E2}$ and $\overline{H2}$. It was shown by Monroe,[1] that an IBC can indeed be used to obtain appoximate solutions to certain internal problems by relatively simple means and that the latter lead naturally to formal solutions to a general class of shielding problems.

Monroe considers the problem of computing fields inside the generalized structure shown in figure 5 when it is illuminated by an arbitrary source S. The structure consists of flat sheets ES_1, ES_2, ...,ES_m of uniform composition and thickness d attached continuously along their edges. This structure includes both open- and closed-form shields as special cases where M2 corresponds to the shield itself and M3 is the shielded volume. By specifying the number, shape, and dimensions of the sheets, one can generate the half-space and the infinite sheet described earlier and the rectangular parallelepiped among many other useful arrangements of flat surfaces.

The composition of the sheets is assumed to fall into the class of materials referred to as good conductors, which is characterized by the relation:

$$\omega \epsilon^* << \sigma 2 \qquad (2.22)$$

where ϵ^* is the real part of the complex permittivity (2.5) and

---

[1] R. L. Monroe, A Theory of Electromagnetic Shielding with Applications to MIL-STD 285, IEEE-299, and EMP Simulation, Harry Diamond Laboratories, HDL-CR-85-052-1, Adelphi, MD (February 1985).

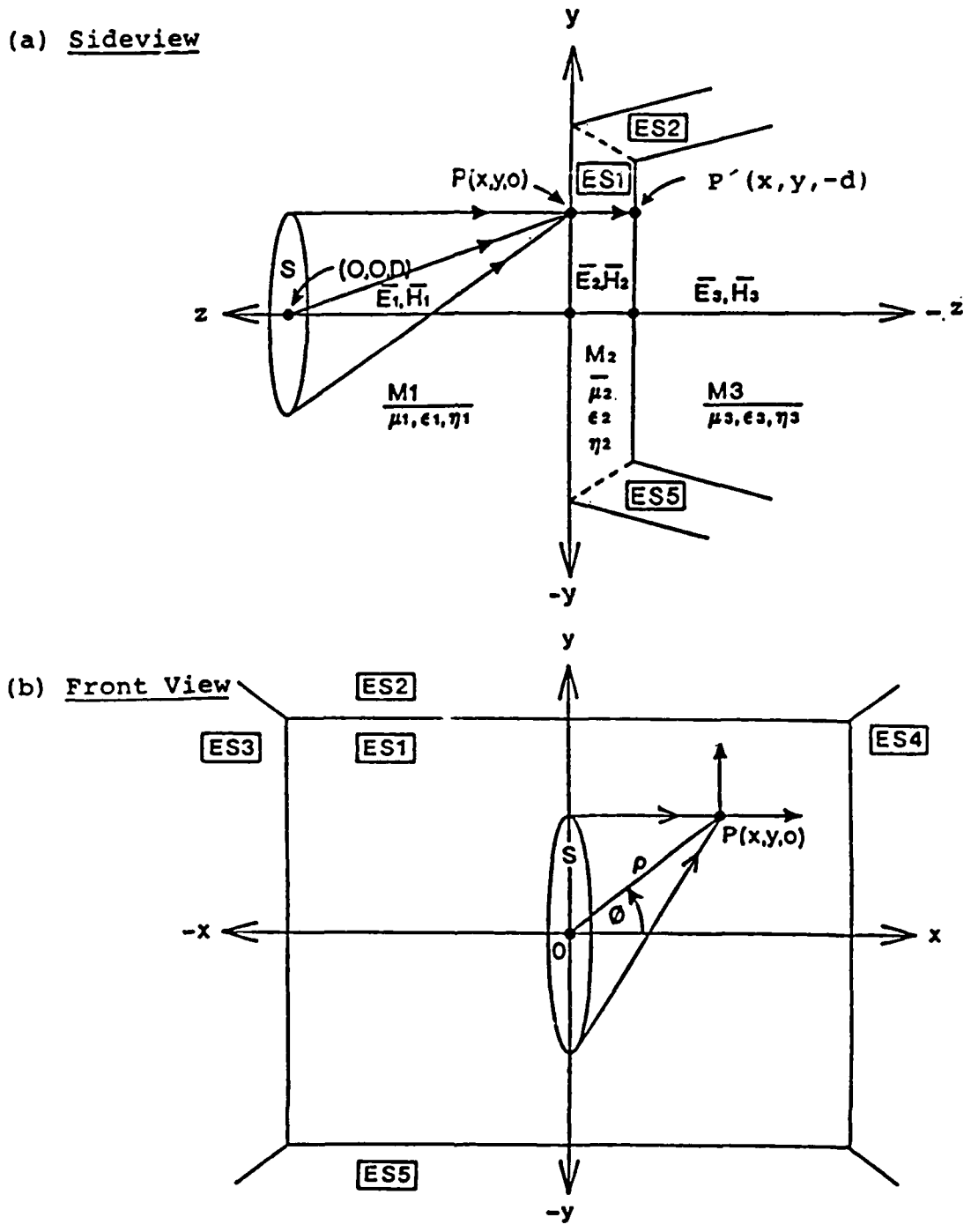

Figure 5. A generalized electromagnetic shield M2 with an arbitrary source S. (Reproduced from ref 1.)

$\sigma 2$ is the conductivity. For these materials, $\eta 2$ and $\gamma 2$ reduce to

$$\eta 2 = (j\omega\ \mu 2/\sigma 2)^{1/2} \tag{2.23}$$

$$\gamma 2 = (j\omega\ \mu 2\sigma 2)^{1/2}. \tag{2.24}$$

Since all primary materials used in shield contruction satisfy (2.22) at all frequencies of interest. and since (2.22) is consistent with (2.4), it is clear that Monroe did not impose a serious limitation on the theory by restricting it to structures composed of good conductors. On the other hand, by accepting this limitation, one is able to simplify the theory using the well-known fact[10] that the net tangential component of the magnetic field at the surface of a good conductor is approximately equal to twice the corresponding component of the incident (source) field.

The objective is to obtain formal expressions for the electric and magnetic fields transmitted into the shielded volume M3 at any point P'(x,y,-d) on the inside surface of ES_1 due to field from S incident on the outside surface of ES_1 (z = 0) where the fields are referred to a rectangular/cylindrical coordinate system that is consistent with the system used to define the IBC. The origin of this system is located on the outside surface of ES_1 and the positive z axis points away from M3. For convenience,

---

[10] R. B. Adler, L. J. Chen, and R. M. Fano, Electromagnetic Energy Transmission and Radiation, John Wiley and Sons, Inc. N.Y. (1960) p 432.

the source is located on the z axis, the origin is located at the geometrical center of ES_1, and the x and y axes are oriented parallel to the edges of ES_1 as shown in figure 5.

The transmitted fields at P'(x,y,-d) are computed in terms of the tangential components of the source magnetic field incident on ES_1 by a five-step process: In the first step, the IBC is used together with standard boundary conditions to show that the x and y components of the electric and magnetic fields at z = 0 in ES_1 can be written in terms of the corresponding components of the magnetic field in M1. That is,

$$\begin{aligned} E2_x(x,y,0) &= -\eta 2\, H1_y(x,y,0) \\ H2_y(x,y,0) &= H1_y(x,y,0) \\ E2_y(x,y,0) &= \eta 2\, H1_x(x,y,0) \\ H2_x(x,y,0) &= H1_x(x,y,0)\ . \end{aligned} \tag{2.25}$$

The second step uses the previously noted property of good conductors to write $H1_x(x,y,0)$ and $H1_y(x,y,0)$ in terms of the corresponding components of the source magnetic field:

$$\begin{aligned} H1_x(x,y,0) &\cong 2\, H1^s_x(x,y,0) \\ H1_y(x,y,0) &\cong 2\, H1^s_y(x,y,0) \end{aligned} \tag{2.26}$$

and subsitutes these expressions in (2.25) to obtain

$$\begin{aligned} E2_x(x,y,0) &= -2\,\eta 2\, H1^s_y(x,y,0) \\ H2_y(x,y,0) &= 2\, H1^s_y(x,y,0) \\ E2_y(x,y,0) &= 2\,\eta 2\, H1^s_x(x,y,0) \end{aligned} \tag{2.27}$$

$$H2_x(x,y,0) = 2\ H1^s_x(x,y,0).$$

The next step is to substitute (2.27) into (2.6) to obtain expressions for the plane wave fields in M2 traveling toward M3 in terms of the tangential components of the source magnetic field incident on ES_1:

$$\begin{aligned} E2_x(x,y,z) &= -\ 2\ \eta 2\ H1^s_y(x,y,0)\ \exp(\gamma 2\ z) \\ H2_y(x,y,z) &= \quad 2\ H1^s_y(x,y,0)\ \exp(\gamma 2\ z) \\ E2_y(x,y,z) &= \quad 2\ \eta 2\ H1^s_x(x,y,0)\ \exp(\gamma 2\ z) \\ H2_x(x,y,z) &= \quad 2\ H1^s_x(x,y,0)\ \exp(\gamma 2\ z) \end{aligned} \tag{2.28}$$

where $\eta 2$ and $\gamma 2$ are given by (2.23) and (2.24). Next, the plane wave fields incident normally on the interface between M2 and M3 are obtained by evaluating (2.28) at $z = -d$:

$$\begin{aligned} E2_x(x,y,-d) &= -\ 2\ \eta 2\ H1^s_y(x,y,0)\ \exp(-\ \gamma 2\ d) \\ H2_y(x,y,-d) &= \quad 2\ H1^s_y(x,y,0)\ \exp(-\ \gamma 2\ d) \\ E2_y(x,y,-d) &= \quad 2\ \eta 2\ H1^s_x(x,y,0)\ \exp(-\ \gamma 2\ d) \\ H2_x(x,y,-d) &= \quad 2\ \eta 2\ H1^s_x(x,y,0)\ \exp(-\ \gamma 2\ d). \end{aligned} \tag{2.29}$$

These generate reflected fields in M2 traveling in the +z direction and transmitted fields in M3 traveling in the -z direction. The final step is to compute the transmitted field at $z = -d$ from (2.29). This is done by multiplying (2.29) by appropriate plane wave trnsnsmission coefficients. The result is:

$$\begin{aligned} E3_x(x,y,-d) &= -\ 2\ \eta 2\ T_E\ H1^s_y(x,y,0)\ \exp(-\ \gamma 2\ d) \\ H3_y(x,y,-d) &= \quad 2\ T_H\ H1^s_y(x,y,0)\ \exp(-\ \gamma 2\ d) \\ E3_y(x,y,-d) &= \quad 2\ \eta 2\ T_E\ H1^s_x(x,y,0)\ \exp(-\ \gamma 2\ d) \end{aligned} \tag{2.30}$$

$$H3_x(x,y,-d) = 2\ T_H\ H1_x^s(x,y,0)\ \exp(-\gamma 2\ d)$$

where T_E and T_H are the transmission coefficients for electric and magnetic plane wave fields incident normally on a planar surface separating two dissimilar media. These coefficients are given by: [2]

$$T_E = 2\ \eta 3/(\eta 2 + \eta 3)$$
$$T_H = 2\ \eta 2/(\eta 2 + \eta 3) \qquad (2.31)$$

where $\eta 2$ is as previously defined and $\eta 3$ is the impedance at $z = -d$ looking into M3.

The preceding are formal expressions for the principal components of the electric and magnetic fields at the surface of the shielded volume ($z = -d$) for the generalized structure in figure 5. To obtain explict expressions for a particular shielding problem, it is necessary to determine the source fields $H1_x^s(x,y,0)$, $H1_y^s(x,y,0)$, and the impedance $\eta 3$. For example, if S is an antenna located a specified distance from ES_1, then $H1_x^s(x,y,0)$ and $H1_y^s(x,y,0)$ can be computed using standard methods from antenna theory. This was done in Monroe[1] for Hertzian dipoles and small rectangular loop antennas. However, if $H1_x^s(x,y,0)$ and $H1_y^s(x,y,0)$

---

[2] S. A. Schelkunoff, Electromagnetic Waves, Van Nostrand, Princeton, NJ (1943).

[1] R. L. Monroe, A Theory of Electromagnetic Shielding with Applications to MIL-STD 285, IEEE-299, and EMP Simulation, Harry Diamond Laboratories, HDL-CR-85-052-1, Adelphi, MD (February 1985).

are known functions or can be estimated from measurements, then these quantities can be used directly in (2.30), and nothing more need be specified about the source. This will be useful in many cases where the source (or sources) generating $H1^s_x(x,y,))$ and $H1^s_y(x,y,0)$ is partially or completely unknown. Examples of the latter include lightning strokes and NEMP (nuclear electromagnetic pulse). By the same token, it follows that two or more sources generating the same magnetic field components tangent to ES_1 will produce the same electric and magnetic fields in M3.

To determine $\eta 3$, it is necessary to specify the geometry of the structure. For open structures, $\eta 3$ can usually be approximated by the wave impedance of the source. This was done by Monroe for the case of an infinite flat sheet with free space on either side exposed to Hertzian dipoles. In this case, the approximation is justified by the evident fact that the structure of the field must be nearly the same on both surfaces of the sheet since M1 and M3 are both of infinite extent. However, the same is not true, in general, if M2 is closed. In this case, the structure of the fields in M3 usually has no simple relationship to that of the source field incident on ES_1. Instead, the structure of the fields in M3 is determined by the geometry of the enclosure and by its size relative to the free space wavelength of the source field. If the cross section of M3 transverse to the z axis is uniform (does not change) from z = - d to z = -L where L

denotes the surface of the sheet opposite ES_1 , then M3 is equivalent to the interior of a section of waveguide closed at both ends. In this case, $\eta 3$ will be determined by one or more of the doubly infinite set of waveguide modes that this structure can support. In Monroe,[1] the principal features of fields transmitted to the interior of a rectangular enclosure were approximated at the point z = -d using a single rectangular waveguide mode- the dominant TE_{10} mode. In section 3, this approach is extended by expanding the fields as doubly infinite series over all TE_{nm} waveguide modes and applying equations (2.29) and (2.30) to each mode at z = 0.

2.3 Shielding by Discontinuous (Slotted) Stuctures Composed of Good Conductors.

If the structure in figure 5 is modified by cutting n narrow rectangular slots through ES_1 at various locations (x_c^i, y_c^i) for i = 1,2,3,....n , where x_c^i and y_c^i are the x and y coordinates of the center of the i-th slot, then the continuous structure is transformed into one with multiple discontinuities. Using (2.10), and (2.14) and a 5 step process analogous to the one used for the

---

[1] R. L. Monroe, A Theory of Electromagnetic Shielding with Applications to MIL-STD 285, IEEE-299, and EMP Simulation, Harry Diamond Laboratories, HDL-CR-85-052-1, Adelphi, MD (February 1985).

continuous structure, Monroe obtained expressions for the fields at the center of the i-th slot incident on M3 at z = - d and the fields transmitted to M3 at the same point. These expressions were then used to describe the principal features of the fields at the center of a slot in one wall of a rectangular enclosure. A similar process yields the following expressions for the fields incident on the surface of the i-th slot at z = -d.

$$
\begin{aligned}
E2^i_x(x,y,-d) &= -\,2\,\eta^i_{2x}\,H1^s_y(x,y,0)\,fe^i_x(x,y,-d) \\
&\qquad \times \exp(-j\omega d\,\mu^i_{2x}/\eta^i_{2x}) \\
H2^i_y(x,y,-d) &= 2\,H1^s_y(x,y,0)\,fh^i_y(x,y,-d)\,\exp(-j\omega d\,\mu^i_{2x}/\eta^i_{2x}) \\
E2^i_y(x,y,-d) &= 2\,\eta^i_{2y}\,H1^s_x(x,y,0)\,fe^i_y(x,y,-d) \\
&\qquad \times \exp(-j\omega d\,\mu^i_{2y}/\eta^i_{2y}) \\
H2^i_x(x,y,-d) &= 2\,H1^s_x(x,y,0)\,fh^i_x(x,y,-d)\,\exp(-j\omega d\,\mu^i_{2y}/\eta^i_{2y})
\end{aligned}
\qquad (2.32)
$$

where all quantities are as previously defined except the form factors fe^i_x, fh^i_y, fe^i_y. and fh^i_x which describe the spatial variation of the incident electric and magnetic field components at z = - d due to the i-th slot. The fields transmitted to M3 from the i-th slot at z = -d are obtained from (2.32) by applying appropriate transmission coefficients. That is,

$$
\begin{aligned}
E3^i_x(x,y,-d) &= TE^i_x\,E2^i_x(x,y,-d) \\
H3^i_y(x,y,-d) &= TH^i_y\,H2^i_y(x,y,-d) \\
E3^i_y(x,y,-d) &= TE^i_y\,E2^i_y(x,y,-d) \\
H3^i_x(x,y,-d) &= TH^i_x\,H2^i_x(x,y,-d)
\end{aligned}
\qquad (2.33)
$$

where the transmission coefficients are given by

$$\begin{aligned} TE_x^i &= 2\,\eta 3/(\eta_x^i + \eta 3) \\ TH_y^i &= 2\,\eta_x^i/(\eta_x^i + \eta 3) \\ TE_y^i &= 2\,\eta 3/(\eta_y^i + \eta 3) \\ TH_x^i &= 2\,\eta_y^i/(\eta_y^i + \eta 3). \end{aligned} \tag{2.34}$$

These formal expressions, like the corresponding expressions for continuous structures, require that $H1_x^s(x,y,0)$, $H1_y^s(x,y,0)$, and $\eta 3$ be specified for the source and structure of interest. Since these factors are not usually affected by slots, the same values of $H1_x^s(x,y,0)$, $H1_y^s(x,y,0)$, and $\eta 3$ used for a continuous structure can also be used for a slotted enclosure of the same size and shape. However, in addition to these, the form factors $fe_x^i(x,y,-d)$, $fh_y^i(x,y,-d)$, $fe_y^i(x,y,-d)$, and $fh_x^i(x,y,-d)$ must also be specified. A precise calculation of these factors will not be attempted in this report. Instead we use approximations based on the assumption that the slot is equivalent to a waveguide with walls composed of good conductors. These points are discussed further in section 4 where the magnetic field in M3 is evaluated for a specific case.

3. MODE EXPANSIONS FOR RECTANGULAR ENCLOSURES EXPOSED TO ARBITRARY, EXTERNAL, TIME HARMONIC, ELECTROMAGNETIC FIELDS

The formal expressions in section 2 can be adapted to give the fields that penetrate a rectangular enclosure by a process analogous to the classical plane wave expansion technique where an electromagnetic field is represented as the sum of an infinite series of plane waves[11]. Since any source field can be represented in this way, plane wave expansions have often been used to simplify external problems (figure 1) by reducing the fields in M1 to the sum of the source field and a series of plane wave reflections from M2. Indeed, the same process could be applied to the shielding problem by computing the plane waves transmitted from M1 to M2. However, the impedance boundary condition makes this unnecessary since it gives the plane wave fields in M2 directly in terms of the source fields tangent to the interface between M1 and M2.

A different expansion is needed for the shielding problem: one that can be used to relate the plane wave fields incident at the M2/M3 interface (equations (2.29) and (2.32)) to the transmitted fields at that interface and to the fields in the interior of M3. Since a rectangular enclosure is equivalent to a section

---

[11] P. C. Clemmow, The Plane Wave Representation of Electromagnetic Fields, Pergamon Press, Oxford (1966).

of rectangular waveguide, the natural choice here is an expansion in terms of the mode functions for this structure. Expanding (2.29) and (2.32) into series composed of mode functions expresses each of these plane wave fields as the sum of an infinite series of plane waves each of which corresponds to a single waveguide mode. In effect, the expansions replace single plane wave fields by an infinite number of elementary fields that are both plane waves and mode functions. Each of these elementary fields is incident normally on the M2/M3 interface and each generates a reflected field in M2 traveling in the +z direction and a transmitted field in M3 traveling in the -z direction. The transmitted field at the interface can be computed in terms of the incident elementary field by using an appropriate plane wave transmission coefficient in the same manner that equations (2.30) and (2.33) were obtained from (2.29) and (2.32). Since the transmitted field at the interface is also a wavequide mode for the enclosure, it can be used to obtain the field at any point inside M3 due to the incident elementary field at the interface by representing the field in M3 by the same mode and applying boundary conditions at the walls and interface. The advantage to this approach is that the total field at any point in M3 can be obtained by summing the contributions at that point due to all the elementary fields in the original expansion. This sum is a complete solution to the shielding problem since it is the field inside M3 due to the external source.

3.1 Normal Mode Functions for an Enlosure Composed of a Good Conductor

The shell structure shown in figure 6 is the ideal version of the most common practical electromagnetic shield. It is a special case of the generalized structure (figure 5) in the form of a rectangular parallelepiped with walls composed of a good conductor as defined in section 2. The walls enclose a volume of free space (M3) with arbitrary dimensions A, B, and C. As in figure 5, we consider fields from an electromagnetic source S entering M3 through the front wall of the enclosure, that is, through the wall directly exposed to the source. (If two or more of the walls are exposed to the same source, or to a different source, then the techniques developed here can be applied to each wall in turn, and the total field at any point in M3 can be obtained by adding contributions from all the walls.) The rectangular/cylindrical coordinate system with origin at the geometric center of the outside surface of the front wall is oriented with x and y axes parallel to the edges of the wall. With the +z axis pointing outward, the inside surface of the front wall lies in the z = -d plane where d is the wall thickness, the inside surface of the back wall lies in the z = -(d + C) plane, and the outside surface of the back wall lies in the z = -(2d + C) plane. Similarly, the inside surfaces of the side walls lie in the $x = \pm A/2$ and $y = \pm B/2$ planes.

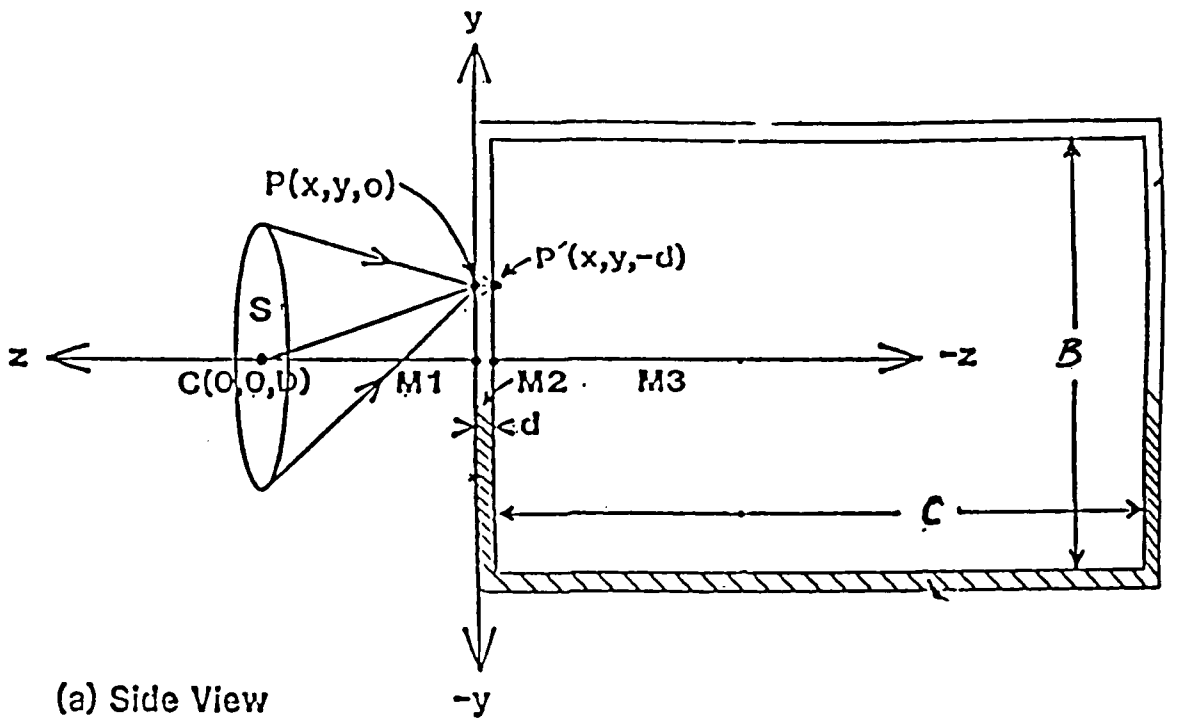

(a) Side View

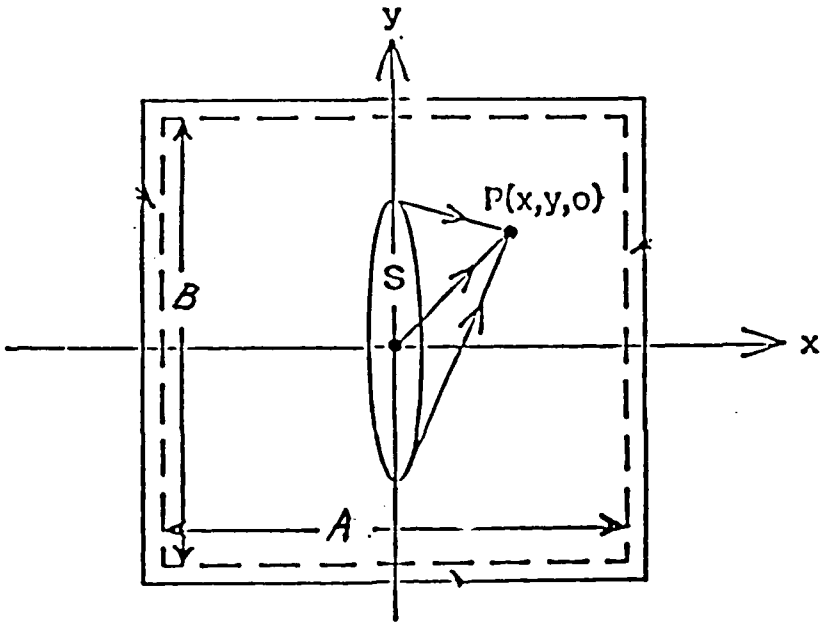

(b) Front View

Figure 6. An arbitrary source S illuminating a continuous enclosure in the form of a rectangular parallelepiped with wall thickness d and inside dimensions A, B, and C.

With this arrangement M3 is defined as follows

$$\text{M3:} \quad \begin{array}{l} -A/2 \leq x \leq A/2 \\ -B/2 \leq y \leq B/2 \\ -(d+C) \leq z \leq -d \end{array} \tag{3.1}$$

and it is seen that for fields traveling into the enclosure along paths parallel to the z axis, the M2/M3 region is a rectangular waveguide driven at $z = -d$ and loaded at $z = -(d + C)$ by a sheet with finite conductivity

The fields in M2/M3 can be represented most conveniently in terms of the normalized TE and TM mode functions[12] for the equivalent waveguide. These functions are solutions to Maxwell's equations satisfying appropriate boundary conditions at the side walls $x = \pm A/2$ and $y = \pm B/2$. The two types of modes are distinguished by the fact that TE modes have no electric field component in the z direction and TM modes have no magnetic component in the z direction. In vector form, the TE mode functions referred to the coordinate system in figure 6 are

$$\bar{e}_{nm}(x,y) = K_{nm}\left[e_x^{nm}(x,y)\ \hat{i}_x + e_y^{nm}(x,y)\ \hat{i}_y\right] \tag{3.2}$$

where $\hat{i}_x$ and $\hat{i}_y$ are unit vectors,

$$e_x^{nm}(x,y) = (m\pi/B)\cos[n\pi(x + A/2)/A]\sin[m\pi(y + B/2)/B]$$

$$e_y^{nm}(x,y) = -(n\pi/A)\sin[n\pi(x + A/2)/A]\cos[m\pi(y + B/2)/B]$$

---

[12] R. E. Collin, Field Theory of Guided Waves, McGraw-Hill, New York (1960).

$$K_{nm} = \left[(n\pi/A)^2 + (m\pi/B)^2\right]^{-1/2} [\epsilon_{on}\epsilon_{om}/AB]^{1/2} \tag{3.3}$$

ϵ_{on} and ϵ_{om} are Neuman's factor:

ϵ_{on} = 1 when n = 0

ϵ_{on} = 2 when n > 0

and all other quantities are as defined previously. These functions give the spatial structure of the electric fields associated with the TE modes. The structure of the transverse components of the magnetic fields associated with the TE modes is given by

$$\bar{h}_{nm}(x,y) = K_{nm}\left[e_y^{nm}(x,y)\ \hat{i}_x + e_x^{nm}(x,y)\ \hat{i}_y\right] \tag{3.4}$$

where all quantities are as defined previously. Similar expressions for TM modes can be obtained by simple transformations of (3.2) and (3.4).

When $\bar{e}_{nm}(x,y)$ and $\bar{h}_{nm}(x,y)$ are multiplied by factors of the form $\exp(\pm \Gamma^{nm} z)$ where Γ^{nm} is the propagation constant for the TE_{nm} mode, the products are also solutions to Maxwell's equations. That is, equations (3.5) and (3.6)

$$\begin{aligned} \bar{e}^{*}_{nm}(x,y,z) &= \bar{e}_{nm}(x,y)\ \exp(\pm \Gamma^{nm} z) \\ \bar{h}^{*}_{nm}(x,y,z) &= \bar{h}_{nm}(x,y)\ \exp(\pm \Gamma^{nm} z) \end{aligned} \tag{3.5}$$

where

$$\Gamma^{nm} = \left[(\omega_c^{nm})^2 + (j\omega)^2\right]^{1/2} (C_o)^{-1} \tag{3.6}$$

and ω_c^{nm} is the cutoff frequency

$$\omega_c^{nm} = \pi C_o \left[(n/A)^2 + (m/B)^2 \right]^{1/2} \tag{3.7}$$

are solutions to Maxwell's equations at all points in the waveguide. When the exponential carries a "+" sign, (3.5) represents TE_{nm} mode fields traveling in the -z direction; conversely, a "-" sign represents fields traveling in the +z direction. Furthermore since Maxwell's equations are linear, fields in the form

$$\begin{aligned} \overline{E3}^{nm}(x,y,z) &= \overline{E3}^{nm}(x,y)\ F_E^{nm}(z) \\ \overline{H3}^{nm}(x,y,z) &= \overline{H3}^{nm}(x,y)\ F_H^{nm}(z)\ , \end{aligned} \tag{3.8}$$

where

$$\begin{aligned} \overline{E3}^{nm}(x,y) &= \varsigma_x^{nm} e_x^{nm}(x,y)\ \hat{i}_x + \varsigma_y^{nm} e_y^{nm}(x,y)\ \hat{i}_y \\ \overline{H3}^{nm}(x,y) &= \xi_x^{nm} e_y^{nm}(x,y)\ \hat{i}_x + \xi_y^{nm} e_x^{nm}(x,y)\ \hat{i}_y \\ F_E^{nm}(z) &= C1\ \exp(+\Gamma^{nm} z) + C2\ \exp(-\Gamma^{nm} z) \\ F_H^{nm}(z) &= C3\ \exp(+\Gamma^{nm} z) + C4\ \exp(-\Gamma^{nm} z) \end{aligned} \tag{3.9}$$

and ς_x^{nm}, ς_y^{nm}, ξ_x^{nm}, ξ_y^{nm}, C1, C2, C3, and C4 are constants, are also solutions to Maxwell's equations. These expressions represent waveguide fields as sums of fields traveling in the +z and -z directions, such as would occur if fields in the waveguide were reflected between a driver and a termination. By applying appropriate boundary conditions at the locations of the driver and the termination, say z = -d and z = -(d + C), the constants in (3.9) can be computed. With $F_E^{nm}(z)$ and $F_H^{nm}(z)$ determined,

(3.8) becomes the correct form for the mode fields in a finite section of waveguide driven at z = -d and terminated at z = -d - C. That is, (3.8) becomes the correct form for the mode fields in M3.

Although a determination of $F_E^{nm}(z)$ and $F_H^{nm}(z)$ is ultimately based on applying boundary conditions at the specfied locations, we can obtain these factors directly without the lengthy calculations required in such a procedure by employing the fact that the mode functions (3.8) satisfy standard transmission line equations. This fact establishes an exact mathematical analogy between the mode functions and solutions to transmission line problems that allows us to transform the latter into the former using simple substitutions such as

$$\begin{aligned} &\overline{E3}^{nm}(x,y,z) \longrightarrow V(z) \\ &\overline{H3}^{nm}(x,y,z) \longrightarrow I(z) \\ &\gamma^{nm} \longrightarrow \gamma \\ &Z_o^{nm} \longrightarrow k \\ &\eta 2 \longrightarrow Z_1 \end{aligned} \tag{3.10}$$

where V(z) and I(z) are the voltage and current along the transmission line, γ is the propagation constant of the line, k is its characteristic impedance, Z_1 is the load impedance, Z_o^{nm} is the characteristic impedance of the TE_{nm} mode:

$$Z_o^{nm} = \frac{\eta_o \; j\omega}{\omega_c^{nm}\left[1 + \left[\frac{j\omega}{\omega_c^{nm}}\right]^2\right]^{1/2}} \tag{3.11}$$

and all other quantities are as defined previously. Since the transmission line analog to the terminated waveguide is a line driven at z = -d by voltage V(-d) and current I(-d) and terminated at z = -d - C by a load impedance Z_l, the solutions to the transmission line equations for this problem[2]:

$$V(z) = V(-d)\left[\frac{Z_l\cosh[\gamma(C+d+z)] + k\sinh[\gamma(C+d+z)]}{Z_l\cosh[\gamma C] + k\sinh[\gamma C]}\right]$$
$$I(z) = I(-d)\left[\frac{k\cosh[\gamma(C+d+z)] + Z_l\sinh[\gamma(C+d+z)]}{k\cosh[\gamma C] + Z_l\sinh[\gamma C]}\right] \qquad (3.12)$$

give the following solutions to the corresponding waveguide problem using (3.10):

$$\overline{E3}^{nm}(x,y,z) = \overline{E3}^{nm}(x,y,-d)\,F_E^{nm}(z)$$
$$\overline{H3}^{nm}(x,y,z) = \overline{H3}^{nm}(x,y,-d)\,F_H^{nm}(z) \qquad (3.13)$$

where

$$\overline{E3}^{nm}(x,y,-d) = \overline{E3}^{nm}(x,y)$$
$$\overline{H3}^{nm}(x,y,-d) = \overline{H3}^{nm}(x,y) \qquad (3.14)$$

$$F_E^{nm}(z) = \frac{\eta 2\cosh\left[\Gamma^{nm}(C+d+z)\right] + Z_o^{nm}\sinh\left[\Gamma^{nm}(C+d+z)\right]}{\eta 2\cosh[\Gamma^{nm}C] + Z_o^{nm}\sinh[\Gamma^{nm}C]}$$
$$F_H^{nm}(z) = \frac{Z_o^{nm}\cosh\left[\Gamma^{nm}(C+d+z)\right] + \eta 2\sinh\left[\Gamma^{nm}(C+d+z)\right]}{Z_o^{nm}\cosh[\Gamma^{nm}C] + \eta 2\sinh[\Gamma^{nm}C]} \qquad (3.15)$$

---

[2] S. A. Schelkunoff, Electromagnetic Waves, Van Nostrand, Princeton, NJ (1943).

and the amplitude factors ς_x^{nm}, ς_y^{nm}, ξ_x^{nm}, and ξ_y^{nm} in $\overline{H3}^{nm}(x,y)$ and $\overline{E3}^{nm}(x,y)$ are determined by the magnitude of the mode fields at z = -d. The same procedure using the well known expression for the input impedance of a loaded transmission line of length C:

$$Z_i = k \left[\frac{Z_l \cosh(\gamma C) + k \sinh(\gamma C)}{k \cosh(\gamma C) + Z_l \sinh(\gamma C)}\right] \tag{3.16}$$

gives the impedance of the TE_{nm} mode at z = -d looking into M3:

$$\eta 3^{nm} = Z_o^{nm}\left[\frac{\eta 2 \cosh(\Gamma^{nm} C) + Z_o^{nm} \sinh(\Gamma^{nm} C)}{Z_o^{nm} \cosh(\Gamma^{nm} C) + \eta 2 \sinh(\Gamma^{nm} C)}\right] \tag{3.17}$$

where all quantities are as defined previously. Both (3.13) and (3.17) will be used in the following sections to obtain the fields in M3.

Mode functions have many other properties useful in the analysis of waveguide problems. Among these is the fact that they can be used to expand arbitrary electromagnetic fields as series summed over an infinite set of discrete modes of a particular type. That is, an arbitrary electromagnetic field with no electric field component in the z direction can be represented by a series composed of TE mode functions. Similarly, an arbitrary field with no H_z component can be expressed as a series composed exclusively of TH mode functions. Since all TE and TH mode functions are trigonometric, both types of expansions will be two dimensional Fourier series over the waveguide cross section. For example, if $\bar{E}(x,y)$ is an arbitrary electric field with no z

component defined over the waveguide cross section, then it can be represented as follows;

$$\bar{E}(x,y) = \sum_{n=0}^{\infty} \sum_{m=0}^{\infty} c_{nm} \bar{e}_{nm}(x,y) \tag{3.18}$$

where the Fourier coefficients c_{nm} are

$$c_{nm} = \int_{-A/2}^{A/2} \int_{-B/2}^{B/2} \bar{E}(x,y) \cdot \bar{e}_{nm}(x,y)\, dx\, dy \,. \tag{3.19}$$

The latter can be written in terms of the x and y components of $\bar{E}(x,y)$ as follows:

$$c_{nm} = c_{nm}^{x} + c_{nm}^{y} \tag{3.20}$$

where

$$\begin{aligned} c_{nm}^{x} &= K_{nm} \int_{-A/2}^{A/2} \int_{-B/2}^{B/2} E_x(x,y)\, e_x^{nm}(x,y)\, dx\, dy \\ c_{nm}^{y} &= K_{nm} \int_{-A/2}^{A/2} \int_{-B/2}^{B/2} E_y(x,y)\, e_y^{nm}(x,y)\, dx\, dy \end{aligned} \tag{3.21}$$

and $e_x^{nm}(x,y)$ and $e_y^{nm}(x,y)$ are given by (3.3). Similarly, the transverse components of an arbitrary magnetic field can be expanded in a Fourier series using $\bar{h}^{nm}(x,y)$.

If the conductivity of the waveguide walls is finite, then TE and TH modes are coupled at the walls and an expansion of an arbitrary field in terms of either TE or TH modes alone is not possible. Thus, the preceding is not valid in the general case. However, if the walls are composed of a good conductor as assumed

here, it has been shown[12,13] that TE and TH mode expansions are valid approximations and, with one exception, the other mode characteristics are the same as those of the perfectly conducting waveguide. Thus, the characteristic impedance of the TE_{nm} mode is still given by (3.11) and the cutoff frequency by (3.7). However, the propagation constant r^{nm} is modified by the addition of an absorption term α^{nm} that depends on the conductivity of the walls. That is, (3.6) is replaced by

$$r^{nm} = \left[(\omega_c^{nm})^2 + (j\omega)^2\right]^{1/2} (C_o)^{-1} + \alpha^{nm} \tag{3.22}$$

where

$$\alpha^{nm} = \frac{2\,R}{B\,\eta_o\left[1 + (\omega_c^{nm}/j\omega)^2\right]^{1/2}} \times \left[\frac{B}{A}\left[\frac{\epsilon_{om}}{2} + (\omega_c^{nm}/i\omega)^2\right]\left[\frac{n^2AB + m^2A^2}{n^2B^2 + m^2A^2}\right] - (1 + \frac{B}{A})(\omega_c^{nm}/j\omega)^2\right] \tag{3.23}$$

$$R = [\omega\,\mu 2/(2\,\sigma 2)]^{1/2}$$

and $\mu 2$ and $\sigma 2$ are the permeability and conductivity of the waveguide walls. When $\sigma 2 \longrightarrow \infty$, $\alpha^{nm} \longrightarrow 0$, and (3.22) reduces to (3.6).

---

[12] R. E. Collin, Field Theory of Guided Waves, McGraw-Hill, New York (1960).

[13] V. M. Papadoppoulos, Quart. J. Mech. and Appl.Math., vol.7, (1954) p 325.

In the following sections, we use mode functions to represent the fields first at the M2/M3 interface and then in the remainder of M3. In M3, the mode fields take the form of (3.7) to account for reflections between the termination at z = -(d + C) z = -(d + C) and the driver (incident field) at z = -d.

3.2 Mode Expansions for Fields Inside a Continuous Enclosure Exposed to Arbitrary, Time Harmonic, External Fields.

The first step in computing the fields in M3 is to expand the fields incident at the M2/M3 interface in terms of mode functions. Since the fields in M2 are TE to a good approximation and since the dominante mode in M3 is also TE, the obvious choice for these expansions are the TE mode functions. Expanding (2.29) using (3.2), (3.3), (3.4), (3.18), and (3.21) gives;

$$
\begin{aligned}
E2_x(x,y,-d) &= -2\,\eta 2\,\exp(-\gamma 2\,d)\sum_{n=0}^{\infty}\sum_{m=1}^{\infty} c_{nm}^{x} e_x^{nm}(x,y) \\
H2_y(x,y,-d) &= \quad 2\,\exp(-\gamma 2\,d)\sum_{n=0}^{\infty}\sum_{m=1}^{\infty} c_{nm}^{x} e_x^{nm}(x,y) \\
E2_y(x,y,-d) &= \quad 2\,\eta 2\,\exp(-\gamma 2\,d)\sum_{n=1}^{\infty}\sum_{m=0}^{\infty} c_{nm}^{y} e_y^{nm}(x.y) \\
H2_x(x,y,-d) &= \quad 2\,\exp(-\gamma 2\,d)\sum_{n=1}^{\infty}\sum_{m=0}^{\infty} c_{nm}^{y} e_y^{nm}(x,y)
\end{aligned}
\qquad (3.24)
$$

where

$$c_{nm}^{x} = K_{nm}^{2} \int_{-A/2}^{A/2} \int_{-B/2}^{B/2} H1_{y}^{s}(x,y,0)\, e_{x}^{nm}(x,y)\, dx\, dy \tag{3.25}$$

$$c_{nm}^{y} = K_{nm}^{2} \int_{-A/2}^{A/2} \int_{-B/2}^{B/2} H1_{x}^{s}(x,y,0)\, e_{y}^{nm}(x,y)\, dx\, dy$$

and all other quantities are as defined previously.

In this representation, each field in (3.24) is the sum of an infinite series of plane wave fields of the form

$$\begin{aligned}
E2_{x}^{nm}(x,y,-d) &= -2\,\eta 2\, \exp(-\gamma 2\, d)\, c_{nm}^{x} e_{x}^{nm}(x,y) \\
H2_{y}^{nm}(x,y,-d) &= 2\, \exp(-\gamma 2\, d)\, c_{nm}^{x} e_{x}^{nm}(x,y) \\
E2_{y}^{nm}(x,y,-d) &= 2\,\eta 2\, \exp(-\gamma 2\, d)\, c_{nm}^{y} e_{y}^{nm}(x,y) \\
H2_{x}^{nm}(x,y,-d) &= 2\, \exp(-\gamma 2\, d)\, c_{nm}^{y} e_{y}^{nm}(x,y)
\end{aligned} \tag{3.26}$$

for $0 \leq n \leq \infty$ and $0 \leq m \leq \infty$. Each of these fields generates reflected fields in M2 traveling in the +z direction and transmitted fields in M3 traveling initially in the -z direction and later in both directions after reflections between the back and front walls. The transmitted mode fields in M3 at z = -d generated by each incident field in (3.26) are given by

$$\begin{aligned}
E3_{x}^{nm}(x,y,-d) &= E2_{x}^{nm}(x,y,-d)\, T_{E}^{nm} \\
H3_{y}^{nm}(x,y,-d) &= H2_{y}^{nm}(x,y,-d)\, T_{H}^{nm} \\
E3_{y}^{nm}(x,y,-d) &= E2_{y}^{nm}(x,y,-d)\, T_{E}^{nm} \\
H3_{x}^{nm}(x,y,-d) &= H2_{x}^{nm}(x,y,-d)\, T_{H}^{nm}
\end{aligned} \tag{3.27}$$

where T_{E}^{nm} and T_{H}^{nm} are the transmission coefficients for the elec-

tric and magnetic fields of the TE_{nm} mode

$$T_E^{nm} = 2\,\eta 3^{nm}/(\eta 2 + \eta 3^{nm})$$
$$T_H^{nm} = 2\,\eta 2/(\eta 2 + \eta 3^{nm}) \qquad (3.28)$$

$\eta 2$ is the characteristic impedance of the wall as defined previously and $\eta 3^{nm}$ is the impedance of the TE_{nm} mode at z = -d looking into M3 as given by (3.17).

With $\overline{E3}^{nm}(x,y,-d)$ and $\overline{H3}^{nm}(x,y,-d)$ given by (3.27), the mode fields at all other locations in M3 can be obtained from (3.13). In component form, the result is

$$E3_x^{nm}(x,y,z) = E3_x^{nm}(x,y,-d)\ F_E^{nm}(z)$$
$$H3_y^{nm}(x,y,z) = H3_y^{nm}(x,y,-d)\ F_H^{nm}(z)$$
$$E3_y^{nm}(x,y,z) = E3_y^{nm}(x,y,-d)\ F_E^{nm}(z) \qquad (3.29)$$
$$H3_x^{nm}(x,y,z) = H3_x^{nm}(x,y,-d)\ F_H^{nm}(z)$$

where the fields at z =-d are

$$E3_x^{nm}(x,y,-d) = \varsigma_x^{nm}\ e_x^{nm}(x,y)$$
$$H3_y^{nm}(x,y,-d) = \xi_y^{nm}\ e_x^{nm}(x,y)$$
$$E3_y^{nm}(x,y,-d) = \varsigma_y^{nm}\ e_y^{nm}(x,y) \qquad (3.30)$$
$$H3_x^{nm}(x,y,-d) = \xi_x^{nm}\ e_y^{nm}(x,y)$$

the amplitude factors are

$$\varsigma_x^{nm} = -\,2\,\eta 2\,\exp(-\gamma 2\,d)\ c_{nm}^{x}\ T_E^{nm}$$
$$\xi_y^{nm} = 2\,\exp(-\gamma 2\,d)\ c_{nm}^{x}\ T_H^{nm}$$
$$\varsigma_y^{nm} = 2\,\eta 2\,\exp(-\gamma 2\,d)\ c_{nm}^{y}\ T_E^{nm} \qquad (3.31)$$
$$\xi_x^{nm} = 2\,\exp(-\gamma 2\,d)\ c_{nm}^{y}\ T_H^{nm}$$

$F_E^{nm}(z)$ and $F_H^{nm}(z)$ are given by (3.15), and all other quantities

are as defined previously.

Since (3.29) gives the fields in M3 due to the nm-th term in the series expansion of (2.29), the total field at any point in M3 due to fields from the external source incident at the M2/M3 interface is equal to the sum of terms computed from (3.29) for all TE modes in the expansion of (2.29). That is,

$$
\begin{aligned}
E3_x(x,y,z) &= \sum_{n=0}^{\infty} \sum_{m=1}^{\infty} E3_x^{nm}(x,y,z) \\
H3_y(x,y,z) &= \sum_{n=0}^{\infty} \sum_{m=1}^{\infty} H3_y^{nm}(x,y,z) \\
E3_y(x,y,z) &= \sum_{n=1}^{\infty} \sum_{m=0}^{\infty} E3_y^{nm}(x,y,z) \\
H3_x(x,t,z) &= \sum_{n=1}^{\infty} \sum_{m=0}^{\infty} H3_x^{nm}(x,y,z) \ .
\end{aligned}
\tag{3.32}
$$

Since (3.32) satisfies both Maxwell's equations at all points in M3 and all boundary conditions at the M2/M3 interface, it represents a unique solution to the shielding problem for a continuous rectangular enclosure.

Combining (3.3), (3.6), (3.7), (3.11), (3.15), (3.17), (3.22), (3.23), (3.25), (3.28), (3.29), (3.30), and (3.31) in (3.32) gives the following result:

The fields at any point inside the rectangular enclosure shown in Figure 6 due to an arbitrary external electromagnetic source illuminating a single wall of the enclosure can be written

in terms of the tangential components of the source magnetic field, $H1^s_x(x,y,0)$ and $H1^s_y(x,y,0)$, incident on the outside surface of that wall as follows:

$$
\begin{aligned}
E3_x(x,y,z) &= -\,2\,\eta 2\,\exp(-\gamma 2\,d)\sum_{n=0}^{\infty}\sum_{m=1}^{\infty} c^x_{nm} e^{nm}_x(x,y)\; T^{nm}_E\; F^{nm}_E(z) \\
H3_y(x,y,z) &= \;\;2\,\exp(-\gamma 2\,d)\sum_{n=0}^{\infty}\sum_{m=1}^{\infty} c^x_{nm} e^{nm}_x(x,y)\; T^{nm}_H\; F^{nm}_H(z) \\
E3_y(x,y,z) &= \;\;2\,\eta 2\,\exp(-\gamma 2\,d)\sum_{n=1}^{\infty}\sum_{m=0}^{\infty} c^y_{nm} e^{nm}_y(x,y)\; T^{nm}_E\; F^{nm}_E(z) \\
H3_x(x,y,z) &= \;\;2\,\exp(-\gamma 2\,d)\sum_{n=1}^{\infty}\sum_{m=0}^{\infty} c^y_{nm} e^{nm}_y(x,y)\; T^{nm}_H\; F^{nm}_H(z)
\end{aligned}
\qquad (3.33)
$$

where

$$\eta 2 = (j\omega\,\mu 2/\sigma 2)^{1/2}$$

$$\gamma 2 = (j\omega\,\mu 2\,\sigma 2)^{1/2}$$

$$c^x_{nm} = K^2_{nm}\int_{-A/2}^{A/2}\int_{-B/2}^{B/2} H1^s_y(x,y,0)\; e^{nm}_x(x,y)\,dx\,dy$$

$$c^y_{nm} = K^2_{nm}\int_{-A/2}^{A/2}\int_{-B/2}^{B/2} H1^s_x(x,y,0)\; e^{nm}_y(x,y)\,dx\,dy$$

$$
\begin{aligned}
K_{nm} &= \left[(n\pi/A)^2 + (m\pi/B)^2\right]^{-1/2}\;[\epsilon_{on}\epsilon_{om}/(AB)]^{1/2} \\
\epsilon_{on} &= 1 \text{ when } n = 0 \\
&= 2 \text{ when } n > 0 \\
e^{nm}_x(x,y) &= (m\pi/B)\cos[n\pi(x+A/2)/A]\sin[m\pi(y+B/2)/B] \\
e^{nm}_y(x,y) &= -\,(n\pi/A)\sin[n\pi(x+A/2)/A]\cos[m\pi(y+B/2)/B] \\
T^{nm}_E &= 2\,\eta 3^{nm}/(\eta 2 + \eta 3^{nm})
\end{aligned}
\qquad (3.34)
$$

$$T_H^{nm} = 2\,\eta 2/(\eta 2 + \eta 3^{nm})$$

$$\eta 3^{nm} = Z_o^{nm}\left[\frac{\eta 2\,\cosh(\Gamma^{nm}C) + Z_o^{nm}\sinh(\Gamma^{nm}C)}{Z_o^{nm}\cosh(\Gamma^{nm}C) + \eta 2\,\sinh(\Gamma^{nm}C)}\right]$$

$$Z_o^{nm} = \frac{\eta_o\, j\omega}{\omega_c^{nm}\left[1 + \left[\frac{j\omega}{\omega_c^{nm}}\right]^2\right]^{1/2}}$$

$$\Gamma^{nm} = \left[(\omega_c^{nm})^2 + (j\omega)^2\right]^{1/2}(C_o)^{-1} + \alpha^{nm}$$

$$\omega_c^{nm} = \pi C_o\left[(n/A)^2 + (m/B)^2\right]^{1/2}$$

$$F_E^{nm}(z) = \frac{\eta 2\,\cosh[\Gamma^{nm}(C+d+z)] + Z_o^{nm}\sinh[\Gamma^{nm}(C+d+z)]}{\eta 2\,\cosh[\Gamma^{nm}C] + Z_o^{nm}\sinh[\Gamma^{nm}C]}$$

$$F_H^{nm}(z) = \frac{Z_o^{nm}\cosh[\Gamma^{nm}(C+d+z)] + \eta 2\,\sinh[\Gamma^{nm}(C+d+z)]}{Z_o^{nm}\cosh[\Gamma^{nm}C] + \eta 2\,\sinh[\Gamma^{nm}C]}$$

and all other quantities are as defined previously.

3.4 Mode Expansions for Fields Inside a Slotted Enclosure

If a rectangular slot as shown in figure 7 is cut through the front wall of the enclosure in figure 6 and the rectangular volume of the slot is filled with a material of permeability $\eta 2'$ and complex permittivity $\epsilon 2'$, then the latter is transformed from a continuous to a discontinuous enclosure, If the conductivity $\sigma 2'$ of the new material is significantly less than that of the replaced material $\sigma 2$, then the fields reaching a specified point in M3 after passing through the slot will be much

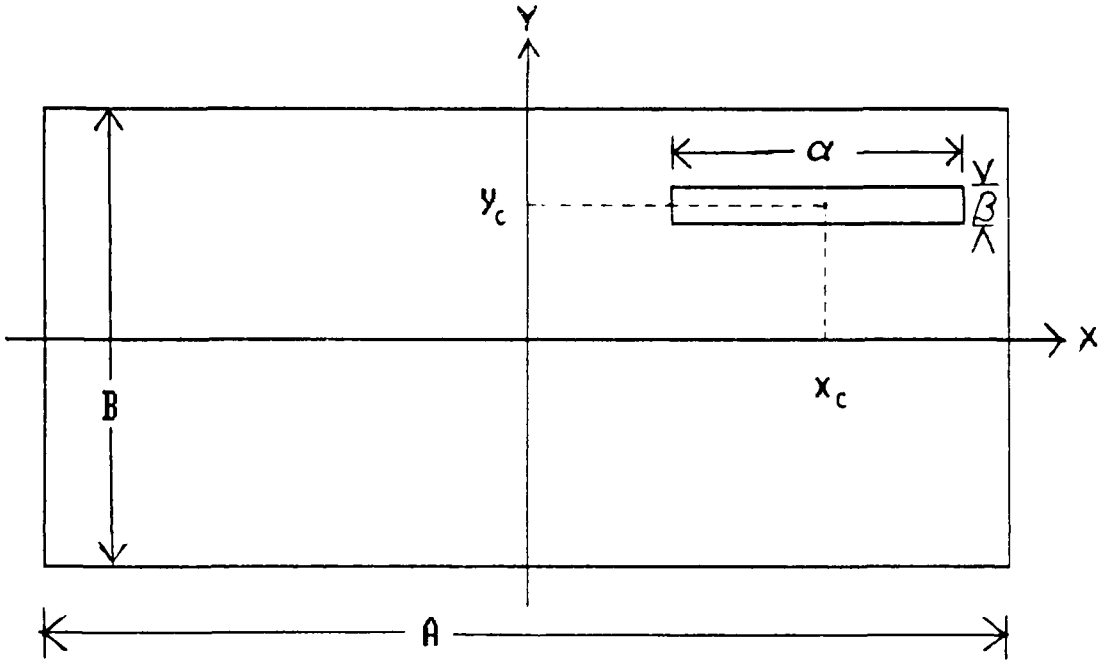

Figure 7. A rectangular slot with center coordinates x_c, y_c and dimensions α and β.

larger than the fields at the same point before the slot was cut, provided all other factors are unchanged. If the coordinates of the center of the slot (x_c, y_c) and its dimensions (α, β) are known, then the fields in M3 due to the presence of the slot can be computed in terms of the products of the tangential compnents of the source magnetic field incident at z = -d and the form factors of the slot. The method used is exactly the same as in the preceding section except that the first step is to expand the slot fields incident at z = - d (equation (2.32) rather than equation (2.29). The final result can be summarized as follows:

The fields at any point inside the rectangular enclosure shown in figure 6 due to an arbitrary electromagnetic source illuminating a rectangular slot located in the front wall of the enclosure as shown in figure 7 can be written in terms of the tangential components of the source magnetic field, $H1_x^s(x,y,0)$ and $H1_y^s(x,y,0)$, incident on the slot as follows:

$$E3_x(x,y,z) = -2\,\eta_x^2 \exp(-\gamma 2_x d) \sum_{n=0}^{\infty} \sum_{m=1}^{\infty} ce_{nm}^x e_x^{nm}(x,y)\, T_{E_x}^{nm}\, F_E^{nm}(z)$$

$$H3_y(x,y,z) = 2 \exp(-\gamma 2_x d) \sum_{n=0}^{\infty} \sum_{m=1}^{\infty} ch_{nm}^x\, e_x^{nm}(x,y)\, T_{H_x}^{nm}\, F_H^{nm}(z) \qquad (3.35)$$

$$E_y(x,y,z) = 2\,\eta_y^2 \exp(-\gamma 2_y d) \sum_{n=1}^{\infty} \sum_{m=0}^{\infty} ce_{nm}^y\, e_y^{nm}(x,y)\, T_{E_y}^{nm}\, F_E^{nm}(z)$$

$$H3_x(x,y,z) = 2 \exp(-\gamma 2_y d) \sum_{n=1}^{\infty} \sum_{m=0}^{\infty} ch_{nm}^y\, e_y^{nm}(x,y)\, T_{H_y}^{nm}\, F_H^{nm}(z)$$

where $\eta 2_x$ and $\eta 2_y$ are the slot impedances when it is driven by x directed and y directed electric fields respectively, $\gamma 2_x$ and $\gamma 2_y$ are the propagation constants of the fields in the slot

$$\gamma 2_x = j\omega \mu 2_x / \eta 2_x$$
$$\gamma 2_y = j\omega \mu 2_y / \eta 2_y \quad , \tag{3.36}$$

$\mu 2_x$ and $\mu 2_y$ are the effective permeabilities of the slot,

$$ce_{nm}^x = K_{nm}^2 \int_{-B/2}^{B/2} \int_{-A/2}^{A/2} H1_y^s(x,y)\ fe_x(x,y,-d)\ e_x^{nm}(x,y)\ dx\ dy$$

$$ch_{nm}^x = K_{nm}^2 \int_{-B/2}^{B/2} \int_{-A/2}^{A/2} H1_y^s(x,y)\ fh_y(x,y,-d)\ e_x^{nm}(x,y)\ dx\ dy$$

$$ce_{nm}^y = K_{nm}^2 \int_{-B/2}^{B/2} \int_{-A/2}^{A/2} H1_x^s(x,y)\ fe_y(x,y,-d)\ e_y^{nm}(x,y)\ dx\ dy \tag{3.37}$$

$$ch_{nm}^y = K_{nm}^2 \int_{-B/2}^{B/2} \int_{-A/2}^{A/2} H1_x^s(x,y)\ fh_x(x,y,-d)\ e_y^{nm}(x,y)\ dx\ dy \quad ,$$

$fe_x(x,y,-d)$, $fh_y(x,y,-d)$, $fe_y(x,y,-d)$, and $fh_x(x,y)$ are form factors as defined in section 2.3,

$$T_{E_x}^{nm} = 2\ \eta 3^{nm} / (\eta 2_x + \eta 3^{nm})$$
$$T_{H_x}^{nm} = 2\ \eta 2_x / (\eta 2_x + \eta 3^{nm})$$
$$T_{E_y}^{nm} = 2\ \eta 3^{nm} / (\eta 2_y + \eta 3^{nm}) \tag{3.38}$$
$$T_{H_y}^{nm} = 2\ \eta 2_y / (\eta 2_y + \eta 3^{nm}) \quad ,$$

and all other quantities are as defined in the preceding section.

If there are two or more slots on the front face with known dimensions and locations and if the impedances, permeabilities, and form factors of these slots can be estimated, then the fields at a given location in M3 due to these slots can be obtained by using the preceding expressions to compute the fields from each slot and then adding the contributions from all slots at that location.

4. FIELDS INSIDE ENCLOSURES EXPOSED TO SPATIALLY UNIFORM EXTERNAL FIELDS GENERATED BY TIME HARMONIC SOURCES

In this section, the general expressions for the fields inside continuous and slotted enclosures are evaluated for the two simplest cases of interest: a continuous enclosure exposed to uniform fields over its front surface, and a slotted enclosure exposed to uniform fields over the area of the slot. These cases can be described more precisely as follows:

$$H1_x^s(x,y,0) \cong H1_x^s(j\omega)$$
$$H1_y^s(x,y,0) \cong H1_y^s(j\omega) \qquad (4.1)$$

over the following areas:

Continuous Enclosure (fig. 6)

$$-A/2 \leq x \leq A/2$$
$$-B/2 \leq y \leq B/2 \qquad (4.2)$$
$$z = 0$$

Slotted Enclosure (fig. 6 and 7)

$$x_c - \alpha/2 \leq x \leq x_c + \alpha/2$$
$$y_c - \beta/2 \leq y \leq y_c + \beta/2 \qquad (4.3)$$
$$z = 0$$

where $H1_x^s(j\omega)$ and $H1_y^s(j\omega)$ are functions of the frequency ω but not of the spatial variables x and y.

These cases occur typically when the source is located far from the enclosure or when the characteristic dimension of the source is larger than that of the enclosure and also larger than

the separation distance. However, they can also occur in less obvious situations. For example, it was shown by Monroe[1] that a small square loop antenna 10.6 in. on a side operating at 10^6 Hz can produce a nearly uniform magnetic field over a significant plane area oriented perpendicular to the plane of the antenna and located 1 m from its center. Furthermore, since the dimensions of most slots are much smaller than than those of the enclosure, it is clear that (4.1) will be satisfied in many cases for slotted enclosures (4.3) when it would not satsfied for continuous enclosures (4.2) of the same size exposed to the same source. Thus, (4.1), (4.2), and (4.3) can describe many situations of practical importance.

4.1 Continuous Enclosure

If $H1_x^s$ satisfies (4.1), then $E3_y(x,y,z)$ and $H3_x(x,y,z)$ must be independent of x or y or both x and y. But it is clear from (3.33) and (3.34) that in order for $E3_y$ and $H3_x$ to be independent of x alone or both x and y it is necessary that n = 0, which implies $E3_y = H3_x \equiv 0$. The latter is, of course, the trivial solution that will only occur when $H1_x^s = 0$. Consequently, a nontrivial solution requires $E3_y$ and $H3_x$ to be independent of

---

[1] R. L. Monroe, A Theory of Electromagnetic Shielding with Applications to MIL-STD 285, IEEE-299, and EMP Simulation, Harry Diamond Laboratories, HDL-CR-85-052-1, Adelphi, MD (February 1985).

y. This implies m = 0. Thus, the solution in this case is obtained by setting m = 0 in the expressions for $E3_y$ and $H3_x$ in (3.33).

Similar considerations show that when $H1_y^s$ satisfies (4.1) the fields $E3_x$ and $H3_y$ are independent of x and the appropriate expressions for these quantities are obtained by setting n = 0 in (3.33).

With these substitutions, (3.33) and (3.34) become

$$
\begin{aligned}
E3_x(y,z) &= -\,2\,\eta 2\,\exp(-\gamma 2\,d)\,H1_y^s(j\omega)\sum_{m=1}^{\infty} c_{0m}^x e_x^{0m}(y)\,T_E^{0m}\,F_E^{0m}(z)\\
H3_y(y,z) &= \quad 2\,\exp(-\gamma 2\,d)\,H1_y^s(j\omega)\sum_{m=1}^{\infty} c_{0m}^x e_x^{0m}(y)\,T_H^{0m}\,F_H^{0m}(z)\\
E3_y(x,z) &= \quad 2\,\eta 2\,\exp(-\gamma 2\,d)\,H1_x^s(j\omega)\sum_{n=1}^{\infty} c_{n0}^y e_y^{n0}(x)\,T_E^{n0}F_E^{n0}(z)\\
H3_x(x,z) &= \quad 2\,\exp(-\gamma 2\,d)\,H1_x^s(j\omega)\sum_{n=1}^{\infty} c_{n0}^y e_y^{n0}(x)\,T_H^{n0}\,F_H^{n0}(z)
\end{aligned}
\tag{4.4}
$$

where

$$
\begin{aligned}
c_{0m}^x &= (2/B)\int_{-B/2}^{B/2}\sin[m\pi(y+B/2)/B]\,dy\\
c_{n0}^y &= (2/A)\int_{-A/2}^{A/2}\sin[n\pi(x+A/2)/A]\,dx\\
e_x^{0m}(y) &= \sin[m\pi(y+B/2)/B]\\
e_y^{n0}(x) &= \sin[n\pi(x+A/2)/A]
\end{aligned}
\tag{4.5}
$$

and all other quantities are either as previously defined or are

obtained from previously defined quantities by setting either n or m equal to zero; e.g., $T_E^{0m} = T_E^{nm}\Big|_{n=0}$ and $F_H^{n0} = F_H^{nm}\Big|_{m=0}$.

Carrying out the indicated integrations and redefining T_E^{0n}, T_E^{m0}, T_H^{0m}, T_H^{n0}, $F_E^{0m}(z)$, etc, we obtain the following result:

The fields at any point inside the rectangular enclosure shown in figure 6 due to an external electromagnetic source that generates spatially uniform fields on one wall of the enclosure can be written in terms of the tangential components of the source magnetic field, $H1_x^s(j\omega)$ and $H1_y^s(j\omega)$, incident on the outside surface of that wall as follows:

$$E3_x(y,z) = -\,2\,\eta 2\,\exp(-\gamma 2\,d)\,H1_y^s(j\omega)\sum_{m=1}^{\infty} c_m^x\,e_x^m(y)\,T_E^m\,F_E^m(z)$$

$$H3_y(y,z) = \quad 2\,\exp(-\gamma 2\,d)\,H1_y^s(j\omega)\sum_{m=1}^{\infty} c_m^x\,e_x^m(y)\,T_H^m\,F_H^m(z)$$

$$E3_y(x,z) = \quad 2\,\eta 2\,\exp(-\gamma 2\,d)\,H1_x^s(j\omega)\sum_{n=1}^{\infty} c_n^y\,e_y^n(x)\,T_E^n\,F_E^n(z) \qquad (4,6)$$

$$H3_x(x,z) = \quad 2\,\exp(-\gamma 2\,d)\,H1_x^s(j\omega)\sum_{n=1}^{\infty} c_n^y\,e_y^n(x)\,T_H^n\,F_H^n(z)$$

where $\eta 2$ and $\gamma 2$ are given in (3.4),

$$c_m^x = -\,2\left[\frac{\cos(m\pi) - 1}{m\pi}\right]$$

$$c_n^y = -\,2\left[\frac{\cos(n\pi) - 1}{n\pi}\right]$$

$$e_x^m(y) = \sin[m\pi(y+B/2)/B]$$

$$e_y^n(x) = \sin[n\pi(x+A/2)/A]$$

$$T_E^m = T_E^{nm}\Big|_{n=0} = 2\,\eta 3^m/(\eta 2 + \eta 3^m)$$

$$T_H^m = T_H^{nm}\Big|_{n=0} = 2\,\eta 2/(\eta 2 + \eta 3^m)$$
$$T_E^n = T_E^{nm}\Big|_{m=0} = 2\,\eta 3^n(\eta 2 + \eta 3^n)$$
$$T_H^n = T_H^{nm}\Big|_{m=0} = 2\,\eta 2/(\eta 2 + \eta 3^n)$$

$$\eta 3^m = \eta 3^{nm}\Big|_{n=0} = Z_o^m\left[\frac{\eta 2\,\cosh(r^m C) + Z_o^m\,\sinh(r^m C)}{Z_o^m\,\cosh(r^m C) + \eta 2\,\sinh(r^m C)}\right]$$
$$\eta 3^n = \eta 3^{nm}\Big|_{m=0} = Z_o^n\left[\frac{\eta 2\,\cosh(r^n C) + Z_o^n\,\sinh(r^n C)}{Z_o^n\,\cosh(r^n C) + \eta 2\,\sinh(r^n C)}\right]$$

$$Z_o^m = Z_o^{nm}\Big|_{n=0} = \frac{\eta_o\ j\omega}{\omega_c^m\left[\ 1 + \left[\frac{j\omega}{\omega_c^m}\right]^2\ \right]^{1/2}}$$
$$Z_o^n = Z_o^{nm}\Big|_{m=0} = \frac{\eta_0\ j\omega}{\omega_c^n\left[\ 1 + \left[\frac{j\omega}{\omega_c^n}\right]^2\ \right]^{1/2}}$$
$$r^m = r^{nm}\Big|_{n=0} = \left[(\omega_c^m)^2 + (j\omega)^2\right]^{1/2}(C_o)^{-1} + \alpha^m$$
$$r^n = r^{nm}\Big|_{m=0} = \left[(\omega_c^n)^2 + (j\omega)^2\right]^{1/2}(C_o)^{-1} + \alpha^n$$
$$\omega_c^m = \omega_c^{nm}\Big|_{n=0} = \pi C_o m/B$$
$$\omega_c^n = \omega_c^{nm}\Big|_{m=0} = \pi C_o n/A$$
$$\alpha^m = \alpha^{nm}\Big|_{n=0}$$
$$\alpha^n = \alpha^{nm}\Big|_{m=0}$$
$$F_E^m = F_E^{nm}\Big|_{n=0}$$
$$F_H^m = F_H^{nm}\Big|_{n=0}$$
$$F_E^n = F_E^{nm}\Big|_{m=0}$$
$$F_H^n = F_H^{nm}\Big|_{m=0}$$

α^{nm} is given by (3.23) and F_E^{nm} and F_H^{nm} are given by (3.15).

While the expressions in (4.6) remain moderately complicated in spite of the simplification afforded by our assumption of spatially uniform incident fields, these expressions are readily ammenable to evaluation by computer. Calculations based on (4.6) indicate that the series converge rapidly and fewer than 10 terms are required to reduce the error below 10% at most locations in the enclosure. In general, more terms are required at locations close to the side walls than near the center line (x = y = 0) where five terms will usually suffice for 10 % accuracy. Figures 8 and 9 are computer plots of the magnitude of $H3_y(y,z)$ versus frequency $f = \omega/2\pi$ at locations close to the center of the front wall (x = y = 0, z = -0.05 m), close to the center of the back wall (x = y = 0, z = -6.05 m), at the geometrical center of the enclosure (x = y = 0, z = -3.05 m), and near the center of the top wall (x = 0, y = 1.75 m) where the enclosure parameters are:

$A = 6.1$ m, $B = 3.66$ m, $C = 6.1$ m, $d = 3.8 \times 10^{-4}$ m,

$\sigma 2 = 4.33 \times 10^{6}$ mhos/m, $\mu 2 = 12.6 \times 10^{-7}$ h/m,

and the source magnetic field is harmonic with unit magnitude:

$H1_y^s(j\omega) = 1.0 \exp(j\omega t) = 1.0 \exp(j2\pi ft)$ (A/m) .

These figures show that the general trend at all locations is an ever more rapidly decreasing magnitude with increasing frequency reflecting a change from a $f^{-1/2}$ variation to f^{-1}, and from f^{-1} to $\exp(-kf^{1/2})$. Superimposed on this trend at frequencies above

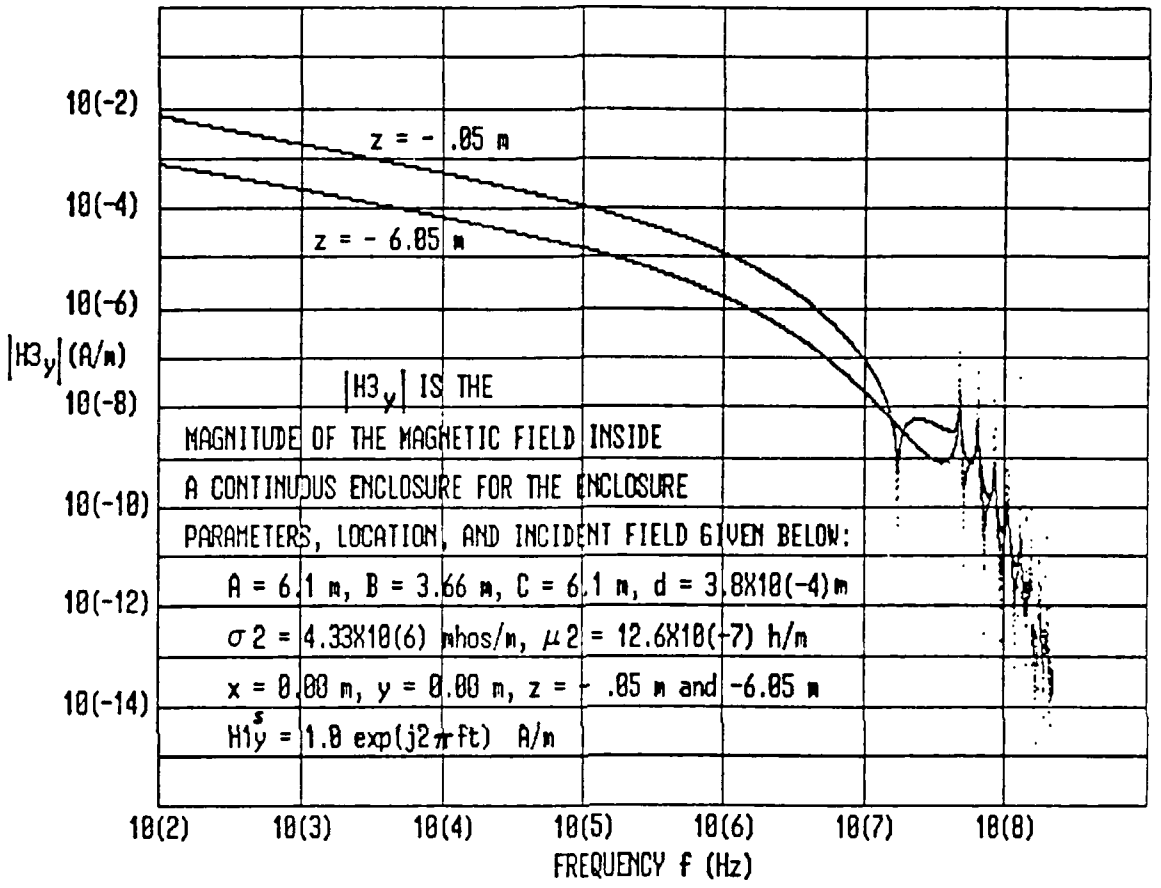

Figure 8. Magnitude of the magnetic field inside a continuous enclosure versus frequency at locations near the center of the front (z=-.05 m) and back walls (z=-6.05 m).

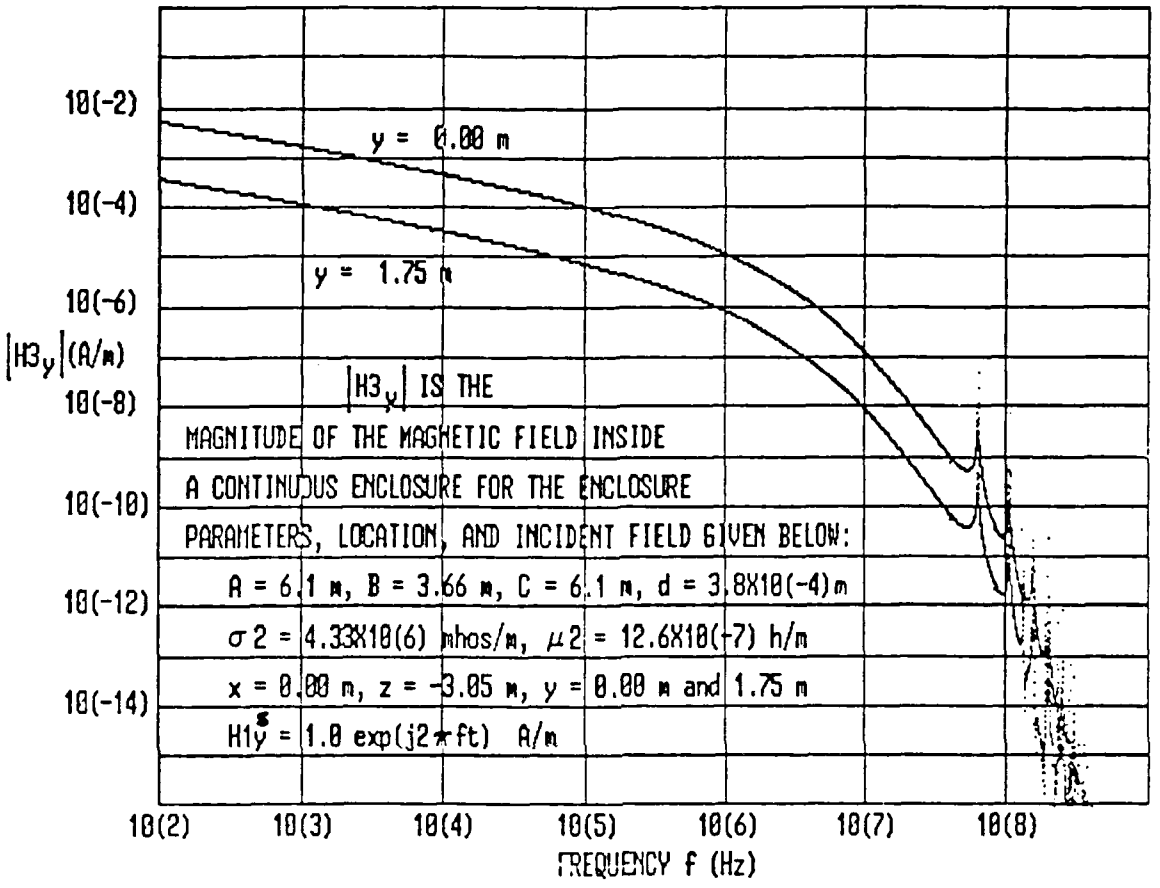

Figure 9. Magnitude of the magnetic field inside a continuous enclosure versus frequency at a location near the center of a side wall (y=1.75 m) and at the center of the enclosure (y=0.0 m).

10^7 Hz are much more rapid variations corresponding to the resonant and antiresonant frequencies of the enclosure. Noteworthy among the latter is the pronounced antiresonance at $f \cong 2 \times 10^7$ Hz seen near the center of the front wall ($x = y = 0$, $z = -0.05$ m) but nowhere else. Figure 8 indicates a spatial variation of just under one order of magnitude between the front and back walls, and figure 9 shows a variation of just over one order of magnitude between the center of the enclosure and a point ($x = 0$, $y = 1.75$ m, $z = -3.05$ m) 0.08 m from the center of the side wall. The former is a reflection of the hyperbolic variation of the internal field with z, and the latter is a reflection of the sinusoidal variation of the internal field with y satisfying the boundary condition $H3_y = 0$ at $y = +1.83$ m.

4.2 Enclosure with an Inductive Slot

If the material filling the slot in figure 7 is free space and the dimensions of the slot are small compared to the wavelength λ of the fields in M1, then the permeability of the slot is equal to the permeability of free space μ_o and the slot impedances are pure inductances. That is, for air-filled slots where

$$\alpha \text{ and } \beta \ll \lambda \tag{4.7}$$

the slot permeabilities are given by

$$\mu_x^2 = \mu_y^2 = \mu_o \tag{4.8}$$

and the slot impedances are

$$\eta 2_x = j\omega L_x$$
$$\eta 2_y = j\omega L_y \qquad (4.9)$$

where L_x is the inductance of the slot when driven by an electric field in the x direction and L_y is the inductance of the slot when driven by an electric field in the y direction. The propagation constants for the fields in the slot are derived from (4.8) and (4.9) as follows:

$$\gamma 2_x = j\omega\, \mu 2_x/\eta 2_x = \mu_o/L_x$$
$$\gamma 2_y = j\omega\, \mu 2_y/\eta 2_y = \mu_o/L_y \quad . \qquad (4.10)$$

Thus, the general expressions for the fields inside a slotted enclosure can be specialized to the case of an inductive slot by substituting (4.9) and (4.10) into (3.35).

If the dimensions α and β satisfy the relation $\beta << \alpha$, then figure 7 describes a narrow rectangular slot with its long axis parallel to the x axis For this "horizontal" air-filled slot, the inductances satisfy the relation $L_x << L_y$, and similarly

$$\eta 2_x << \eta 2_y$$
$$\gamma 2_y << \gamma 2_x \qquad (4.11)$$

by virtue of (4.9) and (4.10). Applying (4.11) to (3.35) gives

$$|E3_x| << |E3_y|$$
$$|H3_y| << |H3_x| \qquad (4.12)$$

provided $|H1^s_x| \cong |H1^s_y|$. That is, $E3_y$ and $H3_x$ are the dominant field components inside an enclosure with a narrow horizontal

slot provided $|H1_y^s|$ is not very much larger than $|H1_x^s|$.

Similarly, if the slot dimensions satisfy $\alpha << \beta$, then figure 7 describes a narrow vertical slot with its long axis parallel to the y axis. In this case, the slot inductances satisfy $L_y << L_x$ and (4.11) becomes

$$\eta_y^2 << \eta_x^2$$
$$\gamma 2_x << \gamma 2_y \ . \tag{4.13}$$

The dominant fields inside the enclosure are now $E3_x$ and $H3_y$. That is,

$$|E3_y| << |E3_x|$$
$$|H3_x| << |H3_y| \tag{4.14}$$

provided $|H1_x^s| \cong |H1_y^s|$.

The preceding shows that, in general, the fields inside an enclosure with a single narrow, air-filled, horizontal or vertical slot will be dominated by a single electric field component and a single magnetic field component and that the remaining components will be negligible by comparison. In the following, we consider the horizontal slot and obtain explicit expressions for $E3_y$ and $H3_x$. The reader will then be able to transform these into the corresponding expressions for $E3_x$ and $H3_y$ inside an enclosure with a vertical slot.

Substituting for η_y^2 from (4.9) and for $\gamma 2_y$ from (4.10) into (3.35) and separating the m = 0 terms in the sum, we obtain

$$E3_y(x,y,z) = 2j\omega L_y \exp(-\mu_o d/L_y)\left[\sum_{n=1}^{\infty} ce_n^y \; e_y^n(x) \; T_E^n \; F_E^n(z) + \sum_{n=1}^{\infty}\sum_{m=1}^{\infty} ce_{nm}^y \; e_y^{nm}(x,y) \; T_{E_y}^{nm} \; F_E^{nm}(z) \right]$$

$$H3_x(x,y,z) = 2 \exp(-\mu_o d/L_y)\left[\sum_{n=1}^{\infty} ch_n^y \; e_y^n(x) \; T_{H_y}^n F_H^n(z) + \sum_{n=1}^{\infty}\sum_{m=1}^{\infty} ch_{nm}^y \; e_y^{nm}(x,y) \; T_{H_y}^{nm} \; F_H^{nm}(z) \right] \qquad (4.15)$$

where

$$ce_{nm}^y = K_{nm}^2 \; H1_x^s(j\omega) \int_{-B/2}^{B/2}\int_{-A/2}^{A/2} fe_y(x,y,-d) \; e_y^{nm}(x,y) \; dx \; dy$$

$$ch_{nm}^y = K_{nm}^2 \; H1_x^s(j\omega) \int_{-B/2}^{B/2}\int_{-A/2}^{A/2} fh_y(x,y,-d) \; e_y^{nm}(x,y) \; dx \; dy$$

$$e_y^{nm}(x,y) = -(n\pi//A) \sin[n\pi(x+A/2)/A] \cos[m\pi(y+B/2)/B]$$

$$T_{E_y}^{nm} = 2 \; \eta 3^{nm}/(j\omega L_y + \eta 3^{nm}) \qquad (4.16)$$

$$T_{H_y}^{nm} = 2 \; j\omega L_y/(j\omega L_y + \eta 3^{nm})$$

$$ce_n^y = ce_{nm}^y\Big|_{m=0}$$

$$ch_n^y = ch_{nm}^y\Big|_{m=0}$$

$$e_y^n(x) = e_y^{nm}(x,y)\Big|_{m=0}$$

$$K_{n0} = K_{nm}\Big|_{m=0}$$

and all other quantities are defined in section 3.

To determine $E3_y$ and $H3_x$ from the preceding expressions, it is necessary first to specify the form factors $fe_y(x,y,-d)$ and

$fh_y(x,y,-d)$ which describe the spatial variation of the incident fields at $z = -d$ for $-A/2 \leq x \leq A/2$ and $-B/2 \leq y \leq B/2$ and then to use these factors to evaluate the Fourier coefficients ce^y_{nm} and ch^y_{nm} by carrying out the indicated integrations. However, exact expressions for fe_y and fh_y are unknown, and therefore in order to proceed, we must resort to approximations. In making these approximations, we will be guided by the fact that the incident fields at $z = -d$ are determined by the fields inside the slot $(x_c - \alpha/2 \leq x \leq x_c + \alpha/2,\ y_c - \beta/2 \leq y \leq y_c + \beta/2)$ and by the boundary conditions over the remainder of the $z = -d$ surface. Since the slot, like the enclosure, is equivalent to a section of rectangular wavegude where TE fields dominate, it follows from the results quoted in section 3 that the spatial variation of the slot fields can be written as sums using TE mode functions appropriate to the slot. That is,

$$e2_y(x,y) = \sum_{s=1}^{\infty} \sum_{r=0}^{\infty} \chi^y_{sr}\, \kappa^{sr}_y(x,y)$$
$$h2_x(x,y) = \sum_{s=1}^{\infty} \sum_{r=0}^{\infty} \Psi^y_{sr}\, \kappa^{sr}_y(x,y) \qquad (4.17)$$

where χ^y_{sr} and Ψ^y_{sr} are the Fourier coefficients of the expansion and

$$\kappa^{sr}_y(x,y) = \nu \sin[s\pi(x-x_c+\alpha/2)/\alpha] \cos[r\pi(y-y_c+\beta/2)/\beta] \qquad (4.18)$$

with

$$\nu = -\pi s/\alpha\ .$$

However, there are no propagating modes in this expansion due to

our assumption that the dimensions of the slot are small compared to the wavelength of the source field, and consequently the field in the slot will be determined by relatively few low-order TE modes with the TE_{10} mode playing a dominant role. Thus, a first order approximation to the structure of the fields in the slot can be obtained from (4.17):

$$e2_y(x,y) = h2_x(x,y) \cong \kappa_y^{10}(x,y)$$
$$= \sin[\pi(x-x_c+a/2)/a] \ . \qquad (4.19)$$

Of course, this is just equivalent to approximating $e2_y$ and $h2_x$ by the first terms in their mode expansions. It implies that the fields in the slot have the structure of a half-sine wave in the x direction and are uniform in the y direction. This appears to be a reasonable assumption for the fields in a narrow slot excited by a uniform external field. Thus the structure of the incident field at z = -d can be approximated by combining the structure of the slot field from (4.19) with continuous extensions of the incident slot field from the slot to the remainder of the z = -d plane. In the case of the electric field, there are no continuous extensions beyond the vicinity of the slot since the remainder of the z = -d plane is composed of a good conductor. Thus, fe_y can be approximated by

$$fe_y(x,y,-d) = p(x)\ q_e(y) \qquad (4.20)$$

where

$$p(x) = \begin{cases} \sin[\pi(x - x_c + a/2)/a] & \text{for } x_c - a/2 \le x \le x_c + a/2 \\ 0 \quad \text{for } -A/2 \le x \le x_c - a/2 \text{ and } x_c + a/2 \le x \le A/2 \end{cases}$$

$$q_e(y) = \begin{cases} 1 & \text{for } y_c - \beta/2 \le y \le y_c + \beta/2 \\ 0 & \text{for } -B/2 \le y < y_c - \beta/2 \text{ and } y_c + \beta/2 < y \le B/2 \end{cases}$$

In the case of the magnetic field, there are continuous extensions of the incident field beyond the slot in the $\pm y$ directions since the slot field at $(x, \pm\beta/2, -d)$ will drive currents in these directions on the z = -d plane. These currents will be reflected at the side walls with a reflection coefficient of nearly +1 resulting in an increase in $H2_x(x,y,-d)$ in the vicinity of $y = \pm B/2$. A precise determination of $fh_y(x,y,-d)$ would model the z = -d plane in the y direction as an asymmetrically driven transmission line with appropriate loads at $y = \pm B/2$. Here, however, we will approximate fh_y analytically as follows:

$$fh_y(x,y,-d) = p(x)\, q_h(y) \tag{4.21}$$

where p(x) is the same sinusoidal function used in (4.19), $q_h(y)$ is defined by

$$q_h(y) = \begin{cases} s_1 y + q_1 & \text{for } -B/2 \le y < y_c - \beta/2 \\ 1 & \text{for } y_c - \beta/2 \le y \le y_c + \beta/2 \\ s_2 y + q_2 & \text{for } y_c + \beta/2 < y \le B/2 \end{cases} \tag{4.22}$$

and

$$\begin{aligned} s_1 &= -1/(y_c - \beta/2 + B/2) \\ s_2 &= -1/(y_c + \beta/2 - B/2) \\ q_1 &= 1 + (y_c - \beta/2)/(y_c - \beta/2 + B/2) \\ q_2 &= 1 + (y_c + \beta/2)/(y_c + \beta/2 - B/2) \end{aligned} \tag{4.23}$$

Figure 10 shows plots of $p(x)$ and $q_h(y)$ for A = 10, B = 8, α = 6, β =0 .5, x_c = +1 and y_c = -2 where the units are arbitrary.

When (4.20) and (4.21) are substituted into (4.16), the integrals can be evaluated in closed form to give explicit expressions for the Fourier coefficients ce_{nm}^{y} and ch_{nm}^{y}. These can then be combined with (4.15) in the following statement:

The principal components of the field at any point inside the enclosure shown in figure 6 due to a uniform electromagnetic source illuminating a narrow, horizontal, air-filled slot with center coordinates x_c and y_c and dimensions α and β, as shown in figure 7, can written in terms of the horizontal component of the source magnetic field $H1_x^s(j\omega)$ incident on the slot as follows:

$$E3_y(x,y,z) = 2j\omega L_y \exp(-\mu_o d/L_y)\left[\sum_{n=1}^{\infty} ce_n^y \; e_y^n(x) \; T_{E_y}^n \; F_E^n(z) \sum_{n=1}^{\infty}\sum_{m=1}^{\infty} ce_{nm}^y \; e_y^{nm}(x,y) \; T_{E_y}^{nm} \; F_E^{nm}(z)\right]$$

$$H3_x(x,y,z) = 2 \exp(-\mu_o d/L_y)\left[\sum_{n=1}^{\infty} ch_n^y \; e_y^n(x) \; T_{H_y}^n \; F_H^n(z) \sum_{n=1}^{\infty}\sum_{m=1}^{\infty} ch_{nm}^y \; e_y^{nm}(x,y) \; T_{H_y}^{nm} \; F_H^{nm}(z)\right] \quad (4.24)$$

where L_y is the slot inductance when driven by a y-directed electric field

$$ce_n^y = - H1_x^s(j\omega) \; \beta \; P_n \; K_n^2 \; n\pi/A$$
$$ch_n^y = - H1_x^s(j\omega) \; Q_o \; P_n \; K_n^2 \; n\pi/A \quad (4.25)$$

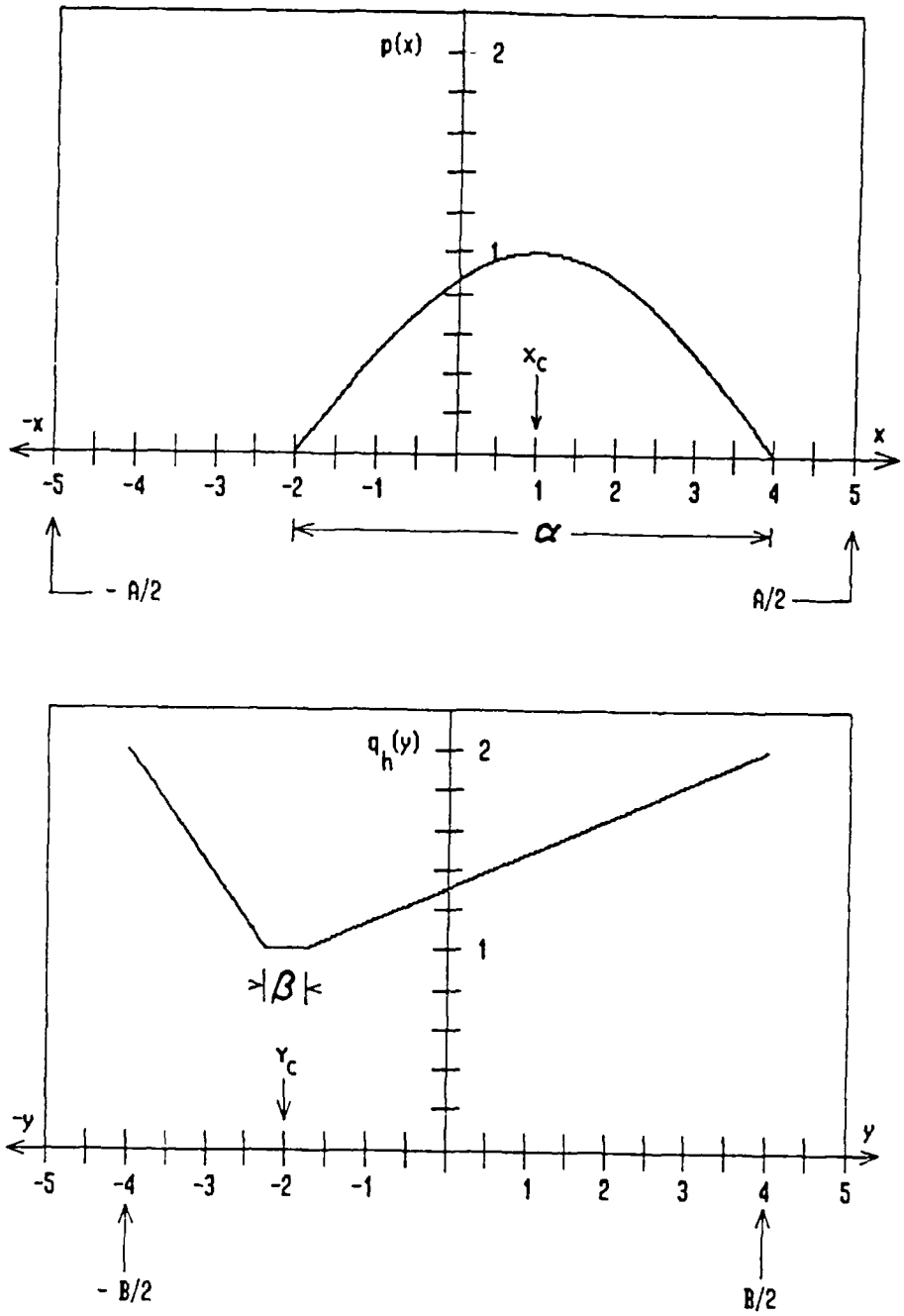

Figure 10. Plots of p(x) and $q_h(y)$ for A = 10. B = 8, α = 6, β = .5, x_c = 1, and y_c = -2. (Arbitrary units).

$$ce^{y}_{nm} = - H1^{s}_{x}(j\omega)\ P_n\ Qe_m\ K^2_{nm}\ n\pi/A$$
$$ch^{y}_{nm} = - H1^{s}_{x}(j\omega)\ P_n\ Qh_m\ K^2_{nm}\ n\pi/A$$

$$P_n = \left[\frac{\alpha A}{2\pi}\right]\left[\frac{\sin[\pi(A-n\alpha)(x_c+\alpha/2)/(\alpha A)] - \pi(x_c-\alpha/2)/\alpha - n\pi/2]}{A - n\alpha}\right.$$

$$- \frac{\sin[\pi(A+n\alpha)(x_c+\alpha/2)/(\alpha A)] - \pi(x_c-\alpha/2)/\alpha + n\pi/2]}{A + n\alpha} \qquad (4.26)$$

$$- \frac{\sin[\pi(A-n\alpha)(x_c-\alpha/2)/(\alpha A)] - \pi(x_c-\alpha/2)/\alpha - n\pi/2]}{A - n\alpha}$$

$$\left. + \frac{\sin[\pi(A+n\alpha)(x_c-\alpha/2)/(\alpha A)] - \pi(x_c-\alpha/2)/\alpha + n\pi/2}{A + n\alpha}\right]$$

provided $A \neq n\alpha$

$$Q_o = \beta + (y_c - \beta/2 + B/2)\left[s_1(y_c - \beta/2 - B/2)/2 + q_1\right]$$

$$- (y_c + \beta/2 - B/2)\left[s_2(y_c + \beta/2 + B/2)/2 + q_2\right] \qquad (4.27)$$

$$Qe_m = \frac{\sin[m\pi(y_c + \beta/2 + B/2)/B] - \sin[m\pi(y_c - \beta/2 + B/2)/B]}{m\pi/B} \qquad (4.28)$$

$$Qh_m = Qe_m + \frac{[s_1(y_c - \beta/2) + q_1]\ \sin[m\pi(y_c - \beta/2 + B/2)/B]}{m\pi/B}$$

$$+ \frac{s_1[\cos[m\pi(y_c - \beta/2 + B/2)/B] - 1]}{(n\pi/B)^2}$$

$$- \frac{[s_2(y_c + \beta/2) + q_2]\sin[m\pi(y_c + \beta/2 + B/2)/B]}{m\pi/B} \qquad (4.29)$$

$$+ \frac{s_2[\cos(m\pi) - \cos[m\pi(y_c + \beta/2 + B/2)/B]}{(m\pi/B)^2}$$

s_1, s_2, q_1, and q_2 are given by (4.23) and all other quantities are as defined previously.

Although the preceding are much more complicated than the corresponding expressions for a continuous enclosure, they are just as amenable to evaluation as the latter with the aid of a computer. Figures 11 and 12 are computer plots of $|H3_x(x,y,z)|$ versus frequency at several locations inside an enclosure with a narrow horizontal slot at the center of one wall ($x_c = y_c = 0$) exposed to a uniform harmonic source of unit magnitude ($\exp(j2\pi ft)$). The enclosure and slot parameters used in these plots are

$A = B = C = 2.7$ m, $d = 6.4\times10^{-3}$ m

$\sigma 2 = 4.33X10^{6}$ mhos/m, $\mu 2 = 12.6\times10^{-7}$ h/m

$\alpha = 0.5$ m, $\beta = 1.6X10\text{-}3$ m, $L_y = 3.2\times10^{-8}$ h

where the slot inductance L_y is computed from the relation

$$L_y = 6.4\ \alpha \times10^{-8}\ \text{h} \qquad (4.29)$$

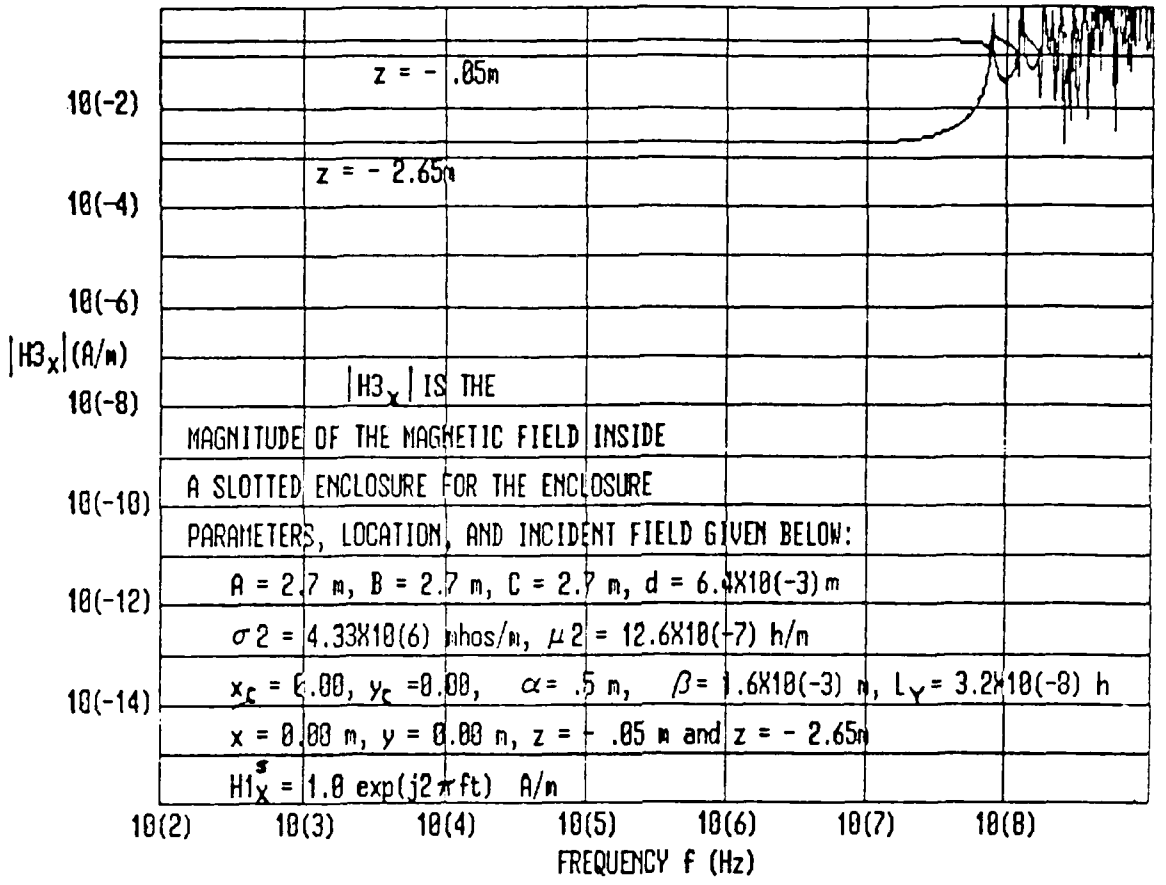

Figure 11. Magnitude of the magnetic field inside an enclosure with a narrow air-filled slot at points near the center of the slot (z = - .05 m) and the center of the back wall (z = - 2.65 m).

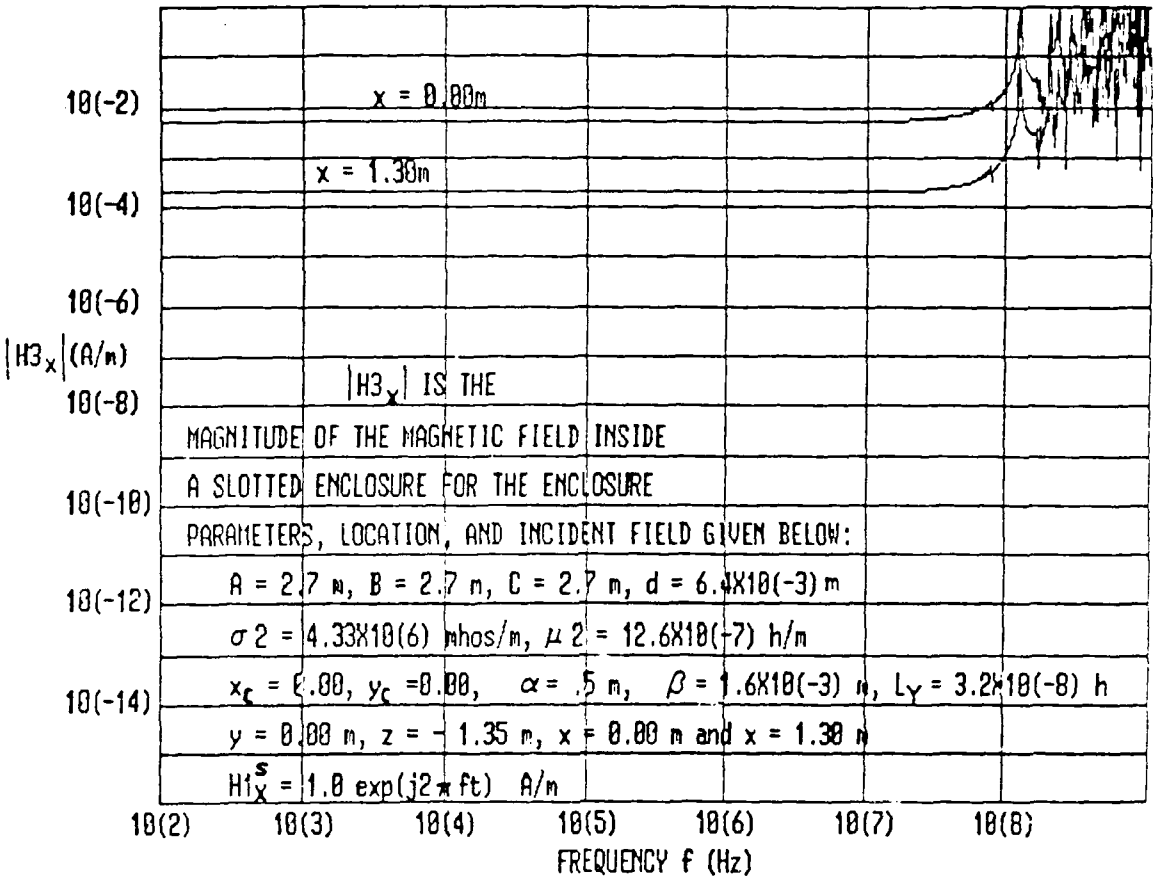

Figure 12. Magnitude of the magnetic field inside an enclosure with a narrow air-filled slot at a point near the center of one side (x = 1.30 m) and at the center of the enclosure (x = 0.00 m).

which is derived from figure 7 of Monroe (1973)[14]. A total of 156 terms were used in the calculations by truncating the series at n = m = 12. Plots obtained using more terms were found to be indistinguishable from the ones in figures 11 and 12. Plots using fewer than 156 terms were found to differ from those in figures 11 and 12 by scale factors that are only weakly dependent on frequency. For example, the lower of the two closely spaced curves in figure 13 is a replot of the curve labeled z = - 0.05 m in figure 11 where 156 terms were used consisting of 144 terms in the double sum over n and m plus 12 terms from the single sum over n. This curve is nearly identical in form to the upper curve which was obtained using only the 12 terms in the sum over n.

The figures suggest that magnetic fields at all locations are virtually independent of frequency below the lowest cutoff frequency of the slotted enclosure. This contrasts with the continuous enclosure where the field is a monotonically decreasing function of frequency below cutoff. The fields in the slotted enclosure also show a significantly greater variation with position than was seen in the continuous enclosure. Thus,in figure 11, the front to back change is two orders of magnitude compared to just under one order of magnitude change in figure 8 in spite of the fact that the slotted enclosure is much smaller. Evidently fields

---

[14]R. L. Monroe, EMP Shielding Effectiveness and MIL-STD 285, Harry Diamond Laboratories, HDL-TR-1336, Adelphi, MD. (July 1973).

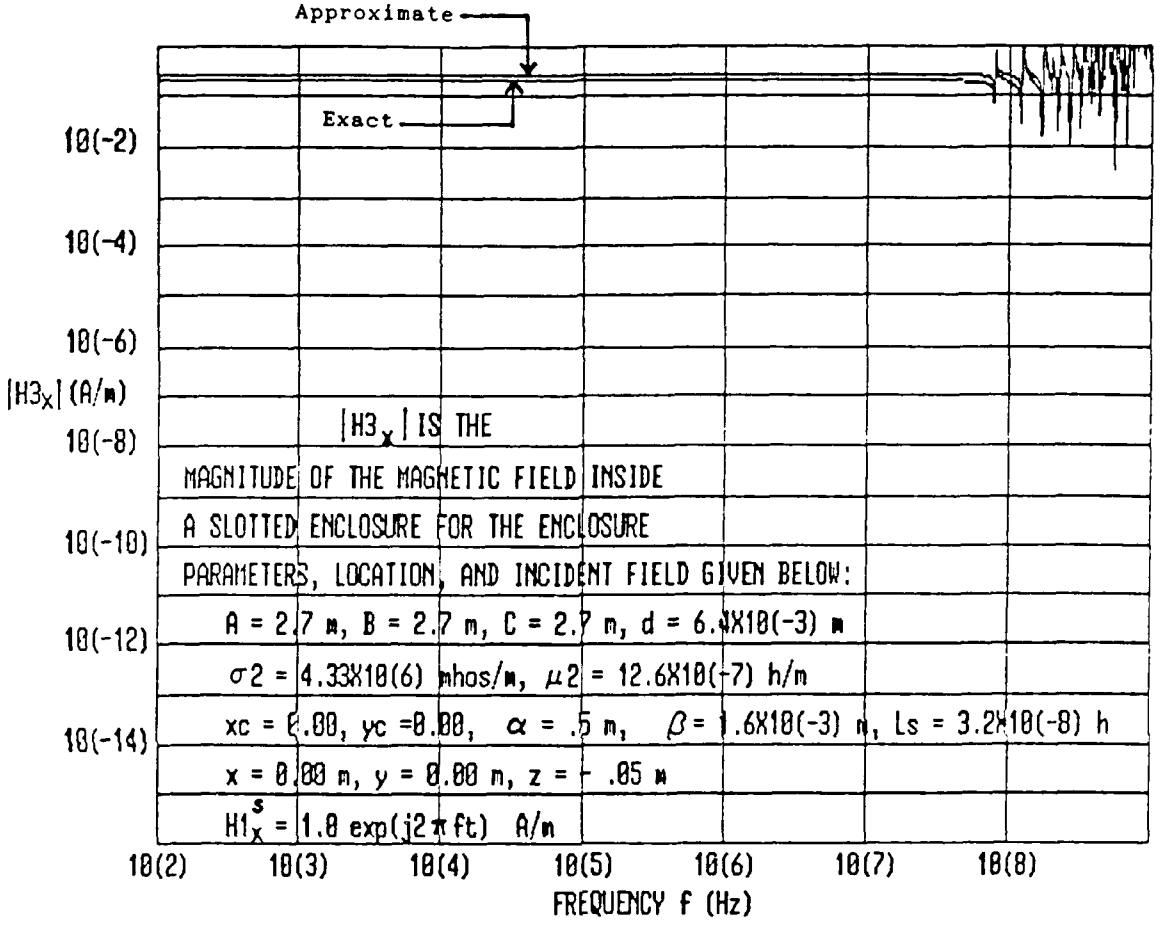

Figure 13. Plots of $|H3_x(x,y,z;j\omega)|$ computed from equation (4.24) using both the single and double sums (lower curve) and the single sum alone (upper curve) where the series are truncated at n = m = 12.

in the slotted enclosure, besides being much larger in magnitude, are more localized than in the continuous enclosure.

Above the cutoff frequency, the magnetic field shows basically the same resonant behavior as in the continuous enclosure but with vastly larger magnitudes. In fact, the figures indicate that the interior field can exceed the exterior field at resonant frequencies. This suggests that a 0.5 m slot makes this enclosure worse than useless as an electromagnetic shield at these frequencies.

5. TIME DOMAIN MAGNETIC FIELDS INSIDE ENCLOSURES DUE TO SPATIALLY UNIFORM, EXTERNAL, TRANSIENT SOURCES

If an external source generates transient magnetic field components that are known functions $h1_x^s(t)$ and $h1_y^s(t)$ of the time t with LaPlace transforms:

$$H1_x^s(j\omega) = L[h1_x^s(t)] \equiv \int_0^\infty \exp(j\omega t)\, h1_x^s(t)\, dt$$
$$H1_y^s(j\omega) = L[h1_y^s(t)] \equiv \int_0^\infty \exp(j\omega t)\, h1_y^s(t)\, dt \qquad (5.1)$$

that are spatially uniform over the areas defined by (4.2) for continuous enclosures and by (4.3) for slotted enclosures, then expressions for the transient fields inside continuous and slotted enclosures exposed to this source can be obtained by substituting (5.1) into (4.6) and (4.24) and computing the inverse LaPlace transform of the resulting expression. Since (4.6) and (4.24) are infinite series each term of which is a function of $j\omega$, this process will consist of a term-by-term application of the inverse LaPlace transform to the series. If the inverse transform of each term in the series can be evaluated, then the result will be new series each term of which is a function of t as well as the internal spatial variables.

In the following sections, we use this procedure to compute magnetic fields inside enclosures exposed to transient fields in

the form of decaying exponentials, damped sinusoids, and rationalized exponentials- a group of functions that alone or in combination can be used to approximate the waveforms of most natural and man-made sources. Although a rigorous mathematical justification of term-by-term inversion of infinite series is a difficult and important problem as Doetsch[15] has emphasized, we will not attempt such a justification here. Our justification will rest on the fact that the time domain series show rapid convergence and produce waveforms that are physically plausible and consistent with measurements.

5.1 Continuous Enclosure

If $H3_x(x,z)$ and $H3_y(y,z)$ from (4.6) are rewritten in the following form

$$H3_x(x,y;j\omega) = \sum_{n=1}^{\infty} S_x^n(x,z;j\omega)$$
$$H3_y(y,z;j\omega) = \sum_{m=1}^{\infty} S_y^m(y,z;j\omega) \qquad (5.2)$$

where the frequency is displayed explicitly as an independent variable through the factor $j\omega$:

$$S_x^n(x,z;j\omega) = 2\exp[-\tau^{1/2}(j\omega)^{1/2}]\ H1_x^s(j\omega)c_n^y e_y^n(x)T_H^n(j\omega)\ F_H^n(z;j\omega) \qquad (5.3)$$

---

[15] G. Doetsch, Guide to the Application of LaPlace Transforms, D. Van Nostrand and Company Ltd., London (1961).

$$S_y^m(y,z;j\omega) = 2\exp[-\tau^{1/2}(j\omega)^{1/2}]\ H1_y^s(j\omega)c_m^x e_x^m(y)T_H^m(j\omega)\ F_H^m(z:j\omega)$$

and

$$\tau = d^2\sigma 2\mu 2 = 4T_c \qquad (T_c = \text{characteristic diffusion time}) \quad (5.4)$$

then the inverse LaPlace transforms of $H3_x(x,z;j\omega)$ and $H3_y(y,z;j\omega)$ are

$$h3_x(x,z;t) = L^{-1}[H3_x(x,z;j\omega)] = \sum_{n=1}^{\infty} h3_x^n(x,z;t)$$

$$h3_y(y,z;t) = L^{-1}[H3_y(y,z;j\omega)] = \sum_{m=1}^{\infty} h3_y^m(y,z;t) \quad (5.5)$$

where

$$h3_x^m(x,z;t) = L^{-1}[S_x^n(x,z;j\omega)]$$

$$h3_y^m(y,z;t) = L^{-1}[S_y^m(y,z;j\omega)] \quad (5.6)$$

and the inverse transform is defined as follows:

$$L^{-1}[G(x,y,z;s)] = \frac{1}{2\pi j}\int_{u-j\infty}^{u+j\infty} \exp(ts)\ G(x,y,z;s)\ ds \quad (5.7)$$

where $j\omega$ is replaced by the complex variable $s = u + jv$.

Thus the problem of computing time domain magnetic fields inside this enclosure reduces to an evaluation of a sequence of inverse LaPlace transforms (5.6) where $S_x^n(x,z;j\omega)$ and $S_y^m(y,z;j\omega)$ are given by (5.3).

Since $S_x^n(x,z;j\omega)$ and $S_y^n(y,z;j\omega)$ are both complicated functions of $j\omega$, for all n and m, we shall not attempt an exact evaluation of these transforms. Instead, we shall use approximations to reduce $S_x^n(x,z;j\omega)$ and $S_y^m(y,z;j\omega)$ to the product of a pair of

functions each of which has an exact transform. This will allow us to express $h3_x^n(x,z;t)$ and $h3_y^m(y,z;t)$ as sequences of convolution integrals in the time domain which can readily be computed to give $h3_x(x,z;t)$ and $h3_y(y,z;t)$.

The approximation is based on the fact that the exponential factor in (5.3) effectively prevents frequencies above a critical value $F_c = 1/(\pi\tau)$ from reaching the interior of the enclosure[1]. Since calculations show that F_c is well below the lowest cutoff frequencies for all room sized shielded enclosures

$$F_c = 1/(\pi\tau) \ll \left[\begin{array}{l} \omega_c^n /(2\pi)|_{n=1} = C_o/(2A) \\ \omega_c^m /(2\pi)|_{m=1} = C_o/(2B) \end{array} \right. \tag{5.8}$$

it follows that only frequencies satisfying

$$\frac{|j\omega|}{\omega_c^n} \ll 1$$

and (5.9)

$$\frac{|j\omega|}{\omega_c^m} \ll 1$$

can affect the interior magnetic fields in this case. Thus, Z_o^n, Z_o^m, r^n, and r^m from (4.6) can be replaced by the following approximations:

$$Z_o^n = \eta_o j\omega/\omega_c{}^n$$
$$Z_o^m = \eta_o j\omega/\omega_c^m$$

---

[1] R. L. Monroe, A Theory of Electromagnetic Shielding with Applications to MIL-STD 285, IEEE-299, and EMP Simulation, Harry Diamond Laboratories, HDL-CR-85-052-1, Adelphi, MD (February 1985).

$$\gamma^n = \omega_c^n/C_o$$
$$\gamma^m = \omega_c^m/C_o \tag{5.10}$$

where

$$\omega_c^n = \pi C_o n/A$$
$$\omega_c^m = \pi C_o m/B \tag{5.11}$$

and the absorption terms in γ^n and γ^m have been neglected. With these approximations, calculations show that

$$\eta 3^n \cong Z_o^n \tanh(\gamma^n C)$$
$$\eta 3^m \cong Z_o^m \tanh(\gamma^m C) \tag{5.12}$$

and

$$T_H^n(j\omega) \cong \frac{2(\mu 2/\sigma 2)^{1/2}}{(\mu 2/\sigma 2)^{1/2} + (j\omega)^{1/2}(\eta_o/\omega_c^n)\tanh[\gamma^n C]}$$
$$T_H^m(j\omega) \cong \frac{2(\mu 2/\sigma 2)^{1/2}}{(\mu 2/\sigma 2)^{1/2} + (j\omega)^{1/2}(\eta_o/\omega_c^m)\tanh[\gamma^m C]} \tag{5.13}$$
$$F_H^n(z;j\omega) = \cosh[\gamma^n(C+d+z)]/\cosh[\gamma^n C]$$
$$F_H^m(z;j\omega) = \cosh[\gamma^m(C+d+z)]/\cosh[\gamma^n C] \ .$$

Substituting (5.13) into (5.3) and the latter into (5.6), we obtain

$$h3_x^n(x,z;t) = L^{-1}[R_1^n(x,z;j\omega)\ R_2^n(j\omega)]$$
$$h3_y^m(y,z;t) = L^{-1}[R_1^m(y,z;j\omega)\ R_2^m(j\omega)] \tag{5.14}$$

where

$$R_1^n(x,z;j\omega) = 2\ H1_x^s(j\omega)\ c_n^y e_y^n(x)\ \cosh[\gamma^n(C+d+z)]/\cosh[\gamma^n C]$$

$$R_2^n(j\omega) = \frac{2(\mu 2/\sigma 2)^{1/2}\ \exp[-\tau(j\omega)^{1/2}]}{(\mu 2/\sigma 2)^{1/2} + (j\omega)^{1/2}(\eta_o/\omega_c^n)\ \tanh[\tau^n C]}$$

$$R_1^m(y,z;j\omega) = 2\ H1_y^s(j\omega)\ c_m^x e_x^m(y)\ \cosh[\tau^m(C+d+z)]/\cosh[\tau^m C] \tag{5.15}$$

$$R_2^m(j\omega) = \frac{2(\mu 2/\sigma 2)^{1/2}\ \exp[-\tau(j\omega)^{1/2}]}{(\mu 2/\sigma 2)^{1/2} + (j\omega)^{1/2}(\eta_o/\omega_c^m)\ \tanh[\tau^m C]}\ .$$

Since $L^{-1}[R_1^n(x,z;j\omega)]$ and $L^{-1}[R_1^m(y,z;j\omega)]$ can be written in terms of the incident time domain source fields (5.1)

$$L^{-1}[H1_x^s(j\omega)] = L^{-1}[L[h1_x^s(t)]] = h1_x^s(t)$$

and

$$L^{-1}[H1_y^s(j\omega)] = L^{-1}[L[h1_y^s(t)]] = h1_y^s(t)$$

which are assumed to be known functions of t for $t > 0$ and since $L^{-1}[R_2^n(j\omega)]$ and $L^{-1}[R_2^m(j\omega)]$ are also known [Campbell and Foster, No. 809][16]

$$L^{-1}[R_2^n(j\omega)] = 2\ r^n(t)$$

$$L^{-1}[R_2^m(j\omega)] = 2\ r^m(t) \tag{5.16}$$

where

$$r^n(t) = \frac{t^{-1/2}}{\pi^{1/2} b^n} \exp\left(-\frac{\tau^2}{4t}\right) - \frac{1}{(b^n)^2} \exp\left[\frac{\tau}{b^n} + \frac{t}{(b^n)^2}\right]$$

---

[16] G. A. Campbell and R.M. Foster, Fourier Integrals for Practical Applications, D. Van Nostrand Company, Inc. Princeton, N.J. (1948).

$$\times \operatorname{erfc}\left[\frac{\tau}{2t^{1/2}} + \frac{t^{1/2}}{b^n}\right] \tag{5.17}$$

$$r^m(t) = \frac{t^{-1/2}}{\pi^{1/2} b^m} \exp\left(-\frac{\tau^2}{4t}\right) - \frac{1}{(b^m)^2} \exp\left[\frac{\tau}{b^m} + \frac{t}{(b^m)^2}\right]$$

$$\times \operatorname{erfc}\left[\frac{\tau}{2t^{1/2}} + \frac{t^{1/2}}{b^m}\right]$$

$$b^n = \frac{\eta_o \tanh[r^n C]}{\omega_c^n (\mu 2/\sigma 2)^{1/2}}$$

$$b^m = \frac{\eta_o \tanh[r^m C]}{\omega_c^m (\mu 2/\sigma 2)^{1/2}} \tag{5.18}$$

and erfc[f(t)] is the complementary error function

$$\operatorname{erfc}[f(t)] \equiv \frac{2}{\pi^{1/2}} \int_{f(t)}^{\infty} \exp(-v^2)\, dv \tag{5.19}$$

it follows from the convolution theorem [Doetsch, No. 23][15] that the inverse transforms in (5.4) can be written in terms of $h1_x^s(t)$, $h1_y^s(t)$, $r^n(t)$, and $r^m(t)$. That is,

$$h3_x^n(x,z;t) = 4\, c_n^y e_y^n(x)\, I^n(t) \cosh[r^n(C+d+z)]/\cosh[r^n C]$$

$$h3_y^m(y,z;t) = 4\, c_m^x e_x^m(y)\, I^m(t) \cosh[r^m(C+d+z)]/\cosh[r^m C] \tag{5.20}$$

---

[15] G. Doetsch, Guide to the Application of LaPlace Transforms, D. Van Nostrand and Company Ltd., London (1961).

where the convolution integrals $I^n(t)$ and $I^m(t)$ are

$$I^n(t) = \int_0^t h1_x^s(t-g)\ r^n(g)\ dg$$

$$I^m(t) = \int_0^t h1_y^s(t-g)\ r^m(g)\ dg\ . \tag{5.21}$$

Substituting (5.20) into (5.5) gives the desired expressions for $h3_x(x,z;t)$ and $h3_y(y,z;t)$. The complete statement is as follows:

Approximate expressions for the time domain magnetic fields at any point inside a continuous enclosure due to a transient external electromagnetic source generating spatially uniform fields on one wall of the enclosure can be written in terms of the tangential components of the source magnetic field $h1_x^s(t)$ and $h1_y^s(t)$ incident on the outside surface of that wall as follows

$$h3_x(x,z;t) = 4 \sum_{n=1}^{\infty} c_n^y e_y^n(x)\ I^n(t)\ \cosh[r^n(C+d+z)]/\cosh[r^nC]$$

$$h3_y(y,z;t) = 4 \sum_{m=1}^{\infty} c_m^x e_x^m(y)\ I^m(t)\ \cosh[r^m(C+d+z)]/\cosh[r^mC] \tag{5.22}$$

where

$$I^n(t) = \int_0^t h1_x^s(t-g)\ r^n(g)\ dg$$

$$I^m(t) = \int_0^t h1_y^s(t-g)\ r^m(g)\ dg$$

$r^n(g)$ and $r^m(g)$ are given by (5.17), r^n and r^m by (5.10), and the remaining quantities are as defined in section 4.1.

When $h1^s_x(t)$ and $h1^s_y(t)$ are specified, the convolution integrals can be evaluated for each n and m, and $h3_x(x,z;t)$ and $h3_y(y,z;t)$ can be computed using a truncated version of (5.22). However, the integrals cannot usually be reduced to closed-form expressions, and, therefore, must be evaluated using a numerical integration technique. Since these techniques replace integrals with sums over the time interval of interest (0,t) for each term in the series, the single sums in (5.22) become double sums. Calculations based on (5.22) where the integrals have been evaluated using the trapezoidal rule with 40 points per interval and the series are truncated at n = m = 10 show excellent convergence for most locations and time intervals. This approach was used to obtain the waveforms in figures 14, 15, 16, and 17, where the internal fields $h3_y$ (solid curves) are multiplied by a scale factor of 10^4 and the incident fields $h1^s_y$ (dotted curves) are given by the following:

Double exponential $h1^s_y(t) = \exp(-4\times10^6 t) - \exp(-4\times10^8 t)$

Rationalized exponential $h1^s_y(t) = 1/[\exp(-3\times10^9) + \exp(2.3\times10^7 t)]$

Damped sinusoid (1.59 MHz) $h1^s_y(t) = \exp(-4\times10^6 t)\sin(1\times10^7 t)$

Damped sinusoid (6.37 MHz) $h1^s_y(t) = \exp(-2.5\times10^6)\sin(4\times10^7 t)$

the enclosure is characterized by

$A = 6.1$ m $B = 3.66$ m $C = 6.1$ m $d = 3.8\text{X}10^{-4}$ m

$\sigma 2 = 4.33\times10^6$ mhos/m $\mu 2 = 12.6\times10^{-7}$ h/m

and the location is the center of the enclosure

$x = y = 0.00$ m , $z = -3.05$ m .

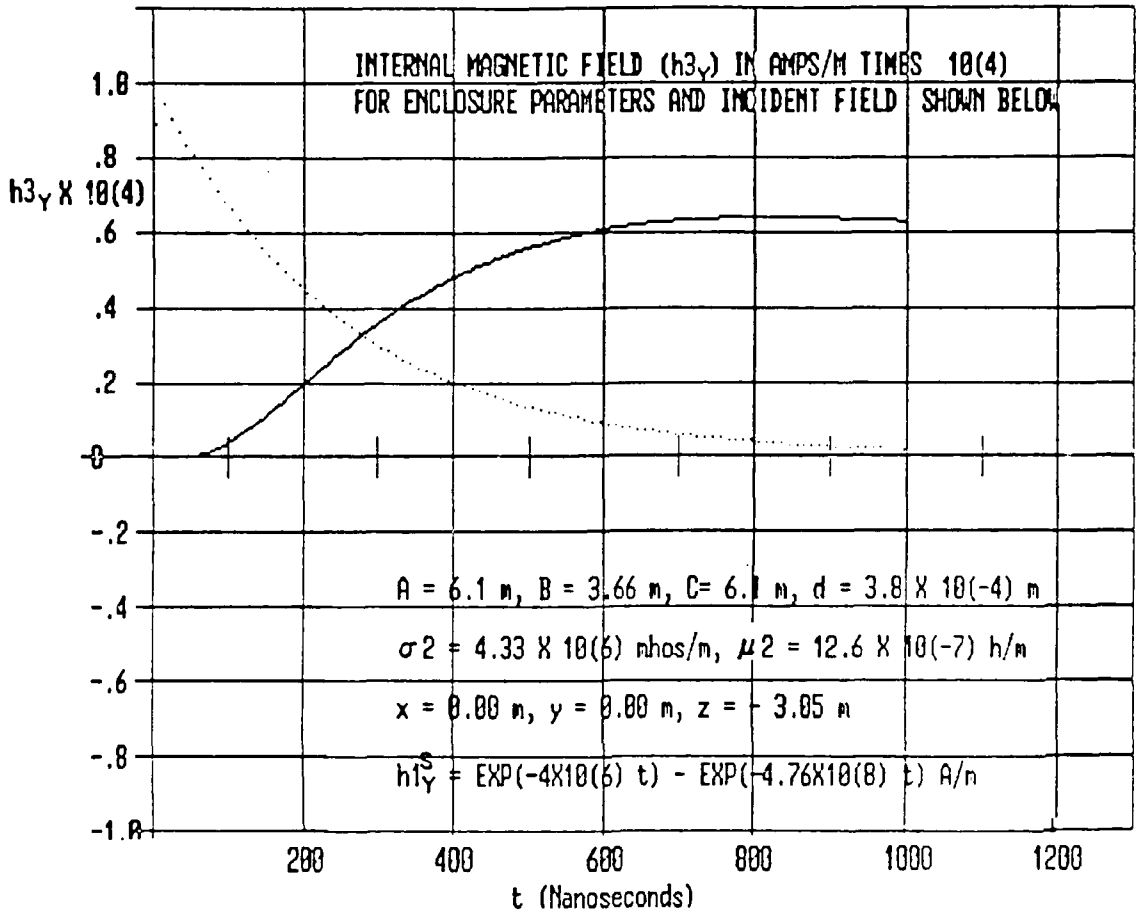

Figure 14. Transient magnetic field $h3_y \times 10^4$ A/m (solid curve) at the center (x = y = 0.00, z = -3.05) of a continuous enclosure with one wall exposed to $h1_y^s$ (dotted curve) with a double exponential waveform.

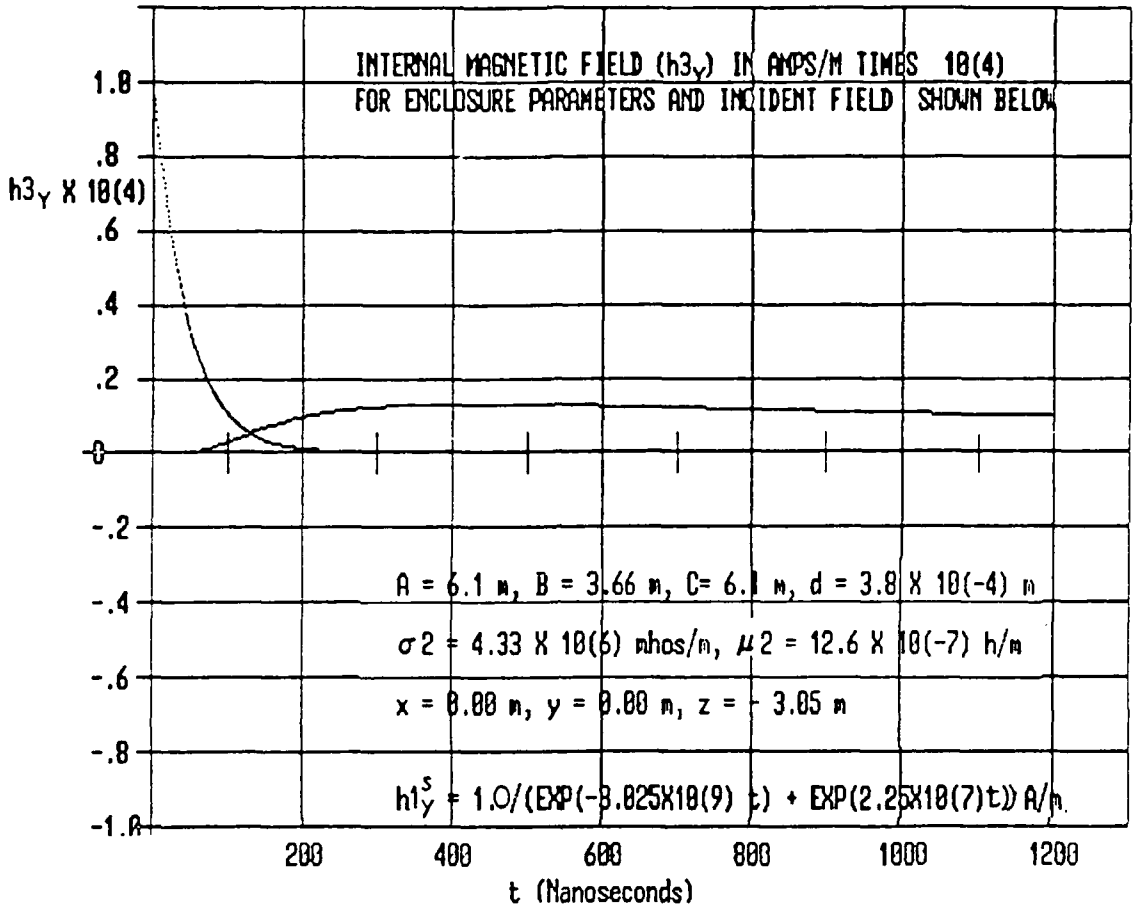

Figure 15. Transient magnetic field $h3_y \times 10^4$ A/m (solid curve) at the center of a continuous enclosure with one wall exposed to $h1_y^s$ (dotted curve) with a rationalized exponential waveform.

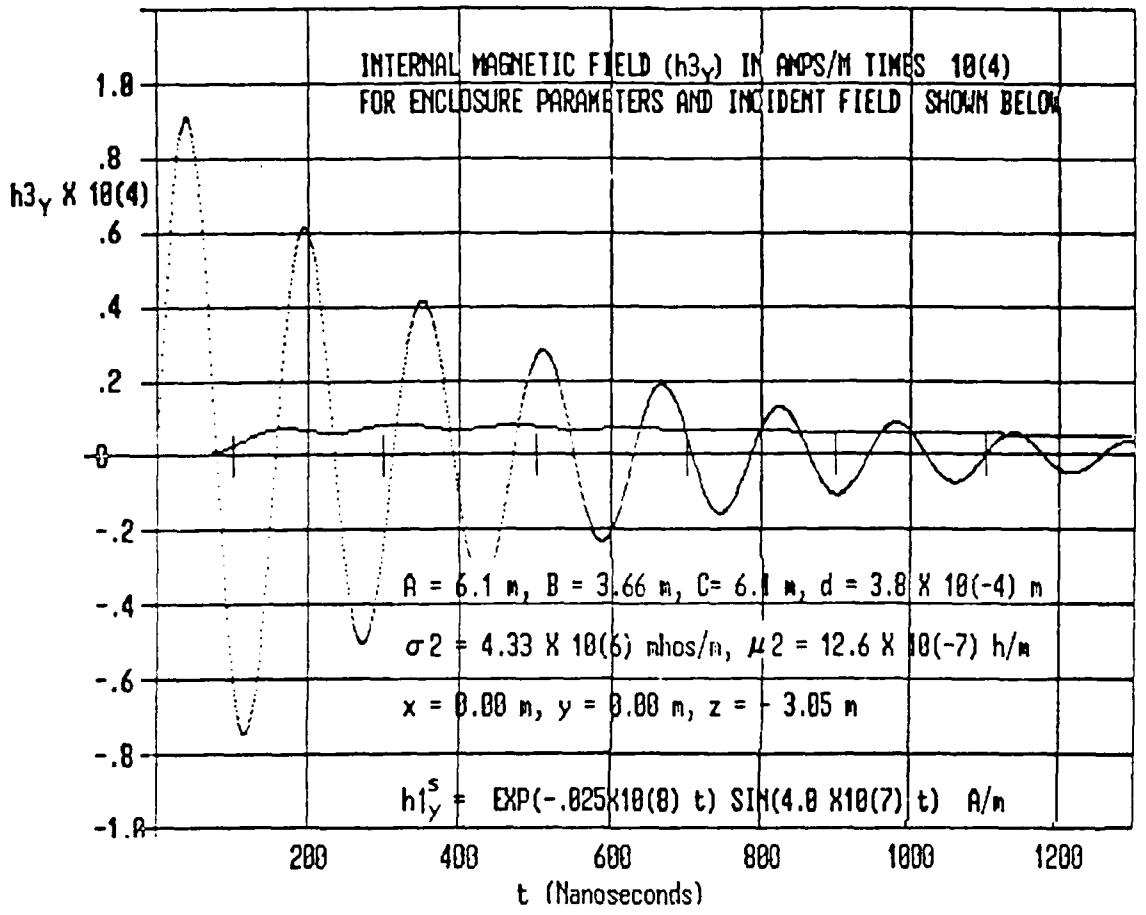

Figure. 16 Transient magnetic field $h3_y \times 10^4$ A/m (solid curve) at the center of a continuous enclosure with one wall exposed to $h1_y^s$ (dotted curve) with an exponentially damped, 6.37 MHz sinusoidal waveform.

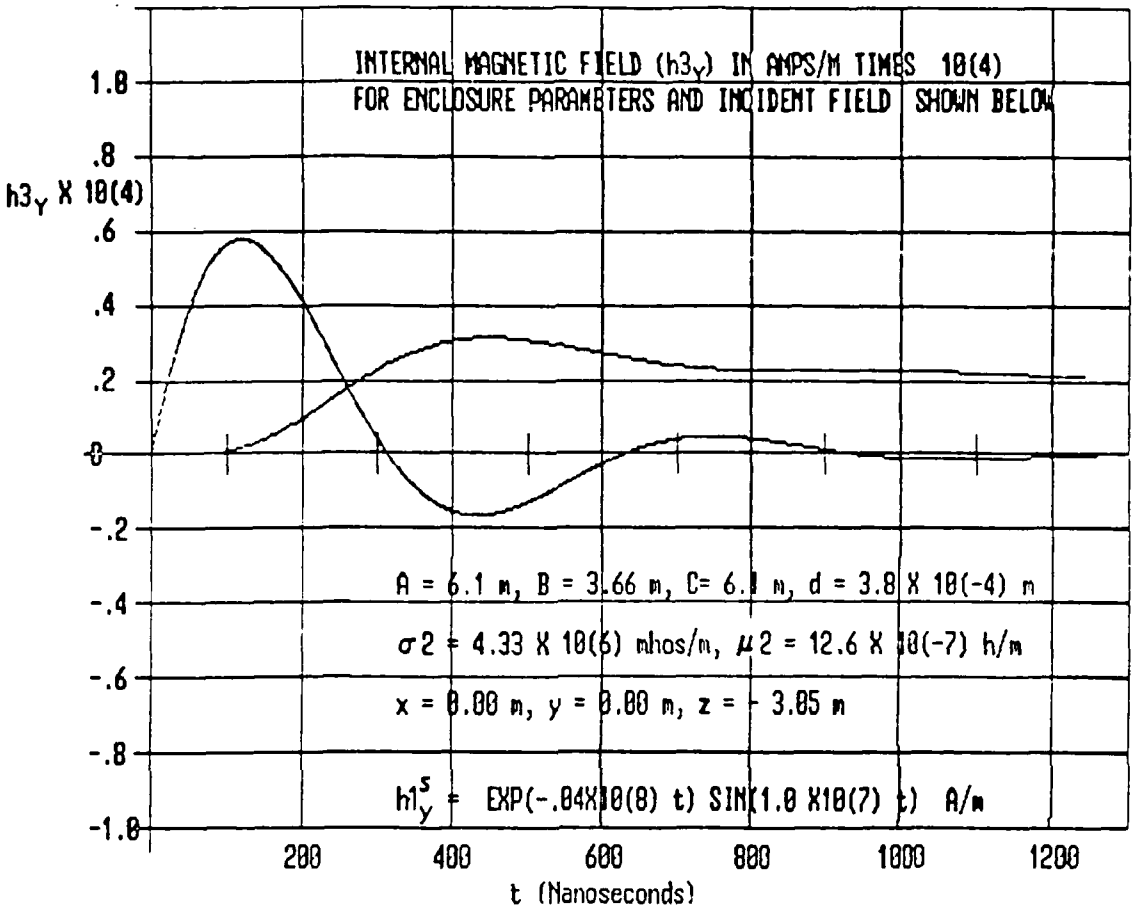

Figure. 17 Transient magnetic field $h3_y \times 10^4$ A/m (solid curve) at the center of a continuous enclosure with one wall exposed to $h1_y^s$ (dotted curve) with an exponentially damped, 1.59 MHz sinusoidal waveform.

These waveforms agree with earlier results of Monroe[1] who based his calculations on a one-term approximation to the transient field at $z = -d$. They show that T_3, the time required for $h3_y$ to reach its maximum, is greater than the characteristic diffusion time of the enclosure T_c, where

$$T_c \equiv \tau/4 = \sigma 2\ \mu 2\ d^2/4 \qquad (5.23)$$

$$\cong 200\ ns, \qquad (1\ ns = 1 \times 10^{-9}\ s)$$

for all four incident waveforms and is independent of T_1, the time reqiured for $h1_y^s$ to reach its peak. For these cases, T_3 depends primarily on the duration of $h1_y^s$ with a longer pulse producing larger value of T_3, that is, a slower "rise" time. This is seen most clearly in figures 14 and 15 where the double-exponential pulse with a duration of 1000 ns produces an internal field with $T_3 \cong 820$ ns while the rationalized exponential with a duration of 200 ns produces $T_3 = 420$ ns. These figures also confirm Monroe's calculations showing that the maximum value of $h3_y$ depends strongly on the pulse duration with long incident pulses generating much larger internal fields than comparable short pulses. Thus, the double exponential with a maximum value (1 A/m) equal to that of rationalized exponential generates an internal field with a maximum value nearly five times larger. This is due to the fact that longer pulses carry more energy at low frequencies which, as shown by figures 8 and 9, are generally less attenuated in passing through the wall of a continuous enclosure.

---

[1] R. L. Monroe, A Theory of Electromagnetic Shielding with Applications to MIL-STD 285, IEEE-299, and EMP Simulation, Harry Diamond Laboratories, HDL-CR-85-052-1, Adelphi, MD (February 1985).

The importance of the frequency content of the incident pulse in determining the magnitude of the internal field is strikingly illustrated by figures 16 and 17 where in both figures the incident pulse is an exponentially damped sine wave. Here, the 1.59 MHz sine wave (Figure 17) generates an internal field three times larger than the field generated by the 6.37 MHz sine wave despite the fact that its amplitude is smaller and its damping greater.

The accuracy of the approximations used to obtain (5.22) can be gauged by computing $|H3_y(y,z;j\omega)|$ from (5.2) with $T_H^m(j\omega)$ and $F_H^m(z:jw)$ determined by (5.13) and comparing the result with $|H3_y(y,z;j\omega)|$ computed with the original expressions (4.6). This is done in figure 18, where the upper curve is obtained from (4.6) and the lower curve is the approximation. For the scale used here, the two curves are indistinguishable at frequencies below 20 MHz. Above 20 MHz, the curves diverge with the approximation falling farther below the exact curve until the first enclosure resonance at approximately 70 MHz is reached. At frequencies above the resonance, the curves partially converge but then diverge again in the vicinity of the second resonance. This alternating divergence and convergence occurs at every resonance and is superimposed on a general downward trend that is virtually the same for both curves. Clearly, the principal difference between the exact and approximate expressions is that the former accounts for the effects of enclosure resonances while the latter does not. However, for the case shown in figure 18 and for most

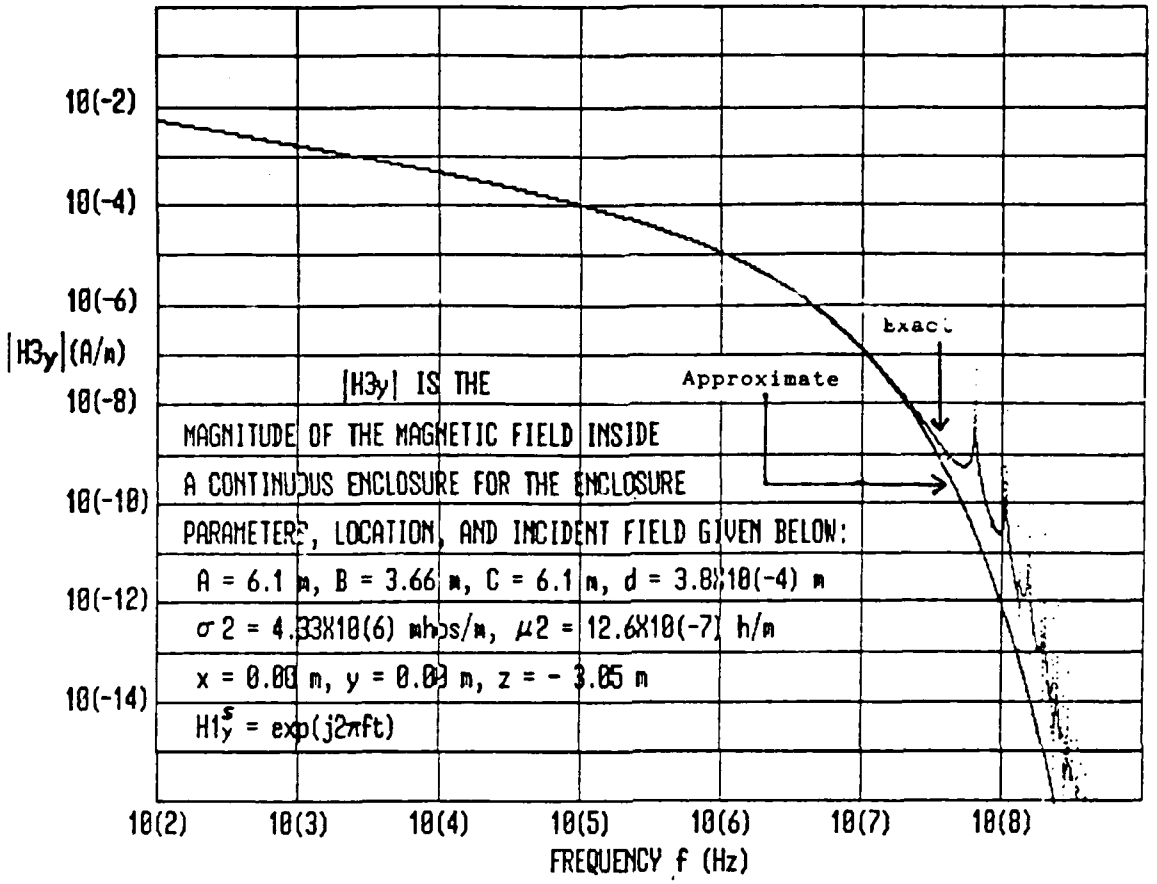

Figure 18. Plots of $|H3_y(x,y,z;j\omega)|$ computed from equation (4.6) using exact expressions for $T_H^m(j\omega)$ and $F_H^m(z;j\omega)$ (upper curve) and using approximate expressions (5.13) for $T_H^m(j\omega)$ and $F_H^m(z;j\omega)$ (lower curve).

cases of interest, the lowest enclosure resonance occurs at a frequency where the field is highly attenuated with respect to the external field, and higher frequency fields are attenuated even more. Thus, enclosure resonances are likely to have little effect on the transient internal field inside most continuous enclosures, and the fact that the approximation fails to account for resonances will have little effect on the accuracy of the transient responses computed with this approximation. Significant errors may occur in the case of a relatively large, thin-walled enclosure where condition (5.8) is violated. When (5.8) is violated, the field at resonance will be less attenuated than the fields at most lower frequencies, and the transient reponse of the enclosure may be dominated by energy coupled into the higher frequencies. This is most likely to occur when the incident field is a narrow-banded pulse centered on, or near, a resonant frequency. In such a case, one should not expect the approximation to yield an accurate transient reponse.

For the enclosure used to obtain figures 14, 15, 16, and 17, the critical frequency F_c equals 0.4 MHz and $C_o/(2B)$ = 41 MHz. Hence, (5.8) is easily satisfied, and the approximation used to compute $h3_y$ in these figures is valid. The same approximation could also be used to compute $h3_x$ for this enclosure since $C_o/(2A)$ = 25 MHz also satisfies (5.8).

5.1 Slotted Enclosure

As in the preceding section, we begin calculating the transient response of a slotted enclosure by rewriting the general frequency domain expression for the internal magnetic field (4.24) in a form that is convenient for term-by-term application of the inverse Laplace transform. That is, we rewrite $H3_x(x,y,z)$ from (4.24) as follows

$$H3_x(x,y,z;j\omega) = \sum_{n=1}^{\infty} S_x^n(x,z;j\omega) + \sum_{n=1}^{\infty}\sum_{m=1}^{\infty} S_x^{nm}(x,y,z;j\omega) \qquad (5.24)$$

where

$$S_x^n(x,z;j\omega) = 2\, H1_x^s(j\omega)\, c_n^y\, e_y^n(x)\, T_{H_y}^n(j\omega)\, F_H^n(z;j\omega)$$

$$S_x^{nm}(x,y,z;j\omega) = 2\, H1_x^s(j\omega)\, c_{nm}^y\, e_y^{nm}(x,y)\, T_H^{nm}(j\omega)\, F_H^{nm}(z;j\omega) \qquad (5.25)$$

$$c_n^y = -\exp(-\mu_o d/L_y)\, Q_o P_n K_n^2\, n\pi/A$$

$$c_{nm}^y = -\exp(-\mu_o d/L_y)\, P_n Q h_m K_{nm}^2\, n\pi/A \qquad (5.26)$$

and apply the inverse transform to this expression to obtain the transient magnetic field:

$$h3_x(x,y,z;t) = L^{-1}[H3_x(x,y,z;j\omega)]$$
$$= \sum_{n=1}^{\infty} h3_x^n(x,z;t) + \sum_{n=1}^{\infty}\sum_{m=1}^{\infty} h3_x^{nm}(x,y,z;t) \qquad (5.27)$$

where

$$h3_x^n(x,z;t) = L^{-1}[S_x^n(x,z;j\omega)]$$

$$h3_x^{nm}(x,y,z;t) = L^{-1}[S_x^{nm}(x,y,z;j\omega)] \qquad (5.28)$$

Thus, to compute the transient internal field, it is necessary to evaluate the sequence of inverse LaPlace transforms (5.28) where

$S_x^n(x,z;j\omega)$ and $S_x^{nm}(x,y,z;j\omega)$ are given by (5.25) and (5.26).

As in the case of the continuous enclosure, it will be necessary to introduce approximations in order to reduce $S_x^n(x,z;j\omega)$ and $S_x^{nm}(x,y,z;j\omega)$ to expressions that will allow us to evaluate their inverse transforms in terms of convolution integrals for all n and m. Since figures 11 and 12 show that enclosure resonances can play an important role in determining the largest field inside a slotted enclosure over a wide range of locations and frequencies, it is clear that approximations (5.9) cannot be extended to the slotted enclosure. Thus, Z_o^n, Z_0^{nm}, r^n, and r^{nm} cannot be replaced by approximations based on (5.9). Instead, we must use

$$\begin{aligned} Z_o^n &= \eta_o j\omega/\varsigma^n(j\omega) \\ Z_o^{nm} &= \eta_o j\omega/\varsigma^{nm}(j\omega) \\ r^n &= \varsigma^n(j\omega)/C_o + \alpha^n \\ r^{nm} &= \varsigma^{nm}(j\omega)/C_o + \alpha^{nm} \end{aligned} \tag{5.29}$$

where

$$\begin{aligned} \varsigma^n(j\omega) &= [(\omega_c^n)^2 + (j\omega)^2]^{1/2} \\ \varsigma^{nm}(j\omega) &= [(\omega_c^{nm})^2 + (j\omega)^2]^{1/2} \end{aligned} \tag{5.30}$$

and

$$\begin{aligned} \omega_c^n &= \pi C_o n/A \\ \omega_c^{nm} &= \pi C_o \left[(n/A)^2 + (m/B)^2\right]^{1/2}. \end{aligned} \tag{5.31}$$

These are the original expressions rewritten in a form that emphasizes their frequency dependence through the factors $\varsigma^n(j\omega)$ and $\varsigma^{nm}(j\omega)$. With Z_o^n, Z_o^{nm}, Γ^n, and Γ^{nm} given by the preceding, the remaining approximations used for the continuous enclosure can be applied to the slotted enclosure without any additional loss of accuracy. Thus, we can again replace $\eta 3^n$, $\eta 3^{nm}$, $F_H^n(z;j\omega)$, and $F_H^{nm}(z;j\omega)$ by

$$\begin{aligned}
\eta 3^n &\cong Z_o^n \tanh[\Gamma^n C] \\
\eta 3^{nm} &\cong Z_o^{nm} \tanh[\Gamma^{nm} C] \\
F_H^n(z;j\omega) &\cong \cosh[\Gamma^n(C+d+z)]/\cosh[\Gamma^n C] \\
F_H^{nm}(z;j\omega) &\cong \cosh[\Gamma^{nm}(C+d+z)]/\cosh[\Gamma^{nm} C]
\end{aligned} \tag{5.32}$$

With these approximations for $\eta 3^n$ and $\eta 3^{nm}$, we obtain

$$\begin{aligned}
T_H^n(j\omega) &= \frac{2j\omega L_y}{j\omega L_y + Z_o^n \tanh[\Gamma^n C]} \\
T_H^{nm}(j\omega) &= \frac{2j\omega L_y}{j\omega L_y + Z_o^{nm} \tanh[\Gamma^{nm} C]}
\end{aligned} \tag{5.33}$$

from (4.16). Combining (5.33) with $F_H^n(z;j\omega)$ and $F_H^{nm}(z;j\omega)$ from (5.32) gives

$$\begin{aligned}
T_H^n(j\omega)\, F_H^n(z;j\omega) &= \frac{2j\omega L_y \cosh[\Gamma^n(C+d+z)]}{j\omega L_y \cosh[\Gamma^n C] + Z_o^n \sinh[\Gamma^n C]} \\
T_H^{nm}(j\omega)\, F_H^{nm}(z;j\omega) &= \frac{2j\omega L_y \cosh[\Gamma^{nm}(C+d+z)]}{j\omega L_y \cosh[\Gamma^{nm} C] + Z_o^{nm} \sinh[\Gamma^{nm} C]}
\end{aligned} \tag{5.34}$$

Substituting (5.34) into (5.25) and the latter into (5.28), we obtain

$$h3_x^n(x,z;t) = L^{-1}[R_1^n(x;j\omega)\, R_2^n(z;j\omega)]$$

$$h3_x^{nm}(x,y,z;t) = L^{-1}[R_1^{nm}(x,y;j\omega)\ R_2^{nm}(z;j\omega)] \tag{5.35}$$

where

$$R_1^n(x;j\omega) = 2\ c_n^y e_y^n(x)\ H1_x^s(j\omega)$$

$$R_2^n(z;j\omega) = \frac{2\ L_y \varsigma^n(j\omega)\ \cosh[\varsigma^n(j\omega)(C+d+z)/C_o]}{L_y \varsigma^n(j\omega)\cosh[\varsigma^n(j\omega)C/C_o] + \eta_o \sinh[\varsigma^n(j\omega)C/C_o]}$$

$$R_1^{nm}(x,y;j\omega) = 2\ c_{nm}^y e_y^{nm}(x,y)\ H1_x^s(j\omega) \tag{5.36}$$

$$R_2^{nm}(z;j\omega) = \frac{2\ L_y \varsigma^{nm}(j\omega)\ \cosh[\varsigma^{nm}(j\omega)(C+d+z)/C_o]}{L_y \varsigma^{nm}(j\omega)\cosh[\varsigma^{nm}(j\omega)C/C_o] + \eta_o \sinh[\varsigma^{nm}(j\omega)C/C_o]}$$

and Z_o^n, Z_o^{nm}, Γ^n, and Γ^{nm} have been replaced by (5.29) and (5.30) after dropping the absorption terms α^n and α^{nm} from the latter.

Following the same approach used for the continuous enclosure, we will compute the inverse transforms of $R_1^n(x;j\omega)$, $R_2^n(z;j\omega)$, $R_1^{nm}(x,y;j\omega)$, and $R_2^{nm}(z;j\omega)$ and use these quantities to write $h3_x^n(x,z;t)$ and $h3_x^{nm}(x,y,z;j\omega)$ in terms of sequences of convolution integrals by applying the convolution theorem to (5.35). Since $h1_x^s(t)$ is the inverse transform of $H1_x^s(j\omega)$, we obtain the inverse transforms of $R_1^n(x;j\omega)$ and $R_2^{nm}(x,y;j\omega)$ immediately;

$$r_1^n(x;t) \equiv L^{-1}[R_1^n(x;j\omega)] = 2\ c_n^y e_y^n(x)\ h1_x^s(t)$$

$$r_1^{nm}(x,y;t) \equiv L^{-1}[R_1^{nm}(x,y;j\omega)] = 2\ c_{nm}^y e_y^{nm}(x,y)\ h1_x^s(t) \tag{5.37}$$

However, the inverse transforms of $R_2^n(z;j\omega)$ and $R_2^{nm}(z;j\omega)$ are not as readily available. These transforms do not appear in any of the standard collections, and, therefore. they must be calculated directly without recourse to tabulated functions. The most

straightforward way to do this is by carrying out partial fraction expansions of $R_2^n(z;j\omega)$ and $R_2^{nm}(z;j\omega)$ and applying the inverse transform to each term in the expansions. Since $R_2^n(z;s)$ and $R_2^{nm}(z;s)$ are meromorphic functions[17] of the complex variable s, these expansions and their inverse transforms will be infinite series. The derivation in appendix A. gives

$$R_2^n(z;j\omega) = \frac{2\,\mathcal{P}}{\mathcal{P}+1} + 2\left[(\omega_c^n)^2 + (j\omega)^2\right] \sum_{k=1}^{\infty} \frac{W_k(z)}{(\omega_c^n)^2 + (\omega_k)^2 + (j\omega)^2}$$

$$R_2^{nm}(z;j\omega) = \frac{2\,\mathcal{P}}{\mathcal{P}+1} + 2\left[(\omega_c^{nm})^2 + (j\omega)^2\right] \tag{5.38}$$

$$\times \sum_{k=1}^{\infty} \frac{W_k(z)}{(\omega_c^{nm})^2 + (\omega_k)^2 + (j\omega)^2}$$

where ω_c^{nm} and ω_c^n are given by (5.31),

$$\mathcal{P} = \frac{L_y C_o}{\eta_o C}$$

$$W_k(z) = \frac{2\,\mathcal{P}\cos[\rho_k(C+d+z)/C_o]}{\mathcal{P}\,[\cos(\rho_k) - \rho_k\sin(\rho_k)] + \cos(\rho_k)} \tag{5.39}$$

$$\omega_k = \rho_k C_o/C$$

and ρ_k $k = 1,2,3....$ are roots of the equation

$$\mathcal{P}\,\rho\cos(\rho) + \sin(\rho) = 0 \tag{5.40}$$

Applying the inverse transform to (5.38) and using transform

---

[17] E. C. Titchmarsh, The Theory of Functions, 2d Ed., Oxford University Press (1939).

pairs 33 and 38 in Doetsch[15] gives

$$r_2^n(z;t) = L^{-1}[R_2^n(z;j\omega)] = \tfrac{1}{2}\,\delta(t) - 2\sum_{k=1}^{\infty} \frac{(\omega_k)^2\, W_k(z)\, \sin(\omega_k^n t)}{\omega_k^n}$$

$$r_2^{nm}(z;t) = L^{-1}[R_2^{nm}(z;j\omega)] = \tfrac{1}{2}\,\delta(t) - 2\sum_{k=1}^{\infty} \frac{(\omega_k)^2\, W_k(z)\, \sin(\omega_k^{nm} t)}{\omega_k^{nm}} \tag{5.41}$$

where $\delta(t)$ is the delta function and

$$\omega_k^n = \left[(\omega_c^n)^2 + (\omega_k)^2\right]^{1/2}$$

$$\omega_k^{nm} = \left[(\omega^{nm})^2 + (\omega_k)^2\right]^{1/2} . \tag{5.42}$$

We can now apply the convolution theorem to (5.35) using (5.37) and (5.40) to obtain

$$h3_x^n(x,z;t) = 2\, c_n^y e_y^n(x)\, I^n(z;t)$$

$$h3_x^{nm}(x,y,z;t) = 2\, c_{nm}^y e_y^{nm}(x,y)\, I^{nm}(z;t) \tag{5.43}$$

where

$$I^n(z;t) = \int_0^t h1_x^s(t-g)\, r_2^n(z;g)\, dg$$

$$I^{nm}(z;t) = \int_0^t h1_x^s(t-g)\, r_2^{nm}(z;g)\, dg \tag{5.44}$$

These expressions can now be substituted into (5.27) to determine $h3_x(x,y,z;t)$. The final result can be stated as follows:

---

[15] G. Doetsch, Guide to the Application of LaPlace Transforms, D. Van Nostrand and Company Ltd., London (1961).

An approximate expression for the time domain magnetic field at any point inside an enclosure with a narrow, horizontal, air-filled slot, as shown in figure 7, due to a transient external source generating a spatially uniform field over the surface of the slot can be written in terms of the tangential component of the source magnetic field $h1_x^s(t)$ incident on the slot as follows

$$h3_x(x,y,z;t) = 2\sum_{n=1}^{\infty} c_n^y e_n^n(x)\ I^n(z;t) + 2\sum_{n=1}^{\infty}\sum_{m=1}^{\infty} c_{nm}^y e_y^{nm}(x,y)\ I^{nm}(z;t) \tag{5.45}$$

where

$$I^n(z;t) = \int_0^t h1_x^s(t-g)\ r_2^n(z;g)\ dg$$

$$I^{nm}(z;t) = \int_0^t h1_x^s(t-g)\ r_2^{nm}(z;g)\ dg$$

c_n^y and c_{nm}^y are given by (5.26), $r_2^n(z;t)$ and r_2^{nm} are given by (5.41), and $e_y^n(x)$ and $e_y^{nm}(x,y)$ are as defined previously.

Since $r_2^n(z;t)$ and $r_2^{nm}(z;t)$ are infinite series for each n and m, $I^n(z;t)$ and $I^{nm}(z;t)$ will also be infinite series for each n and m. Consequently, the single sum in (5.45) is actually a double sum, and the double sum is a triple sum. When the functional form of $h1_x^s(t)$ is specified, $I^n(z;t)$ and $I^{nm}(z;t)$ can be computed and $h3_x(x,y,z;t)$ can be written explicitly in terms of these sums. For example, if $h1_x^s(t)$ can be written in the form of the difference between two decaying exponentials:

$$h1_x^s = h_o[\exp(-\gamma_1 t) - \exp(-\gamma_2 t)] \tag{5.46}$$

then

$$h3_x(x,y,z;t) = 2\sum_{n=1}^{\infty}\sum_{k=0}^{\infty} c_n^y e_y^n(x)\ I_k^n(z;t) + 2\sum_{n=1}^{\infty}\sum_{m=1}^{\infty}\sum_{k=0}^{\infty} c_{nm}^y e_y^{nm}(x,y)\ I_k^{nm}(z;t) \tag{5.47}$$

where

$$I_0^n(z;t) = I_0^{nm}(z;t) = \tfrac{1}{2}\, h1_x^s(t) = \tfrac{1}{2}\, h_o[\exp(-\gamma_1 t) - \exp(-\gamma_2 t)]$$
$$I_k^n(z;t) = -2(\omega_k)^2 W_k(z)\ J_k^n(t)/\omega_k^n$$
$$I_k^{nm}(z;t) = -2(\omega_k)^2 W_k(z)\ J_k^{nm}(t)/\omega_k^{nm} \tag{5.48}$$

$$J_k^n(t) = \tfrac{1}{2}\, h_o\left[\frac{\omega_k^n \exp(-\gamma_1 t) + \gamma_1 \sin(\omega_k^n t) - \omega_k^n \cos(\omega_k^n t)}{(\gamma_1)^2 + (\omega_k^n)^2} - \frac{\omega_k^n \exp(-\gamma_2 t) + \gamma_2 \sin(\omega_k^n t) - \omega_k^n \cos(\omega_k^n t)}{(\gamma_2)^2 + (\omega_k^n)^2}\right]$$

$$J_k^{nm}(t) = \tfrac{1}{2}\, h_o\left[\frac{\omega_k^{nm} \exp(-\gamma_1 t) + \gamma_1 \sin(\omega_k^{nm} t) - \omega_k^{nm} \cos(\omega_k^{nm} t)}{(\gamma_1)^2 + (\omega_k^{nm})^2} - \frac{\omega_k^{nm} \exp(-\gamma_2 t) + \gamma_2 \sin(\omega_k^{nm} t) - \omega_k^{nm} \cos(\omega_k^{nm} t)}{(\gamma_2)^2 + (\omega_k^{nm})^2}\right]$$

Similar expressions can be obtained when $h1_x^s(t)$ assumes other functional forms, such as the damped sinusoid. However, when the convolution integrals cannot be evaluated in closed form, one must resort to numerical integration. This has the effect of replacing double sums with triple sums and triple sums with quadruple sums and can greatly complicate the process of computing $h3_x(x,y,z;t)$.

The solid curves in figures 19, 20, 21, 22, 23, 24, 25, and 26 are plots of $h3_x(x,y,z,;t)$ computed with (5.47) and (5.48) for the same enclosure used to obtain figures 11, 12, and 13 where the center of the slot coincides with the center line of the enclosure ($x_c = y_c = 0$). These curves represent time histories of the magnetic field at points on the center line of the enclosure ranging from the center of the back surface of the slot ($x = y = 0$, $z = -6.44\times10^{-3}$ m) to the center of the back wall ($x = y = 0$, $z = -2.7$ m). The incident field (5.46) is characterized by $h_o = 1.1$ A/m, $\tau_1 = 1 \times 10^7$ s^{-1}, and $\tau_2 = 5 \times 10^8$ s^{-1}. These parameters produce a pulse (dotted curve) with a peak field of 1 A/m at $t = 8$ ns. It should be noted that $h3_x(x,y,z;t)$ and $h1_x^s(t)$ are plotted to the same vertical scale in figures 19 and 20, but $h3_x(x,y,z;t)$ is multiplied by a factor of 10 in the remaining figures. The time scale is in nanoseconds (ns) where 1 ns = 1×10^{-9}s, and $t = 0$ ns corresponds to the arrival of the incident field at $z = 0$.

The computer time required to complete the calculations for these figures was significantly reduced by including only the sum over n and k in (5.47), that is, by dropping the triple sum over n, m, and k. The approximation is justified in this case by figure 13, which shows that the difference between the exact and approximate expressions is relatively small and virtually independent of frequency at a location ($x = y = 0$, $z = -0.05$ m)

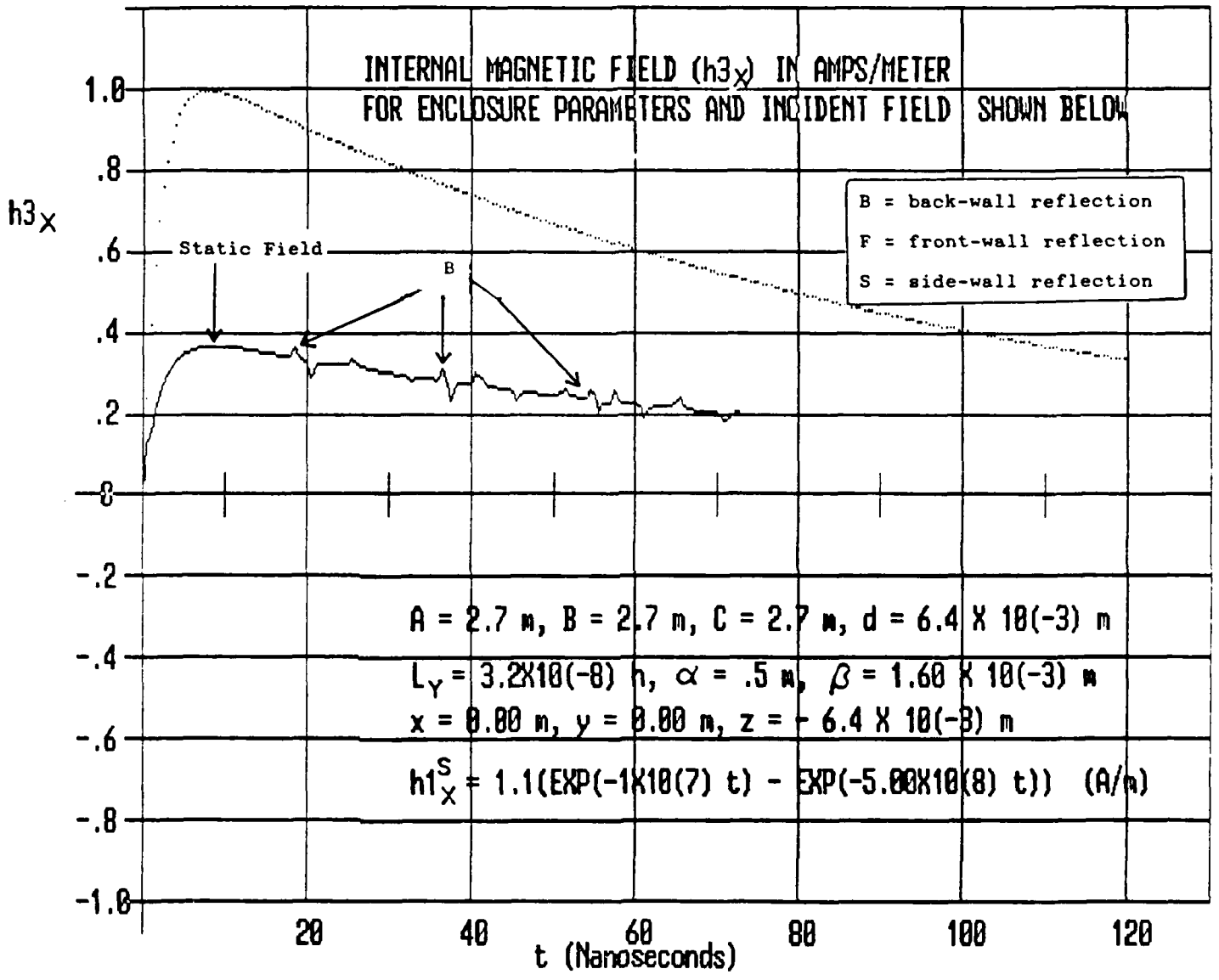

Figure 19. Transient magnetic field $h3_x$ (A/m) inside a slotted enclosure at the point ($x=y=0, z=-6.4X10^{-3}m$).

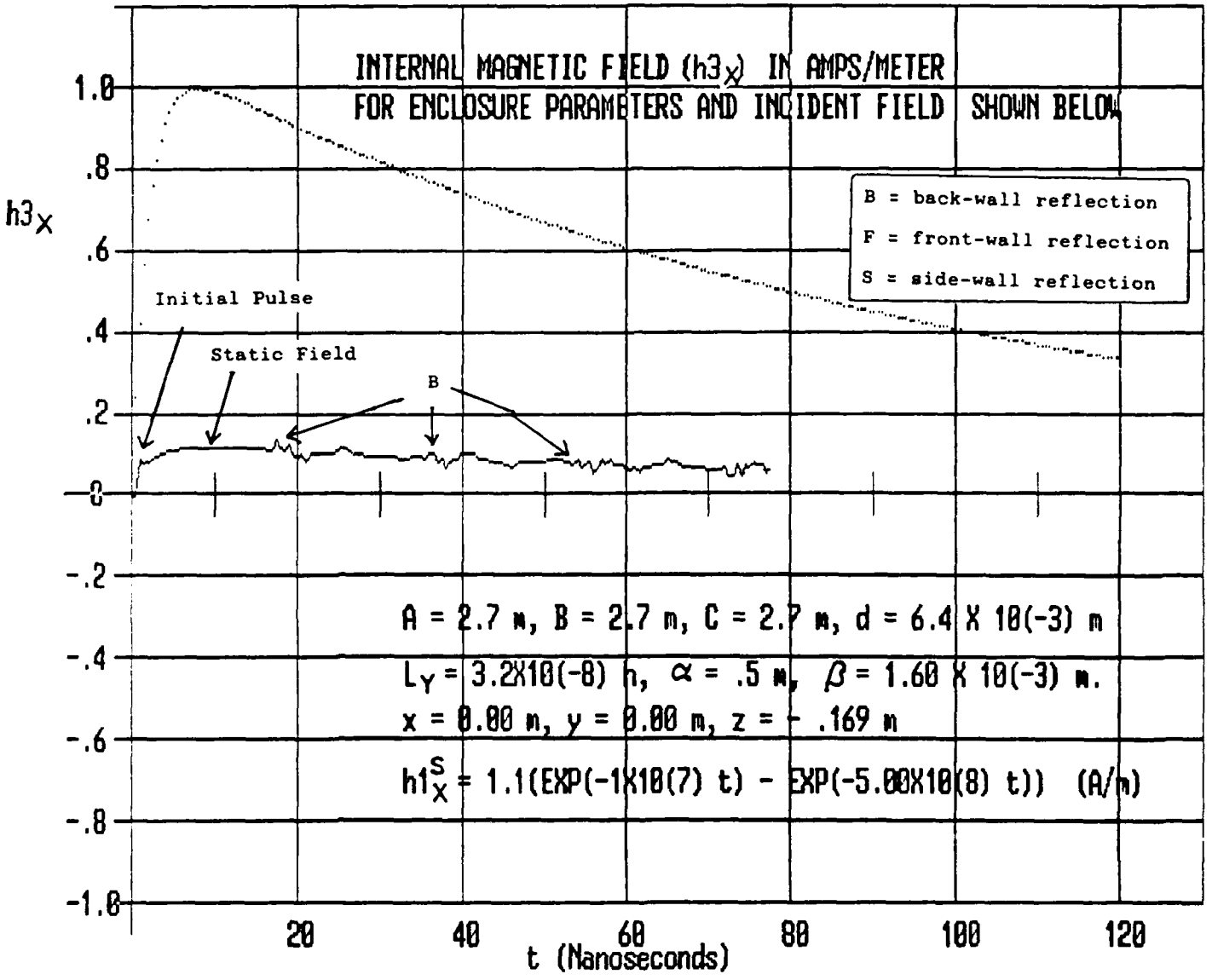

Figure 20. Transient magnetic field $h3_x$ (A/m) inside a slotted enclosure at the point (x=y=0, z=-.169 m).

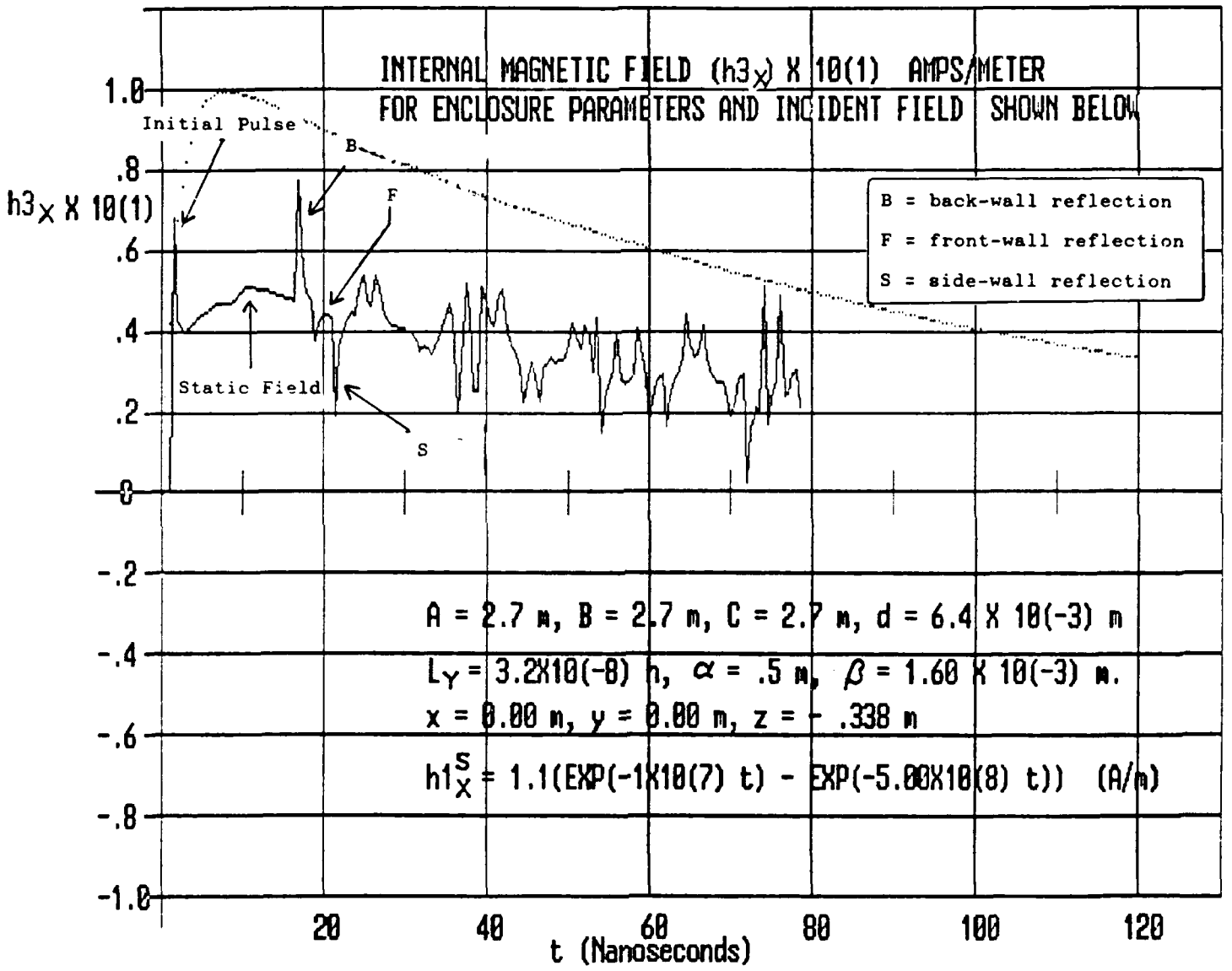

Figure 21. Transient magnetic field $h3_x$ X 10 (A/m) inside a slotted enclosure at the point (x=y=0, z=-.338 m).

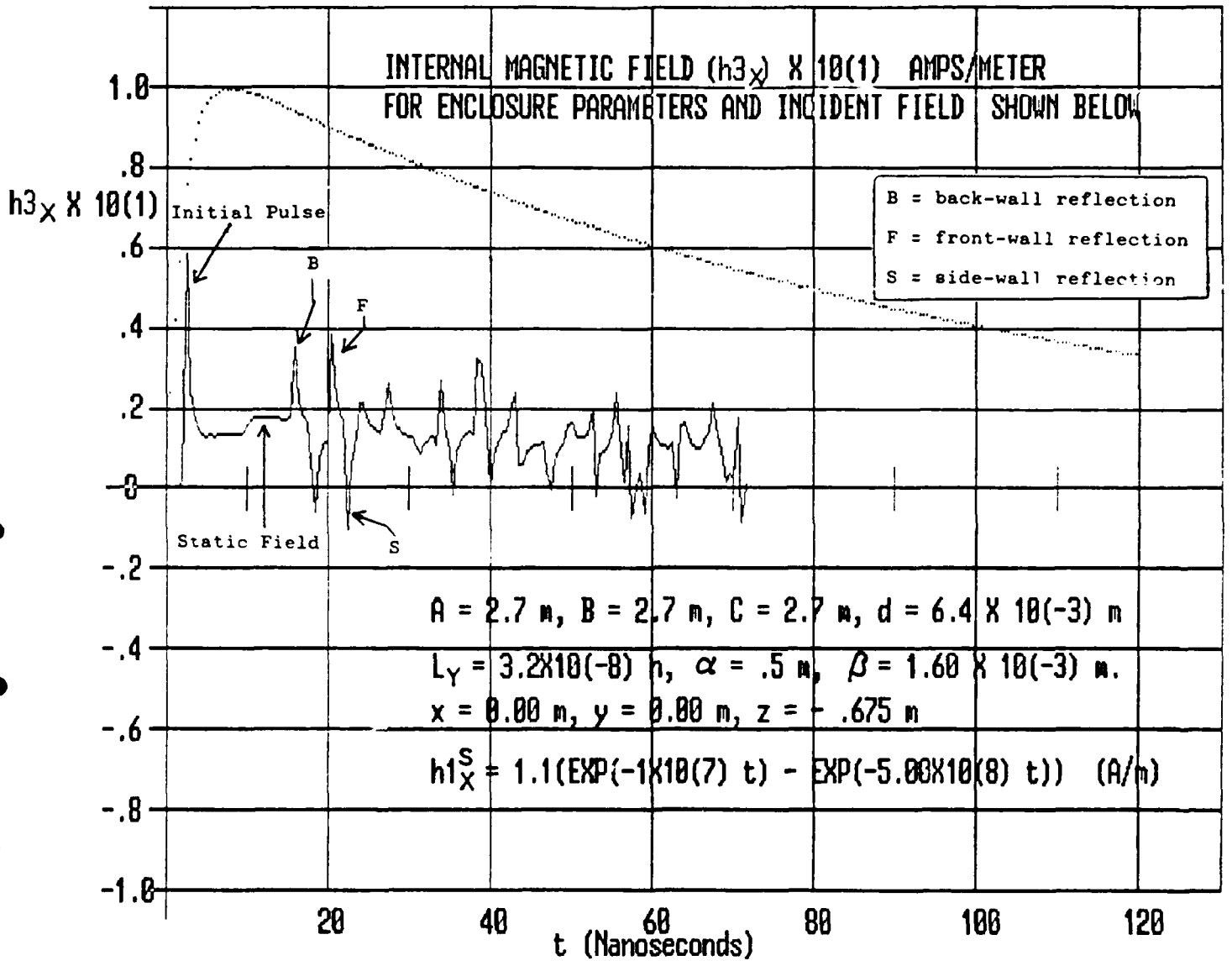

Figure 22. Transient magnetic field $h3_x$ X 10 (A/m) inside a slotted enclosure at the point (x=y=0, z=-.675 m)

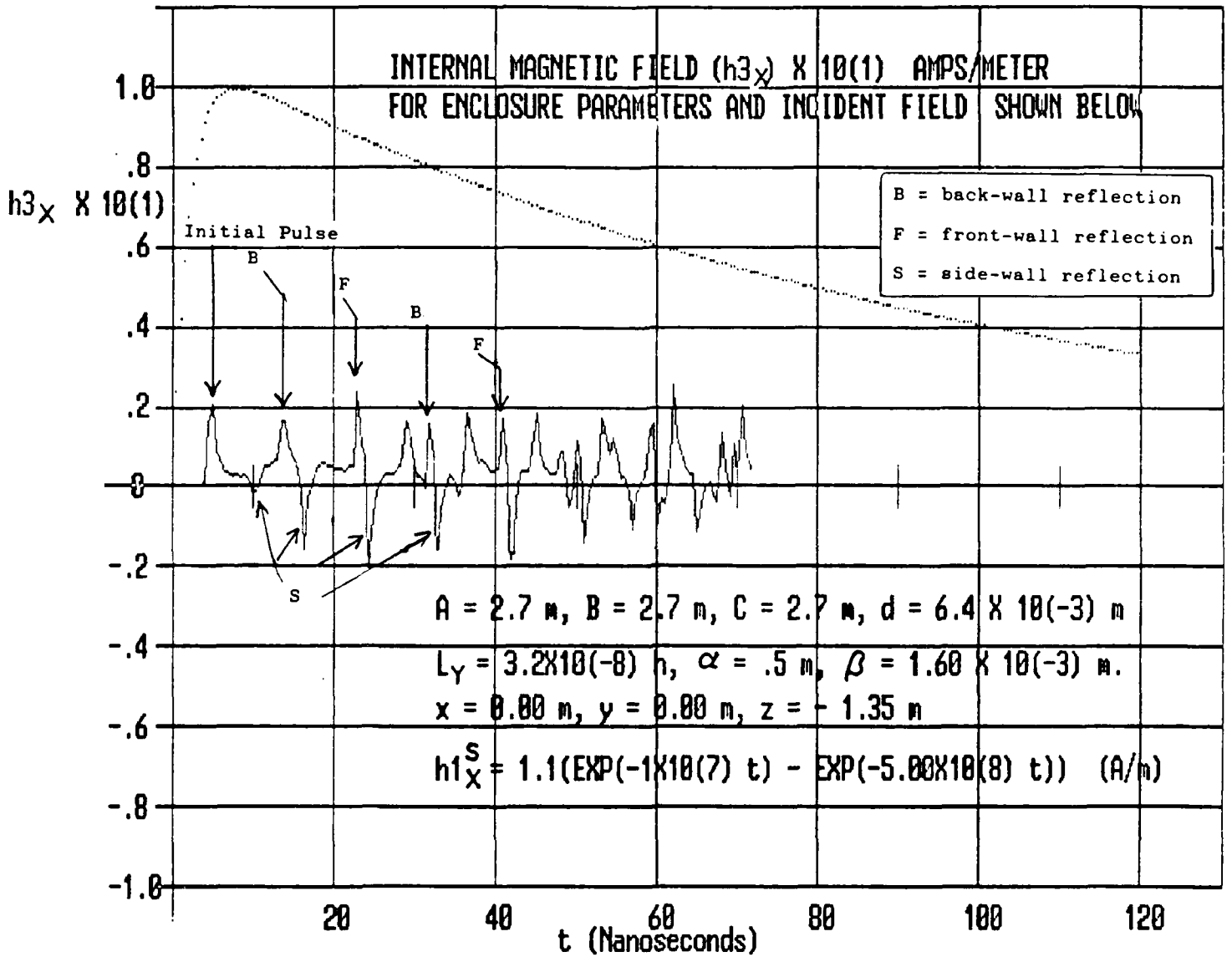

Figure 23. Transient magnetic field $h3_x$ X 10 (A/m) inside a slotted enclosure at the point (x=y=0, z=-1.35 m).

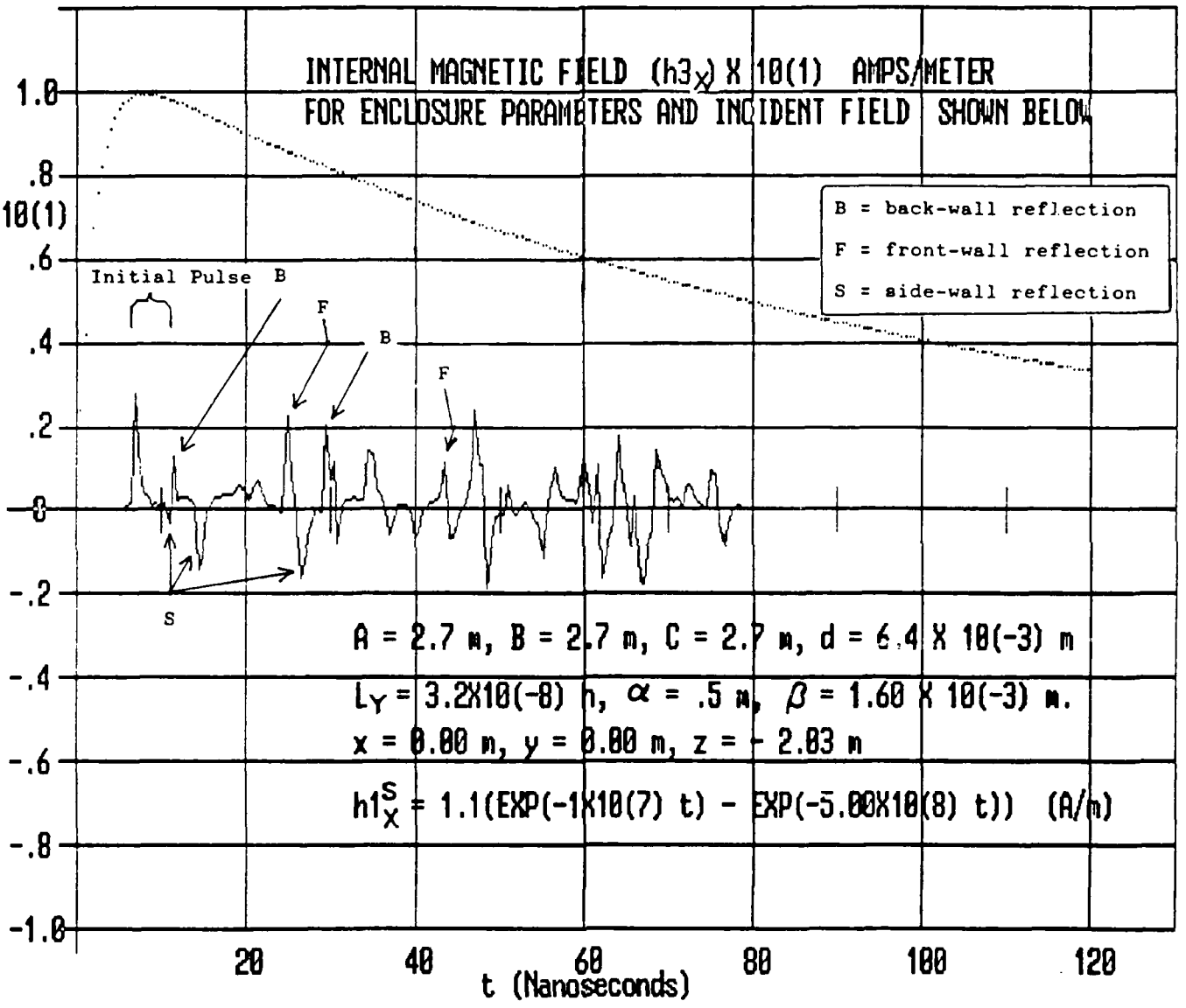

Figure 24. Transient magnetic field $h3_x$ X 10 (A/m) inside a slotted enclosure at the point (x=y=0, z=-2.03 m).

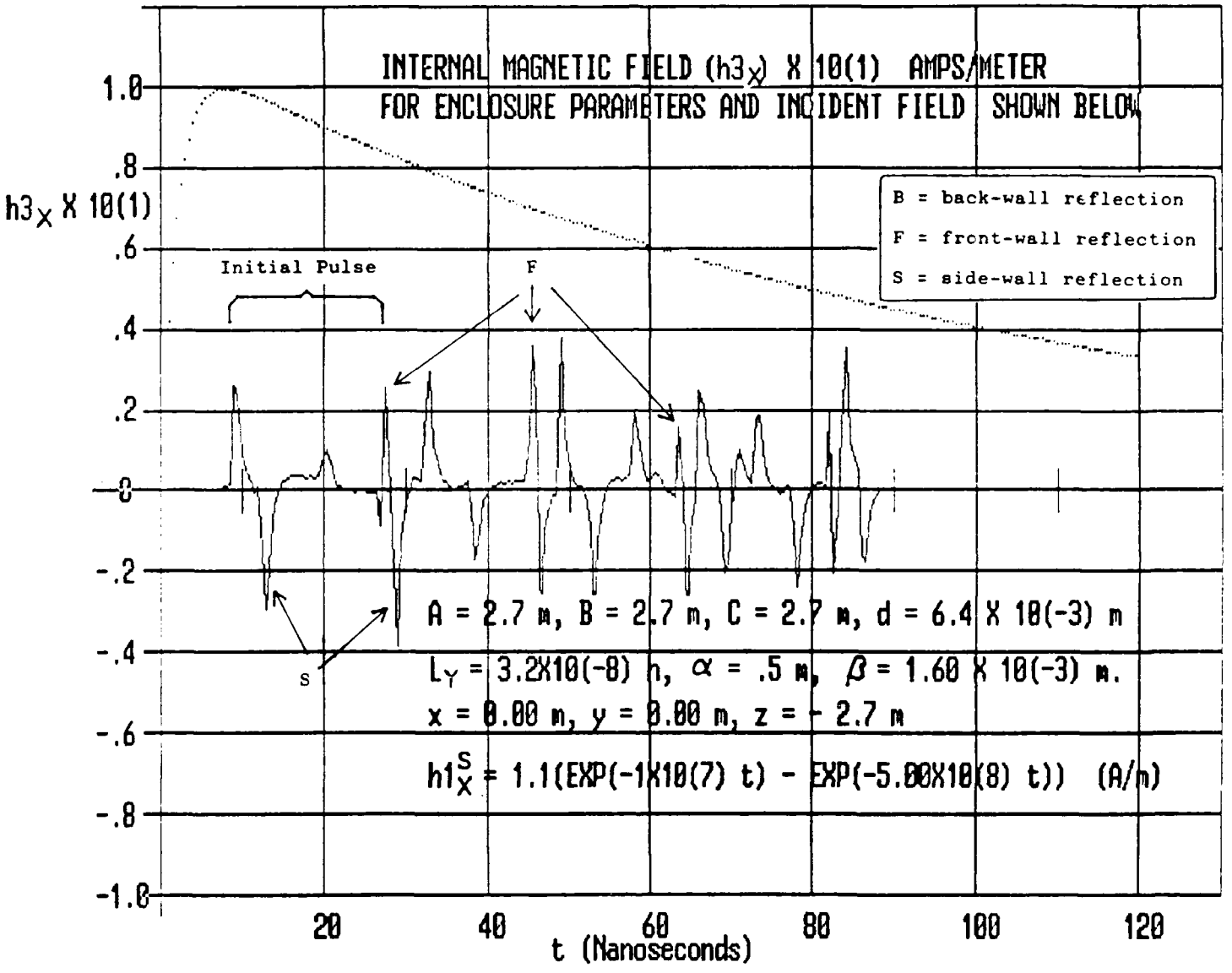

Figure 25. Transient magnetic field $h3_x$ X 10 (A/m) inside a slotted enclosure at the point (x=y=0, z=-2.7 m).

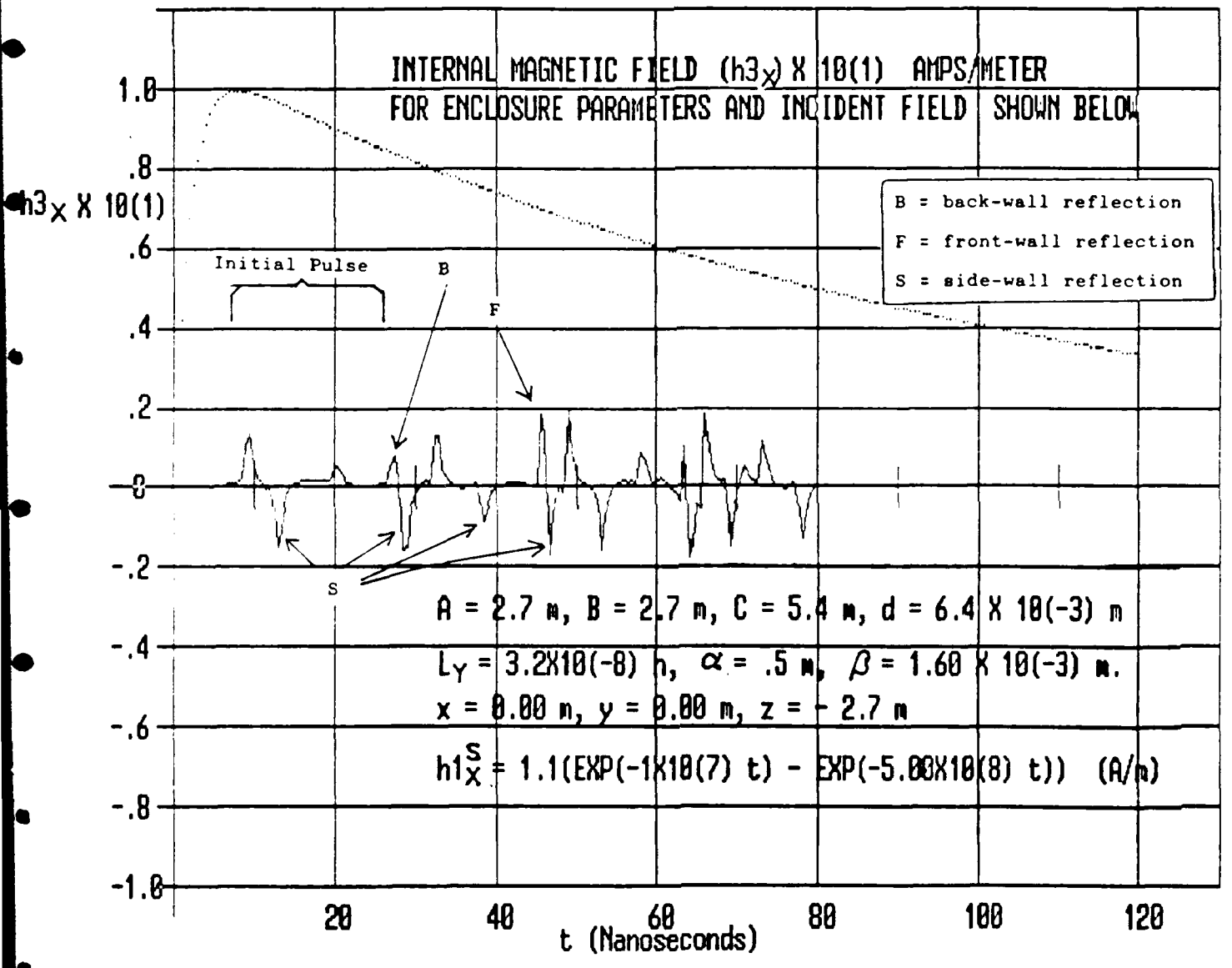

Figure 26. Transient magnetic field $h3_x$ X 10 (A/m) inside a slotted enclosure where C = 5.4 m at the point (x=y=0, z=-2.7 m).

close to the slot. Moreover, other calculations for this case show that the difference becomes even smaller as the field point moves farther away from the slot. Thus, we can expect figures 19 to 26 to accurately represent the wave form of the transient field while somewhat overestimating its magnitude at locations close to the slot. These curves were generated by truncating the series at n = 12 and k =72 and calculating $h3_x$ at time intervals of .5 ns using a PC-XT operating at 4.77 MHz. A 70 ns record required a running time of approximately 11 hours.

The field at the slot as shown in figure 19 is consistent with the one term approximation of Monroe [1] in that it consists of a unipolar (dc) pulse carrying a smaller bipolar (ac) pulse that recurs with certain variations at a fixed interval (18+ ns) corresponding to the time required by a signal moving at approximately the speed of light to reflect from the back wall and return to the front. Since the same features are seen at other points in the enclosure, we will follow Monroe and refer to these as the static or stationary field and the propagating field. As shown in figure 19, the form of the static field is close to that of the incident field and, like the latter, it approaches zero exponentially as $t \to \infty$. On the other hand, the propagating field has a much more complicated structure that changes with each

---

[1] R. L. Monroe, A Theory of Electromagnetic Shielding with Applications to MIL-STD 285, IEEE-299, and EMP Simulation, Harry Diamond Laboratories, HDL-CR-85-052-1, Adelphi, MD (February 1985).

reflection and bears no obvious resemblance to the incident field. Clearly, the static field is derived mainly from those frequencies in the incident pulse that are below the lowest TE cutoff frequency for the enclosure (flat portion of the curves in fig. 11), while the propagating field is derived from frequencies above the cutoff. Thus the propagating field will be continually reflected between the front and back walls and will continue to propagate after the static field has decayed to insignificance.

Since the static field is composed of frequencies below TE cutoff, we would expect it to decay rapidly with distance from the slot. This expectation is borne out by figures 21, 22, and 23 where it is seen that the peak static field at z = -0.68 m is only 1/20th of the peak field at the surface of the slot. When the field point moves an additional 0.65 m from the slot to the center of the enclosure as in figure 24, the static field is reduced to a barely visible level. Thus the static field is large compared to the propagating field only at points very close to the slot. At most locations in the enclosure, the propagating field dominates as shown by figures 24, 25 and 26.

The rapid decay of the static field with distance from the slot as shown by figures 20, 21, and 22 reveals the origin of the propagating field as an initial pulse that is formed from the earliest and most rapidly increasing part of the internal field. This pulse which is obscured by the static field in figure 19 is

seen first in figure 20 as a spike that peels away from the front of the static field and arrives at the observation point (z = -0.169 m) with a time delay of less than 1 ns. However, the full complexity of the initial pulse and the reflected fields it generates can be seen only at observation points where the static field is reduced to a level that allows the use of an expanded vertical scale as in figures 21 to 26. Figure 21 shows clearly the basic sequence of events that is repeated at every point inside the enclosure. First the initial pulse arrives at z = -0.338 m after a time delay relative to the external field equal to twice the time delay seen at z = -0.169. Approximately 2 to 3 ns later, the initial pulse is interrupted by the greatly reduced static field which is interrupted in turn at t ≅ 16 ns by the arrival of the reflected pulse generated by the initial pulse at the back wall. Since the reflection coefficent at the back wall is +1 , the amplitude and polarity of this reflected pulse are at first identical to that seen in the initial pulse. However, at later times (t = 18+ ns and t = 22 ns) pulses of opposite polarity appear giving the propagating field its characteristic bipolar appearance.

The presence of negative pulses is puzzling at first since they are obviously part of the field reflected from the back wall but cannot be created by such a reflection. The explanation provided by a study of the remaining figures in this series (especially fig. 24, 25, and 26) is that the initial pulse is already

bipolar by the time it reaches the back wall. This bipolarity is the result of oblique reflections from the side walls where the boundary condition requiring that $h3_x = 0$ at $x = \pm A/2$ produces a reflection coefficient of -1. Thus, an initial pulse generated with positive polarity (same polarity as the external field) at the slot $z = -6.4 \times 10^{-3}$ m becomes a bipolar pulse due to interactions with the sides of the enclosure and is further modified by reflections from the front, back, and side walls as it propagates in the enclosure. The negative sections or phases of the propagating field are labeled "side-wall" reflections in the figures; however, most of these are produced by a series of reflections involving the side wall together with the back and/ or front walls.

The earliest evidence of a negative phase in the initial pulse is the ripple that occurs in figure 21 just before the static field reaches its peak at $t \cong 10$ ns. This negative phase reappears at t = 18+ ns after reflection from the back wall, at t = 22 ns after reflection from the front wall, and at later times corresponding to the arrival of additional reflections from the back and front walls. The amplitude of the negative phase arriving from the back wall at t = 18 ns is sufficient to cancel most of the positive phase reflected from the front wall which arrives simultaneously at this location.

The principal features of the transient response are seen even more clearly in figure 22 where z = - 0.675 m. At this location, the initial pulse arrives after a time delay equal to twice the delay seen in figure 21, and its negative phase produces a more pronounced ripple as it rides on the rising portion of the static field. Since the location is now closer to the back wall and farther from the front wall, the back-wall reflection arrives earlier and the front-wall reflection later than in figure 21. This difference in arrival times effectively separates the front-wall reflection from the back-wall reflection allowing positive and negative phases of each reflection to be seen without interference.

The time delay of the initial pulse and the separation of the front- and back-wall reflections increase still more when the location moves to the center of the enclosure (z = -1.35 m). As shown in figure 23, the positive phase of the initial pulse arrives after a delay of 4+ ns, and the first back-wall reflection arrives 9+ ns later. All subsequent reflections of the positive phase are also spaced 9+ ns apart. This is exactly what one would expect at this location for a pulse traveling at a constant velocity. Furthermore, since the static field is small, the negative phase of the initial pulse is clearly visible for the first time at t = 10 ns. Subsequent reflections of the negative phase are indicated on the figure; however, these, unlike posi-

tive phase reflections, do not appear at completely regular intervals.

At the point z = -2.03 m midway between the center of the enclosure and the center of the back wall (fig. 24), the delay of the initial pulse increases to 7+ ns, and the separation between the initial pulse and its reflection from the back wall is small enough so that its negative phase partially cancels the positive phase of the reflection at t = 12 ns.

Figure 25 shows the initial pulse arriving at the center of the back wall (z = -2.7 m) with a delay of 9+ ns and combining with the reflected field to give a net field with the same form as the incident field, The initial pulse is interrupted at t = 27 ns by the return of its positive phase after reflection from the front wall. Succeeding reflections from the front wall arrive at intervals of 18+ ns corresponding to the time required for the pulse to travel from the back wall to the front wall and return. The 18 ns interval between the arrival of the initial pulse and the return of its positive phase, combined with the absence of the static field, provides the clearest picture of the initial pulse to be seen in these figures. It shows that the pulse includes not just a single cycle of positive and negative phases but also a second cycle with reduced magnitudes beginning at t = 20 ns. Evidently, the initial pulse consists of a train of such cycles generated by side-wall reflections. The folding of this train back onto itself at each reflection from the front and back

walls accounts for the increasing complexity with time of the transient waveform.

Since the reflection coefficient of the back wall is +1, we should expect the initial pulse to be doubled in magnitude when it combines with its reflection at z = -2.7 m in figure 25. One way to verify this result is to recompute the field at z = -2.7 m for the same enclosure with the back wall removed. This has been done in figure 26 by setting C = 5.4 m, that is, by analytically moving the the back wall to z = -5.4 m. Comparing figure 25 to 26, we see that the peak magnitude of the initial field in figure 25 is indeed much larger than it is in figure 26, although it falls somewhat short of being twice as large. This discrepancy may be due to plotting inaccuracies associated with our choice of a 0.5 ns time interval for these calculations.

6. COMPARISON BETWEEN COMPUTED AND MEASURED FIELDS INSIDE SHIELDED ENCLOSURES

Although rectangular enclosures have been used for at least sixty years as electromagnetic shields, there is surprisingly little experimental data in the avaliable literature that is directly relevant to this type of shield. Most published data relates to shields with simpler geometry, such as the plane sheet and the sphere. This is probably due to a desire to avoid the complexity of the rectangular geometry by using more amenable structures that might be expected to approximate the rectangular enclosure for certain ranges of frequency, for example, the sheet for very high frequencies and the sphere for very low frequencies. Moreover, those reports that do provide data on rectangular enclosures frequently fail to disclose all the relevant information. Examples of commonly omitted information are the enclosure dimensions, the location of the internal field sensor, and the locations and orientation of slots and seams.

In this section, we reproduce two of the most complete sets of experimental shielding data for rectangular enclosures and compare this data to calculations based on the theoretical expessions we have developed in the preceding sections. Both sets are frequency domain data and, as is the usual practice for measurements of this type, are expressed in terms of the shielding

effectiveness (or shielding efficiency) SE of the enclosure. SE is defined as follows:

$$SE = -20 \log\left[\frac{|H_p|}{|H_p^o|}\right] \quad \text{(dB)} \qquad (6.1)$$

where H_p is the pth component of the magnetic field measured at a specified location inside the enclosure generated by a specified source outside the enclosure and H_p^o is the same component generated by the same source at the same location when the enclosure walls and ceiling have been removed. That is, H_p is the shielded field at a location, H_p^o is the unshielded field at the same location due to the same source, and the logarithmic difference between the magnitudes of these quantities in dB is defined as the shielding effectiveness of the enclosure at that location. This definition is intended to characterize the shielding properties of the enclosure in a way that is independent of the source except for its frequency. If SE can be measured in a way that is independent of the source, then it can be used to predict the shielding performance of the enclosure against the magnetic field from any source, provided that the frequency of source is known. However, in general, it is not possible to measure SE at any point inside an enclosure in a way that is independent of the source. This is due to the fact that two different sources S_1 and

S_2 will produce unshielded fields, say H_p^{o1} and H_p^{o2}, that vary in different ways throughout the volume such that in general at any location

$$|H_p^1|/|H_p^{o1}| \neq |H_p^2|/|H_p^{o2}| \tag{6.2}$$

where H_p^1 and H_p^2 are the shielded fields corresponding to S_1 and S_2 respectively. Nevertheless, there are classes of sources for which

$$|H_p^1|/|H_p^{o1}| = |H_p^2|/|H_p^{o2}| \tag{6.3}$$

for any sources S_1 and S_2 belonging to such a class. In this case, when SE is obtained from (6.1) using measurements made with one source belonging to this class, it characterizes the shielding of the enclosure with respect to all sources in that class. That is, once SE is determined in this way, it can be used to predict the shielding properties of the enclosure against magnetic fields from any source belonging to this class. An example of a class of sources for which (6.3) holds is the class of all sources that generate spatially uniform unshielded fields throughout the region of interest. For any two sources S_1 and S_2 belonging to this class

$$H_p^{o1} = A_o(j\omega)\, H_p^{o2} \tag{6.4}$$

at each point where $A_o(j\omega)$ may be a constant or a function of frequency but is independent of the spatial variables. In this case, the shielded fields will obey the same relationship:

$$H_p^1 = A_o(j\omega)\, H_p^2 \tag{6.5}$$

at each point and (6.3) will be satisfied. Consequently, SE as

defined by (6.1) completely characterizes the shielding properties of the enclosure with respect to the class of sources that expose the enclosure to spatially uniform fields.

We can use our expression for the field inside a continuous enclosure exposed to uniform fields on one wall to compute the theoretical shielding effectiveness of these structures against the class of uniform sources by substituting $H3_p(x,y,z;j\omega)$ from (4.6) for the shielded field H_p and $H1_p^s(j\omega)$ for the unshielded field H_p^o in (6.1):

$$SE(x,y,z;\omega) = -20 \log\left[\frac{|H3_p(x,y,z;j\omega)|}{|H1_p^s(j\omega)|}\right] . \qquad (6.6)$$

(When more than one wall is exposed to the field the contributios from all must be added at the specified location to determine the total unshielded field $H3_p(x,y,z;j\omega)$). Calculations using (6.6) can then be compared with measurements based on (6.1) to determine whether or not the theory is supported by experiment. It should be noted from (6.6) that SE is a function of the spatial variables even though the unshielded field is not.

6.1 Continous Copper Enclosure with Soldered Joints

In 1964, J. B. Hays[18] published the results of shielding measurements that had been carried out by E. D. Sunde[19] on an 8 x 8 x 8 ft. cubical structure constructed from 10 mil copper sheets soldered together along their edges. The experimental set-up used in these measurements is represented schematically in part A) of figure 27. It consists of a signal generator driving a circular coil 80 ft. in diameter surrounding the copper cube which contains a smaller coil used as a magnetic field detector. The purpose of the large coil and generator is to produce an unshielded magnetic field with a single spatially uniform component H_y^o over the volume occupied by the enclosure. This allows easy determination of H_y^o ,which can then be combined with the shielded field H_y measured by the loop detector to give SE using (6.1). With this setup, Sunde was able to measure the shielding effectiveness of the copper cube over a frequency range from less than 100 Hz to 40 kHz. His data (reproduced from curve d of fig. 1 in reference 18) is shown as the broken line in part B) of figure 27.

The solid curve in part B) is the computed shielding effectiveness obtained with the aid of $H3_y(y,z;j\omega)$ from equation

---

[18] J. B. Hays, IEEE Spectrum, Vol 1 , May (1964).

[19] E. D. Sunde, Switching Center Shielding Against Atmospheric Induction, Bell Telephone Laboratories (unpublished memorandum).

(a) experimental setup

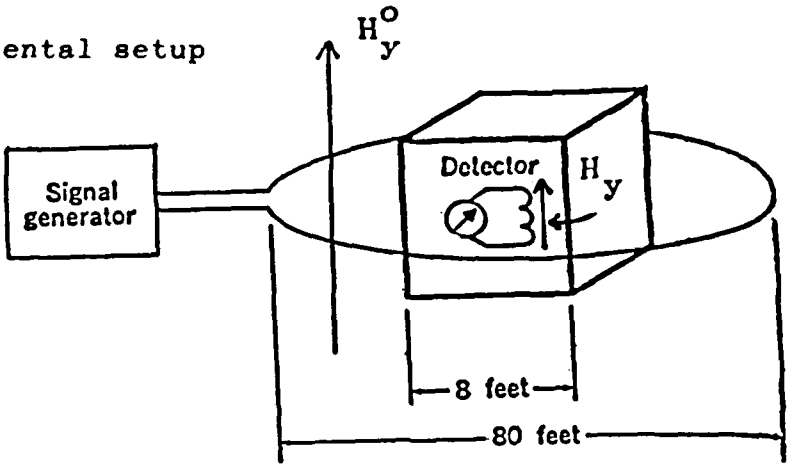

(b) comparison of measured and computed shielding effectiveness

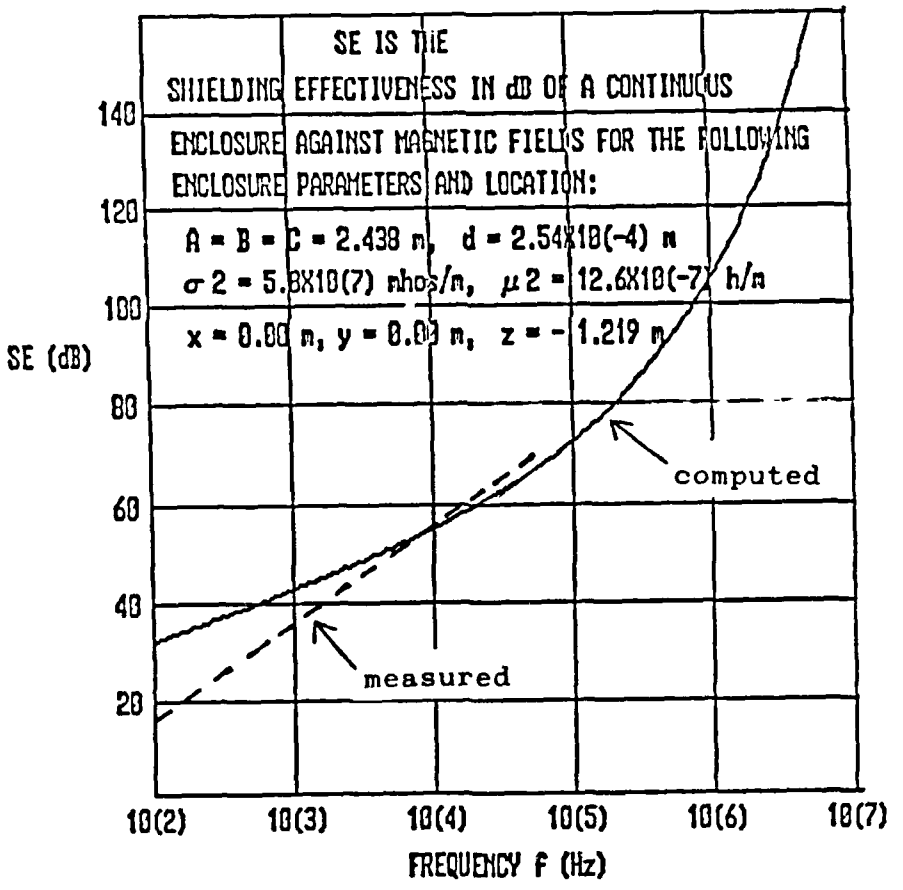

Figure 27. Shielding effectiveness (SE) of a cubical copper enclosure with soldered joints: experimental setup and comparison of measured and computed shielding effectiveness.

4.6). In applying this expression to the setup shown in part B), it was assumed that the detector was located at the center of the cube which in our standard coordinate system is given by x = y = 0, z = -1.219 m. (The actual location was not mentioned by Hays, but it appears highly likely that a desire to preserve symmetry would have dictated this choice). Since the total field at the center of a uniformly illuminated cube is the sum of equal contributions from fields entering through each of the cube's four vertical walls, the theoretical expression for the shielded field at this location is 4 $H3_y(0,-1.219;j\omega)$ and the computed shielding effectiveness is obtained by evaluating

$$SE(0,0,-1.219;\omega) = -20 \log\left[\frac{4\ |H3_y(0,-1.219;j\omega)|}{|H1_y^s(j\omega)|}\right] \qquad (6.7)$$

as a function of $f = \omega/2\pi$ for

$A = B = C = 2.438$ m, $d = 2.54\times10^{-4}$ m

$\sigma 2 = 5.8\times10^{7}$ mhos/m, $\mu 2 = 12.6\times10^{-7}$ h/m.

Comparison of the two curves shows good agreement at the higher frequencies. There is, however, a divergence below 4 kHz that causes the measured values of SE to fall below the computed values. This divergence may be due to the fact that condition (2.8) is not satisfied at these frequencies for 10 mil copper sheets. That is, the thickness of the sheet is not larger than the skin depth of the field in the sheet at these frequencies as assumed by the theory. This means that multiple reflections can

occur inside the sheet which may result in a larger internal field and a smaller shielding effectiveness than can be accounted for by the theory in its present form.

6.2 Slotted Steel Enclosure

The effect of slot length α on the shielding effectiveness of a cubical steel enclosure was investigated by E. M. Honig, Jr.[20] using the experimental setup shown in part (a) of figure 28. Unlike the arrangement employed by Sunde for the continuous enclosure, this setup is not designed to generate a spatially uniform source field. Instead, a small loop source is used to generate a strongly nonuniform field throughout the volume occupied by the enclosure. The advantages of Honig's setup are that it can be used at higher frequencies and generally produces a greater dynamic range for measurements on enclosures of this size than does Sunde's. Its disadvantage is that measurements of SE made in this way using (6.1) depend on the location of the source. That is, the same source located at a different position with respect to the enclosure and the detector would produce a different value of SE. Similarly, a larger or smaller source at the same position might produce a different value of SE. To mitigate this limitation, Honig has chosen the setup

---

[20] E. M. Honig, IEEE Trans. Electromagn. Compat., Vol EMC-19, No.4 (Nov. 1977). p 377.

(a) experimental setup

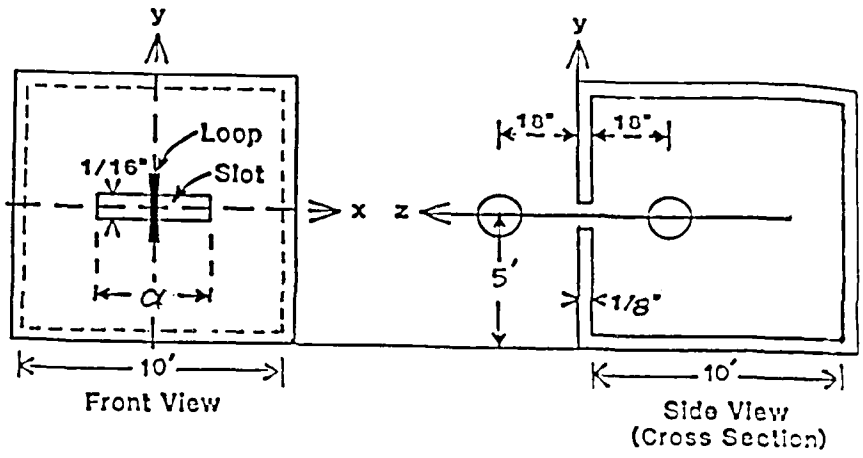

(b) comparison of measured and computed shielding effectivenness

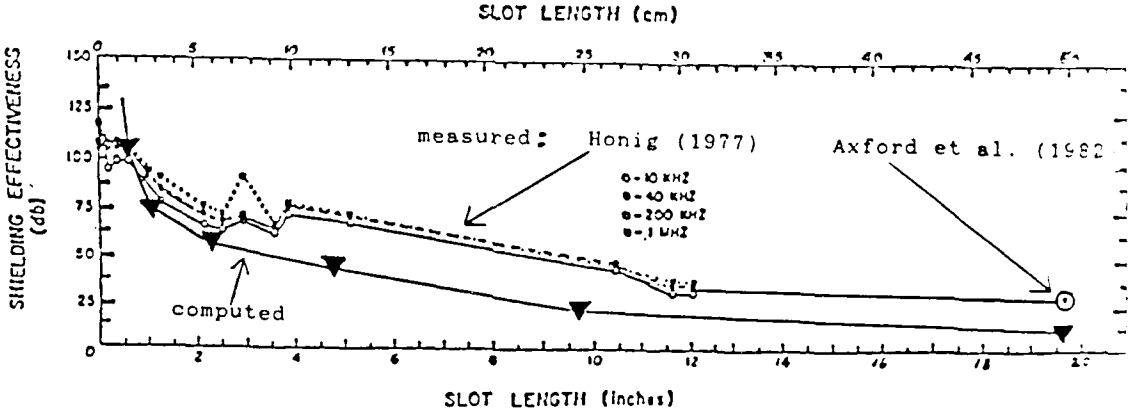

Figure 28. Shielding effectiveness (SE) of a slotted steel cube: experimental setup and comparison of measured and comput shielding effectiveness.

called for by two widely used standards for shielding measurements: MIL-STD 285[21] and IEEE 299[22] which specify that the source and the detector shall be identical circular loop antennas 12 in. in diameter lying in the same plane (coplanar arrangement) with centers 18 in. from the enclosure wall. With this set-up, Honig's measurements can be compared directly to other measurements made using these same standards, even though they would not in general be comparable to measurements made on the same enclosure using a different source such as Sunde's large loop. In accordance with these standards, Honig orients the plane of his loops perpendicular to the long axis of the slot. This orientation produces the most efficient coupling through slots of any size and insures that his measured values of shielding effectiveness will be the smallest possible for this setup. It allows him to measure the shielding effectiveness of slots ranging from 1 to 30.5 cm in length at frequencies of 10 kHz, 40 kHz, 200 kHz, and 1 MHz for each slot. The procedure is to remove the enclosure wall containing the slot and measure the unshielded field H_x^o at the detector loop due to the source loop and then to replace the wall and measure the shielded field H_x at the

---

[21]Dept of Defense, MIL-STD-285, Method of Attenuation Measurements for Enclosures, Electromagnetic Shielding, for Electronic Test Purposes (25 June 1956).

[22]IEEE, Proposed IEEE Recommended Practices for Measurement of Shielding Effectiveness of High Performance Shielding Enclosures, IEEE 299, IEEE Inc. NY (June 1969).

detector without changing the arrangement of the loops from that shown in the figure. The latter step is then repeated as the slot length is increased in specified increments. The measured shielding effectivness for each length is determined by (6.1).

Honig's data from figure 8 in his report is plotted versus slot length in part (b) of figure 28 along with a data point obtained by Axford et al.[23] who measured the shielding effecetiveness of a cubical steel enclosure with a 50 cm slot using a very similar setup. The data shows a strong general trend in the direction of decreasing shielding effectiveness with increasing slot length. However, there is a notable subset of the data (α = 7.5 , 10, and 13.5 cm) where this trend is reversed. The plot also shows that, with the exception of one point (α = 7.5 cm), the data for each slot is closely grouped indicating that the shielding effectiveness is virtually independent of the source frequencies used in these measurements.

Although Honig's loop source generates a nonuniform unshielded field $\bar{H}^{o}(x,y,z;j\omega)$ throughout most of the volume occupied by the slotted enclosure, it will produce a nearly uniform

---

[23]R. Axford, R. McCormack, and R. Mittra, Evaluation of the Applicability of Standard CW EMI/RFI Shielding Effectiveness Test Techniques to Assessment of EMP Hardness of Tactical Shelters, Construction Engineering Research Laboratories, CERL-TM-M-307 Urbana, IL (March 1982).

field over a slot positioned like the one shown in the figure provided the slot is not too long. For such a slot, we can calculate the field $H3_x(x,y,z;j\omega)$ at any point inside the enclosure in terms of the tangential compnent of the unshielded loop field $H_x^o(0,0,0;j\omega)$ incident on the slot by setting $H_x^o(0,0,0;j\omega) = H1_x^s(j\omega)$ in equation (4.24). With this substitution, the shielded field at the center of the detector loop (0,0,-0.49 m) due to the source loop is $H3_x(0,0,-0.49\ m;j\omega)$, and the theoretical expression for the shielding effectivness that would be measured at that location using Honig's set-up is

$$SE(0,0,-.49m;\omega) = -20\ \log\left[\frac{|H3_x(0,0,-.49m;j\omega)|}{|H_x^o(0,0,-.49m;j\omega)|}\right] \qquad (6.8)$$

where $H_x^o(0,0,-0.49\ m;j\omega)$ is the unshielded source field at the center of the detector loop. Since $H3_x(0,0,-0.49\ m;j\omega)$ is computed in terms of $H_x^o(0,0,0,;j\omega)$, it is also convenient to write the field $H_x^o(0,0,-0.49\ m;j\omega)$ in terms of $H_x^o(0,0,0;j\omega)$. This is easily done using the fact that points (0,0,0) and (0,0,-0.49 m) are both in the near field of the source loop where the magnitude of the field is inversely proportional to the cube of the distance to the center of the loop[1]. In this case, since (0,0,-0.49 m) is twice as far from the center of the source loop as (0,0,0), the

---

[1]R. L. Monroe, A Theory of Electromagnetic Shielding with Applications to MIL-STD 285, IEEE-299, and EMP Simulation, Harry Diamond Laboratories, HDL-CR-85-052-1, Adelphi, MD (February 1985).

magnitude of $H_x^o(0,0,-0.49\ m;j\omega)$ will be equal to 1/8 that of $H_x^o(0,0,0;j\omega)$. Thus (6.8) can be rewritten

$$SE(0,0,-.49m;\omega) = -\ 20\ \log\left[\frac{8\ |H3_x(0,0,-.49m;j\omega)|}{|H_x^o(0,0,0;j\omega)|}\right] . \qquad (6.9)$$

Since $H3_x(0,0,-0.49\ m;j\omega)$ is directly proportional to $H_x^o(0,0,0;j\omega)$, this term drops out when (6.9) is evaluated; and SE is seen to depend on the source only through the factor 8.

The calculated shielding effectivness for Honig's setup is denoted by the solid triangles at α = 1.56, 3.13, 6.25, 12.5, 25, and 50 cm in part (b) of figure 28. This plot was obtained by evaluating (6.9) for each α (expressed in meters) at a frequency of 10 kHz. Only a single frequency was required because previous calculations (fig. 11 and 12) based on equation (4.24) demonstrated that $H3_x(x,y,z;j\omega)$ is independent of frequency for frequencies below the cutoff frequency of the enclosure. The enclosure parameters used in these calculations are

$A = B = C = 2.7\ m\ ,\ d = 6.4\times10^{-3}\ m$

$\sigma 2 = 4\times10^{6}$ mhos/m, $\mu 2 = 12.6\times10^{-5}$ h

and the slot inductance for each slot length α (meters) was computed with equation (4,29):

$L_y = 6.4 \times 10^{-8}\ \alpha$ (henries)

which was derived from figure 7 of Monroe[14]. Since Honig did not specify the location of the slots, it was assuned that they are centered at the center of the wall where $x_c = y_c = 0$.

Comparison of the measured and computed shielding effectiveness curves shows good agreement for slots less than 6 cm in length. A divergence occurs at $\alpha = 7.5$ cm, where the measured shielding effectiveness is larger than the preceding measurments at 5.5 and 6.5 cm rather than smaller as shown by the computed curve. Similar divergences occur at $\alpha = 10$ and 13.5 cm. These data points run counter to the general trend of both measured and computed curves and are difficult to explain on physical grounds since they would require a type of antiresonant behavior that appears to be ruled out at the frquencies used in the measurements. Consequently, the validity of these three points appears to be open to question. If they were eliminated, the measured curve like the computed curve would show SE as a monotonically decreasing function of α, and the overall agreement would be noticeably improved. For very small slots (< 1 cm), SE exceeds the dynamic range of Honig's measurements (100 to 125 dB), and, therefore, valid comparisons cannot be made. However, the figure suggests that SE will continue to increase monotonically as slot

---

[14]R. L. Monroe, EMP Shielding Effectiveness and MIL-STD 285, Harry Diamond Laboratories, HDL-TR-1336, Adelphi, MD. (July 1973).

length decreases, until it approches the shielding effectiveness of an enclosure with no slot, that is, until it approaches the shielding effectiveness of a continuous steel enclosure. To calculate this limit, it would be necessary to use a modified version of (6.9) where $h3_x(0,0,-0.49\ m;j\omega)$ is computed with an expression similar to (4.6).

7. CONCLUSIONS

In the preceding pages, we have used a theory of electromagnetic shielding based on impedance boundary conditions to obtain general expressions for the fields at any point inside slotted and continuous rectangular enclosures exposed on one side to arbitrary external source fields. These expressions consist of infinite series summed over the TE waveguide modes where each term is the product of one or more mode functions and a Fourier coefficient. In the case of the slotted enclosure, the Fourier coefficients are determined by the spatial distribution of the magnetic field incident on the inside surface of the wall due to the slot, and for the continuous enclosure they are determined by the spatial distribution of the magnetic field incident on the outside surface of the wall. These coefficients were evaluated in closed form for the case where the outside surface of the slot is exposed to a spatially uniform magnetic field and for the case where the entire outside surface of the continuous enclosure is exposed to a spatially uniform magnetic field. Frequency domain calculations based on these expressions showed that the series converge rapidly. This allowed easy plotting of the internal magnetic fields as functions of frequency with the aid of a microcomputer. The plots show that at frequencies below the cutoff frequency the field inside a typical slotted enclosure is independent of frequency and the field inside a continuous

enclosure is a monotonically decreasing function of frequency. At frequencies above cutoff, the fields in both slotted and continuous enclosures show very complex behavior associated with cavity resonances. The spatial variation of the internal fields is determined by the boundary conditions at the inside surfaces of the walls. The field reaches its maximum at the exposed wall and decreases monotonically as one moves to the opposite wall.

The frequency domain expressions were replaced by series approximations and transformed into the time domain using a term by term application of the inverse LaPlace transform. The transformed series were found to converge, and they were used to compute and plot the transient response of the internal magnetic fields when one wall of the enclosure is exposed to time-varying external fields in the form of decaying exponentials, damped sinusoids, or rationalized exponentials. These plots showed quite different responses for the continuous and slotted enclosure in agreement with the results of Monroe [1] who computed the transient fields at one point on the inside surface of the exposed wall using one-term approximations. It was found that the characteristics of the field inside a continuous enclosure are determined to a great extent by the diffusion time factor τ (eq 5.4) and by

---

[1] R. L. Monroe, A Theory of Electromagnetic Shielding with Applications to MIL-STD 285, IEEE-299, and EMP Simulation, Harry Diamond Laboratories, HDL-CR-85-052-1, Adelphi, MD (February 1985).

the duration of the incident field. The former determines the shortest, that is, fastest, rise time possible by the internal field, and the latter determines its largest value. Plots of the fields inside slotted enclosures showed a transient response consisting of the sum of stationary and propagating fields. The stationary field dominates close to the slot where it forms a reduced replica of the external field. However, its peak field decreases rapidly with distance from the slot so that at most locations in the interior it is negligible compared to the propagating field. The latter travels at approximately the speed of light and undergoes repeated reflections from the front, back, and sides of the enclosure. These reflections produce a waveform that becomes increasingly complex with time. The separation of the internal field into these two constituents corresponds to a separation of the incident field into the sum of frequencies lying above and below the cutoff frequency with the propagating field formed from frequencies above cutoff and the stationary field formed from those below. The peak value of the stationary field depends principally on the length of the slot, while the peak of the propagating field depends on the rise time of the external field. That is, longer slots produce larger stationary fields and faster rise times produce larger propagating fields.

Finally, calculations based on the frequency domain expressions were used to compare the theoretical results with two sets of experimental data: one set by E. D. Sunde[18,19] for a continuous cubical enclosure formed from soldered copper sheets and the other by E. M. Honig[20] for a cubical steel enclosure with one wall penetrated by single slot with a variable length. Since the data was presented in terms of the measured shielding effectiveness SE of each enclosure, it was necessary to construct theoretical expressions for SE corresponding to the experimental setups of both Sunde and Honig using $H3_y(y,z;j\omega)$ from equation (4.6) and $H3_x(x,y,z;j\omega)$ from equation (4.24). Computed values of SE were then plotted together with the experimental values for easy comparison. In the case of the copper enclosure, good agreement is found for frequencies above 4 kHz, but a significant divergence occurs at extremely low frequencies. For the slotted enclosure, there is good agreement for slots less than 6 cm in length, but a divergence is seen for longer slots where some of the experimental data points show longer slots providing greater shielding than some shorter slots. Since good agreement is seen

---

[18] J. B. Hays, IEEE Spectrum, Vol 1 , May (1964).

[19] E. D. Sunde, Switching Center Shielding Against Atmospheric Induction, Bell Telephone Laboratories (unpublished memorandum).

[20] E. M. Honig, IEEE Trans. Electromagn. Compat., Vol EMC-19, No.4 (Nov. 1977). p 377.

where the theory is expected to be most accurate (high frequencies for continuous enclosures and short slot lengths for slotted enclosures), the overall comparison provides a satisfactory verification of the theory within its present limits.

These results establish a theoretical basis for the principal features of electromagnetic shields formed from rectangular enclosures. However, they do not exhaust the subject. There remain many areas open for further investigation relating to both the general shielding theory and its application to practical shielded enclosures.

One area for possible future development is an extension of the general shielding theory to include thin-walled structures where conditions (2.8) and (2.20) ar not satisfied. Such an extension might eliminate the divergence between measured and computed SE for the thin-walled copper enclosure at extremely low frequencies and clear the way for accurate calculations at still lower frequencies. It might also close the gap between theory and measurement for enclosures with long slots and lead to corresponding results for an enclosure with a resonant slot. (Although the effect of a resonant slot can be partially accounted for simply by replacing η_x^2 or η_y^2 in (3.35) with a general

expression for the slot impedance[14], this would not change the fact that condition (2.20) would not be satisfied, and consequently the accuracy of the resulting expression could not be guaranteed). To make this extension with assurance, it would be necessary to replace the simple impedance boundary conditions (2.2) and (2.10) with more general forms that account for multiple reflections inside the walls and slots of the enclosure. If these boundary conditions can be developed, then there appears to be no reason why the remainder of the extension cannot be carried out in nearly the same manner as the original. The extension would, of course, be more complicated than the original, but its likely advantage would compensate for the added complexity

An extension of the theory to enclosures with slots filled with lossy dielectrics could also be very useful. This extension would include both the inductive (air filled) and resistive slots as special cases and would be a natural model for the radio frequency gasket- a device that is often used in practical enclosures to reduce the magnitude of unwanted fields in open seams. It could also be used to model the effect of paints and metal oxides that tend to build up in any unintended opening. These results could be incorporated directly into the theory in its present form by regarding the slot as a rectangular waveguide

---

[14]R. L. Monroe, EMP Shielding Effectiveness and MIL-STD 285, Harry Diamond Laboratories, HDL-TR-1336, Adelphi, MD. (July 1973).

filled with a lossy dielectric and adapting the existing theory[12] of these structures to the shielding problem.

A reader who has followed the development to this point will no doubt be able to suggest many other areas for further research on this interesting subject.

---

[12] R. E. Collin, Field Theory of Guided Waves, McGraw-Hill, New York (1960).

LITERATURE CITED

[1]R. L. Monroe, A Theory of Electromagnetic Shielding with Applications to MIL-STD 285, IEEE-299, and EMP Simulation, Harry Diamond Laboratories, HDL-CR-85-052-1, (February 1985).

[2]S. A. Schelkunoff, Electromagnetic Waves, Van Nostrand, Princeton, NJ (1943).

[3]T. B. A. Senior, Appl. Sci. Res., 8(B) (1960), 418.

[4]T. B. A. Senior, IEEE Trans. on Antennas Propagt., AP-29, No. 2 (1981). 826.

[5]M. A. Leontovich, Investigation of Radiowave Propagation, Part II, Moscow: Academy of Sciences (1948).

[6]S. M. Rytov, J. Exp. Theor. Phys. USSR, 10 (1940), 180.

[7]I. L. Alpert, J. Tech. Phys., USSR, 10 (1940), 1358..

[8]E. L. Feinberg, J. Phys. USSR, 8 (1944), 317.

[9]W. Jarva, IEEE Trans. EMC, EMC-12 (1970), 12.

[10]R. B. Adler, L. J. Chen, and R. M. Fano, Electromagnetic Energy Transmission and Radiation, John Wiley and Sons, Inc., NY (1960) p 432.

[11]P. C. Clemmow, The Plane Wave Representation of Electromagnetic Fields, Pergamon Press, Oxford (1966)

[12]R.E. Collin, Field Theory of Guided Waves, McGraw-Hill, NY (1960).

[13]V. M. Papadoppoulos, Quart. J. Mech. and Appl. Math., vol. 7 (September 1954) 325.

[14]R. L. Monroe, EMP Shielding Effectiveness and MIL-STD 285, Harry Diamond Laboratories, HDL-TR-1336, Adelphi, MD (July 1973).

[15]G. Doetsch, Guide to the Application of LaPlace Transforms, D. Van Nostrand and Company, London (1961).

[16]G. A. Campbell and R. M. Foster, Fourier Integrals for Practical Applications, D. Van Nostrand and Company, Princeton NJ (1948).

[17]E. C. Titchmarsh, The Theory of Functions, 2d Ed., Oxford University Press (1939).

[18]J. B. Hays, IEEE Spectrum, vol 1, (May 1964).

[19]E. D. Sunde, Switching Center Shielding Against Atmospheric Indution, Bell Telephone Laboratories (unpublished memorandum).

[20]E. M. Honig, IEEE Trans. EMC, EMC-19 (1977), 377.

[21]Department of Defense, MIL-STD-285, Method of Attenuation Measurements for Enclosures, Electromagnetic Shielding for Electronic Test Purposes (25 June 1956).

[22]IEEE, Proposed IEEE Recommended Practices for Measurement of Shielding Effectiveness of High Performance Shielding Enclosures, IEEE 299, IEEE Inc. NY (June 1969).

[23]R. Axford, R. McCormack, and R. Mittra, Evaluation of the Applicability of Standard CW EMI/RFI Shielding Effectiveness Test Techniques to Assessment of EMP Hardness Of Tactical Shelters, Construction Engineering Research Laboratories, CERL-TM-M-307 Urbana, IL (March 1982).

APPENDIX A-PARTIAL FRACTION EXPANSIONS OF $R_2^n(z;j\omega)$ AND $R_2^{nm}(z;j\omega)$

Our objective here is to obtain partial fraction expansions of $R_2^n(z;j\omega)$ and $R_2^{nm}(z;j\omega)$ which are defined by equation (5.36) on page 106. This procedure can be shortened by noting that both of these quantities can be written in the form:

$$R(z;\varsigma) = \frac{2\,\rho\,\varsigma\,\cosh[\varsigma(C+d+z)/C]}{\rho\,\varsigma\,\cosh(\varsigma) + \sinh(\varsigma)} \tag{A-1}$$

where ς is a complex variable and ρ is a real parameter. To recover $R_2^n(z;j\omega)$ and $R_2^{nm}(z;j\omega)$ from (A-1), it is only necessary to replace ς by

$$\varsigma = (C/C_o)\left[(\omega_c')^2 + (j\omega)^2\right]^{1/2} \tag{A-2}$$

ρ by

$$\rho = \frac{L_y C_o}{\eta_o\, C} \tag{A-3}$$

and ω_c' by ω_c^n and ω_c^{nm} respectively.

Since $R(z;\varsigma)$ is a single valued function of ς whose only singularities are simple poles, it satisfies the definition of a meromorphic function and can be expanded as a series of partial fractions[1] in the form

$$R(z;\varsigma) = R(z;0) + \sum_k W_k\left[\frac{1}{\varsigma - \varsigma_k} + \frac{1}{\varsigma_k}\right] \tag{A-4}$$

---

[1] E. C. Titchmarsh, The Theory of Functions, 2d Ed., Oxford University Press (1939).

where ς_k is the kth pole of $R(z;\varsigma)$, W_k is its residue, the sum is taken over all poles, and

$$R(z;0) = 2\,\mathcal{P}/(\mathcal{P}+1) \tag{A-5}$$

Now the poles of $R(z;\varsigma)$ are the nonzero roots of

$$F(\varsigma) = \mathcal{P}\,\varsigma\cosh(\varsigma) + \sinh(\varsigma) \tag{A-6}$$

and it can easily be shown that these form a doubly infinite sequence of paired imaginary numbers

$$\varsigma_k = \pm j\rho_k \qquad k = 1,2,3,. \quad \ldots\infty \tag{A-7}$$

where ρ_k satisfy

$$\mathcal{P}\,\rho\cos(\rho) + \sin(\rho) = 0\ . \tag{A-8}$$

Thus (A-4) becomes

$$R(z;\varsigma) = R(z;0) + \sum_{k=1}^{\infty} W_k^+ \left[\frac{1}{\varsigma - j\rho_k} + \frac{1}{j\rho_k}\right] + \sum_{k=1}^{\infty} W_k^- \left[\frac{1}{\varsigma + j\rho_k} - \frac{1}{j\rho_k}\right] \tag{A-9}$$

where W_k^+ are the residues for the $+j\rho_k$ poles and W_k^- are the residues for the $-j\rho_k$ poles. Evaluating the residues, we find

$$W_k^+(z) = -\,W_k^-(z) = \frac{2\mathcal{P}j\rho_k\cos[\rho_k(C+d+z)/C]}{\mathcal{P}[\cos(\rho_k)-\rho_k\sin(\rho_k)] + \cos(\rho_k)} \tag{A-10}$$

Using the first equation in (A-10), we can combine the two sums in (A.9) as follows

$$R(z;\varsigma) = R(z;0) + \sum_{k=1}^{\infty} W_k^+(z)\left[\frac{1}{\varsigma - j\rho_k} - \frac{1}{\varsigma + j\rho_k} + \frac{2}{j\rho_k}\right] \tag{A-11}$$

$$= R(z,0) + 2\,\varsigma^2 \sum_{k=1}^{\infty} \frac{W_k^+(z)}{j\rho_k[\varsigma^2 - (j\rho_k)^2]}\ .$$

The latter can be rewritten using (A-2), (A-3), and (A-10), as follows

$$R(z;j\omega) = \frac{2\,\rho}{\rho + 1} + 2\left[(\omega_c')^2 + (j\omega)^2\right] \sum_{k=1}^{\infty} \frac{W_k(z)}{(\omega_c')^2 + (\omega_k)^2 + (j\omega)^2}$$

where

$$W_k(z) = W_k^+(z)/(j\rho_k)$$

$$\omega_k = \rho_k C_o/C$$

and the partial fraction expansions of $R_2^n(z;j\omega)$ and $R_2^{nm}(z;j\omega)$ can be obtained from the preceding by replacing ω_c' with ω_c^n and ω_c^{nm}.

DISTRIBUTION

Commander

US Army Communications Command

ATTN: CC-OPS-TT

ATTN: CC-ENGR

ATTN: CC-OPS-WR, O.P. Connell

Ft. Huachuca, AZ 85613

Administrator

Defense Technical Information Center

Cameron Station, Building 5

ATTN: DTIC-DDA (2 copies)

Alexandria, VA 22314

National Communications System

Department of Defense

Office of the Manager

ATTN: NCS-TS, D. Bodson

Washington, DC 20305

Assistant to the Secretary of Defence

Atomic Energy

ATTN: Executive Assistant

Washington, DC 20301

Director

Defense Communications Agency

ATTN: Code B410, Parker

Washington, DC 20305

Director

Defense Nuclear Agency

ATTN: NATA

ATTN: RAEV

ATTN: DDST

ATTN: RAEE

ATTN: TITL

Washington, DC 20305

US Amy Engineer Division, Huntsville

DIvision Engineer

ATTN: HNDED FD, T. Bolt

P.O. Box 1600

Huntsville, AL 35807

Air Force Weapons Laboratory/DYC

ATTN: NTC4, TESD, IESM

Kirtland, AFB, NM 87117

Lawrence Livermore National Lboratory

ATTN: Technical Information Department Library

ATTN: L-156, H. Cabayan, L. Martin

P.O. Box 808

Livermore, CA 94550

Computer Sciences Corporation

Systems Division

ATTN: A. Schiff

1400 San Mateo Boulevard, SE

Abuquerque, NM 87108

Electromagnetic Applications, Inc.

ATTN: R. Perala

12567 West Cedar Drive

Suite 250

Lakewood, CO 80228

IIT Research Institute

ATTN: J. Bridges

ATTN: I. Mindel

10 West 35 th Street

Chicago, IL 60616

Mission Research Corporation

ATTN: W. Stark

4935 North 30th Street

Colorado Springs, CO 80919

Mission Research Corporation

EM System Applications Division

ATTN: A. Chodorow

1720 Randolph Road, SE

Albuquerque, NM 87106

Richard L. Monroe Associates

3634 Alton Place N.W.

Washington, DC 20008

Science Applications, Inc.

P.O. Box 1303

ATTN: W. Chadsey

McLean, VA 22102

SRI International

ATTN: A. Whittson

ATTN: E. Vance

333 Ravenswood Avenue

Menlo Park, CA 94025

TRW Defense and Space Systems Group

ATTN: J. Penar

One Space Park

Redondo Beach, CA 92078

US Army Laboratory Command

ATTN: TECHNICAL DIRECTOR, AMSLC-TD

2800 Powder Mill Road

Adelphi, MD 20783-1145

Installation Support Activity

ATTN: Library, SLCIS-IM-TL (3 copies)

ATTN: Library, SLCIS-IM-TL (Woodbridge)

ATTN: Legal Office, SLCIS-CC

2800 Powder Mill Road

Adelphi, MD 20783-1145

USAISC

ATTN: Record Copy, ASNC-ADL-TS

ATTN: Technical Reports Branch, SLCIS-IM-TR

2800 Powder Mill Road

Adelphi, MD 20783-1145

Harry Diamond Laboratories

ATTN: D/Division Directors

2800 Powder Mill Road

Adelphi, MD 20783-1197

Harry Diamond Laboratories

ATTN: Chief, SLCHD-NW-E

ATTN: Chief, SLCHD-NW-EC

ATTN: Chief, SLCHD-NW-ED

ATTN: Chief, SLCHD-NW-EE

ATTN: SLCHD-NW-EC, W. Coburn, COTR (9 copies)

ATTN: SLCHD-NW-RE, A. Cuneo

2800 Powder Mill Road

Adelphi, MD 20783-1197